Copy No. 5

1 ARL-TR-81-13

2 EFFECTS OF IONOSPHERIC TURBULENCE ON SPS PILOT SIGNAL

5 Final Report under Contract NAS9-16086

3 James R. Clynch

1 EE7 / Jack Seyl

NASA CR-160959

4 APPLIED RESEARCH LABORATORIES
THE UNIVERSITY OF TEXAS AT AUSTIN
POST OFFICE BOX 8029, AUSTIN, TEXAS 78712

6 24 February 1981

Final Report

1 March - 1 December 1980

Prepared for:

NATIONAL AERONAUTICS AND SPACE ADMINISTRATION
LYNDON B. JOHNSON SPACE CENTER
HOUSTON, TX 77058

TABLE OF CONTENTS

LIST OF FIGURES

LIST OF TABLES

I. INTRODUCTION

The proposed solar power satellite (SPS) will deliver its power from geosynchronous orbit to an earth station via a microwave beam at 2.45 GHz. A phased transmitting array will focus the beam on the receiving array. The reference for phasing the transmitting antenna is derived from a phase locked loop, which includes an uplink of the received power phase called the pilot signal. This system was proposed to achieve the high degree of pointing accuracy required and as a safety feature to cause the transmitting array elements to become randomly phased if the power beam drifts off the receiving site.

Because the pilot signal will travel the same path as the power beam, there is concern that phase noise will be imposed on this signal as it passes through the ionosphere, especially since the region of the ionosphere it traverses may be modified by the power beam. It is the objective of this study to obtain data on the ionospheric turbulence generated by the power beam and relate that to induced phase noise on the 2.45 GHz pilot beam.

It is not possible to duplicate the SPS configuration with currently available equipment. However, it was possible to take data from the ionosphere heated by the facility at Platteville, Colorado.[1] This facility can broadcast 1.8 MW of power in a 11° conical beam. To relate the effects of the Platteville heater to the SPS, some adjustments for the differing frequencies and power densities are required. The SPS will have a 5 GW beam passing through a 10 km diam circle, giving an average power density of 64 W/m^2, whereas the Platteville facility will have a maximum power density of 300 $\mu W/m^2$ at 300 km, a difference of five orders of magnitude. However, the heating is

expected to frequency scale as $1/f^3$ or $1/f^2$, depending on the processes involved. Thus, the Platteville facility operating at 10 MHz can simulate between 20 and 4000 W/m^2 at SPS frequencies, depending on the scaling.

One important factor in this comparison is the relative values of the peak plasma density and the heating frequency. In the SPS case, the heating frequency will be much greater than the highest possible ionosphere plasma frequency. When the heating frequency is at or below the peak plasma frequency, large quantities of energy are deposited in the ionosphere by resonant mechanisms.[2] This must be avoided in the current experiment if we are to obtain a valid comparison, using whatever scaling laws prevail. Unfortunately, the Platteville facility was limited to 10 MHz and below during the time this experiment was conducted. Thus data could only be acquired at night, when the plasma frequency was below 10 MHz. Due to the high level of solar activity, the operational frequency of 9.9 MHz was only 1.2-1.8 times the plasma frequency during data acquisition. The proximity of the heater frequency to the plasma frequency may make these data difficult to extrapolate to SPS frequencies.

The experiment consisted of monitoring the Doppler frequencies on the coherent UHF and VHF frequency pairs on the Navy navigation satellites and the GEOS-C geodetic satellite. These satellites are all in near-earth orbit at an altitude of about 1000 km and have orbital periods of about 105 min. Ground sites were chosen such that the line of sight (LOS) passed through the heating beam. Measurement of the differential Doppler allowed the rate of change of the columnar content to be measured. Since the satellite, and hence the LOS, were moving very rapidly, the ionospheric electron density turbulence could be measured as a function of space.

The initial objective was to acquire about ten satellite passes, probing the beam at various altitudes. The data were to be recorded on magnetic tape with a chart recorder as a backup. A component in the tape recording system was damaged in shipment and never functioned

correctly despite efforts to repair it in the field. A backup recording system was used for a time, and electron columnar content data from three heating passes were obtained with 200 Hz time resolutions. This system recorded only the differential Doppler. Chart recordings were obtained on all passes, but only the amplitude data are calibrated.

II. EXPERIMENTAL CONFIGURATION

A. Geometry

One of the principal advantages of using the Platteville site over Arecibo for this experiment was the availability of receiver sites. Predictions of satellite positions for the experimental period in late April 1980 were used to pick sites that were effectively on the path of the shadow of the heater beam as projected by the satellite. Four sites were chosen which had a reasonable variety of passes from which to probe the heater beam. These sites are listed in Table I and shown schematically in Fig. 1.

The heater beam has a beamwidth of 11.5° at 10 MHz, and all these experiments used a heating frequency near that value. The diameter of the beam is 60 km at an altitude of 300 km. A circle of that diameter is also shown in Fig. 1. Due to the earth's magnetic field, the actual energy may have deviated 10 km north or south of the heater beam at 300 km, depending on the polarization.

The magnetic field over the heater has a dip angle of 67.6° and an azimuth of 12.6° at 300 km altitude. These angles vary only a fraction of a degree over a 200 km altitude range and over a 100 km horizontal extent.

In addition to the data acquired by ARL:UT, differential Doppler data were collected by the permanent Tranet II station at the Physical Science Laboratory (PSL), New Mexico State University, located at Las Cruces, New Mexico. While it is possible for PSL to view the heater beam above 80 km altitude, the elevation angles to the heated region are

TABLE I

LOCATIONS OF HEATER AND RECEIVER SITES

	Geodetic Latitude (°N)	Longitude (°E)	Ground Range to Heater (km)	Azimuth to Heater (deg)
Heater	40.183	-104.726	--	--
Sterling	40.621	-103.170	142	252
Loveland	40.406	-104.996	32	136
Ft. Morgan	40.272	-103.703	80	265
Boulder	39.982	-105.249	49	62
Las Cruces	32.279	-106.754	914	10

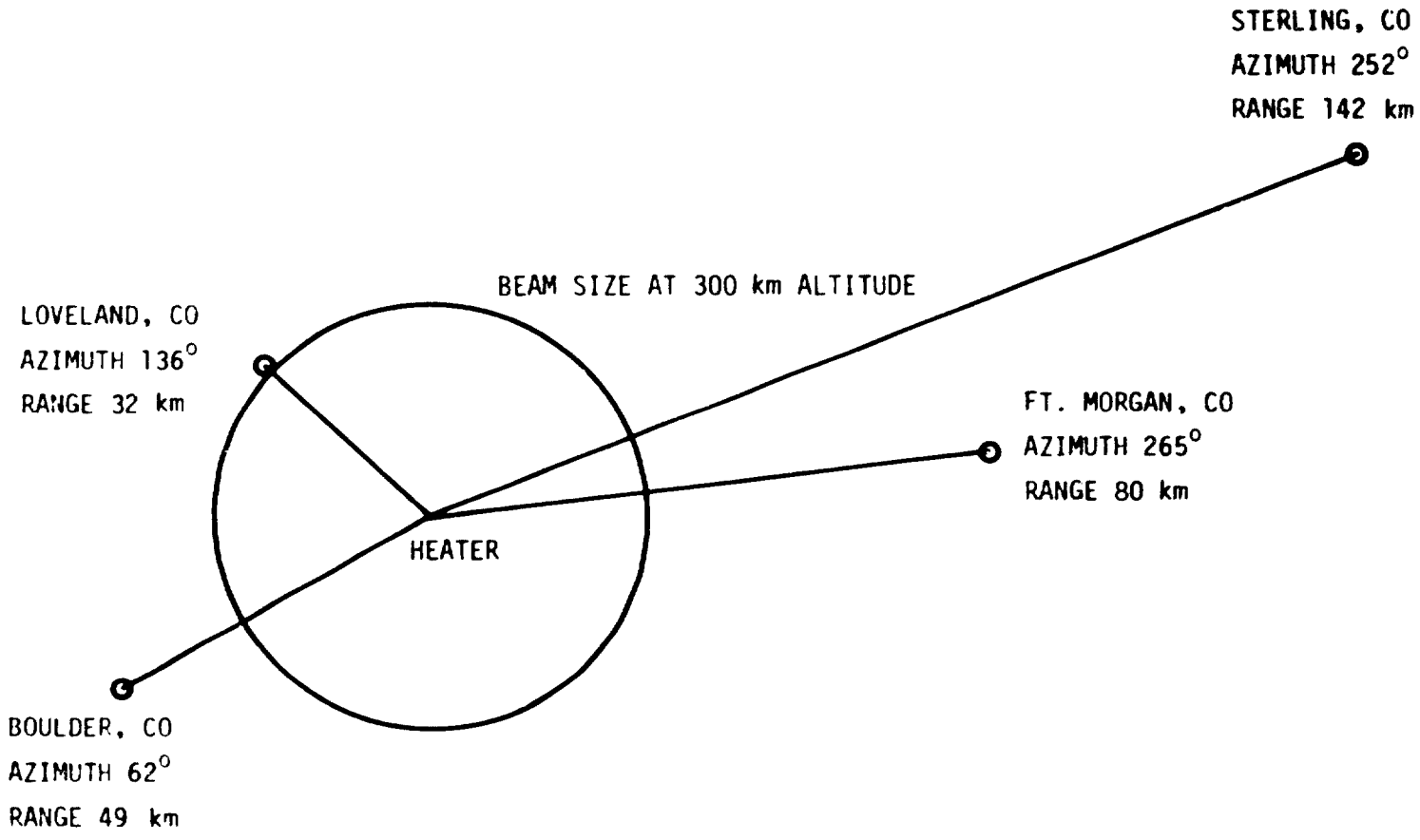

FIGURE 1

RELATIVE LOCATIONS OF HEATER AND RECEIVING SITES

very low, e.g., 16° to an altitude of 350 km. These data are useful, however, as background data and for the observation of very large scale effects.

B. Electronics

A diagram of the major components in the ground system is shown in Fig. 2. The cassette tape recording was intended to be the primary data. In addition, the data were recorded on a strip recorder and paper tape, which is the original data format for the commercial receiver used.

The data were acquired with a modified version of a geoceiver built by Magnavox and designed to receive either 150 MHz/400 MHz or 162 MHz/324 MHz pairs of signals originating on satellites. The data are partially processed internally and the number of UHF Doppler counts, the number of refraction correction counts (discussed below), and the time are punched on paper tape about every 30 sec. The unit used by ARL:UT had been modified to record paper tape data at a 10 sec interval and to bring out internal signals which allow better resolution of ionospheric parameters.

The geoceiver subtracts a harmonic of a stable crystal from the UHF (400 MHz/324 MHz) signal leaving only the Doppler shift riding on a small offset frequency of a few kilohertz. The local oscillator signal for the VHF signal is another harmonic of the same oscillator, and the ratios of these harmonics is the same as that of the received signals. In addition to this VHF harmonic, the Doppler of the UHF signal scaled down by the frequency ratio is subtracted from the VHF signal. The resulting signal would be at dc (in reality, a 2.5 MHz reference carrier) if there were no dispersion. The cycles of the difference between the 2.5 MHz reference and the VHF processed signal are counted. This number is then multiplied by 1/8 for the 400/150 MHz system or 1/2 for the 324/162 MHz system to give the refraction correction count (RCC).

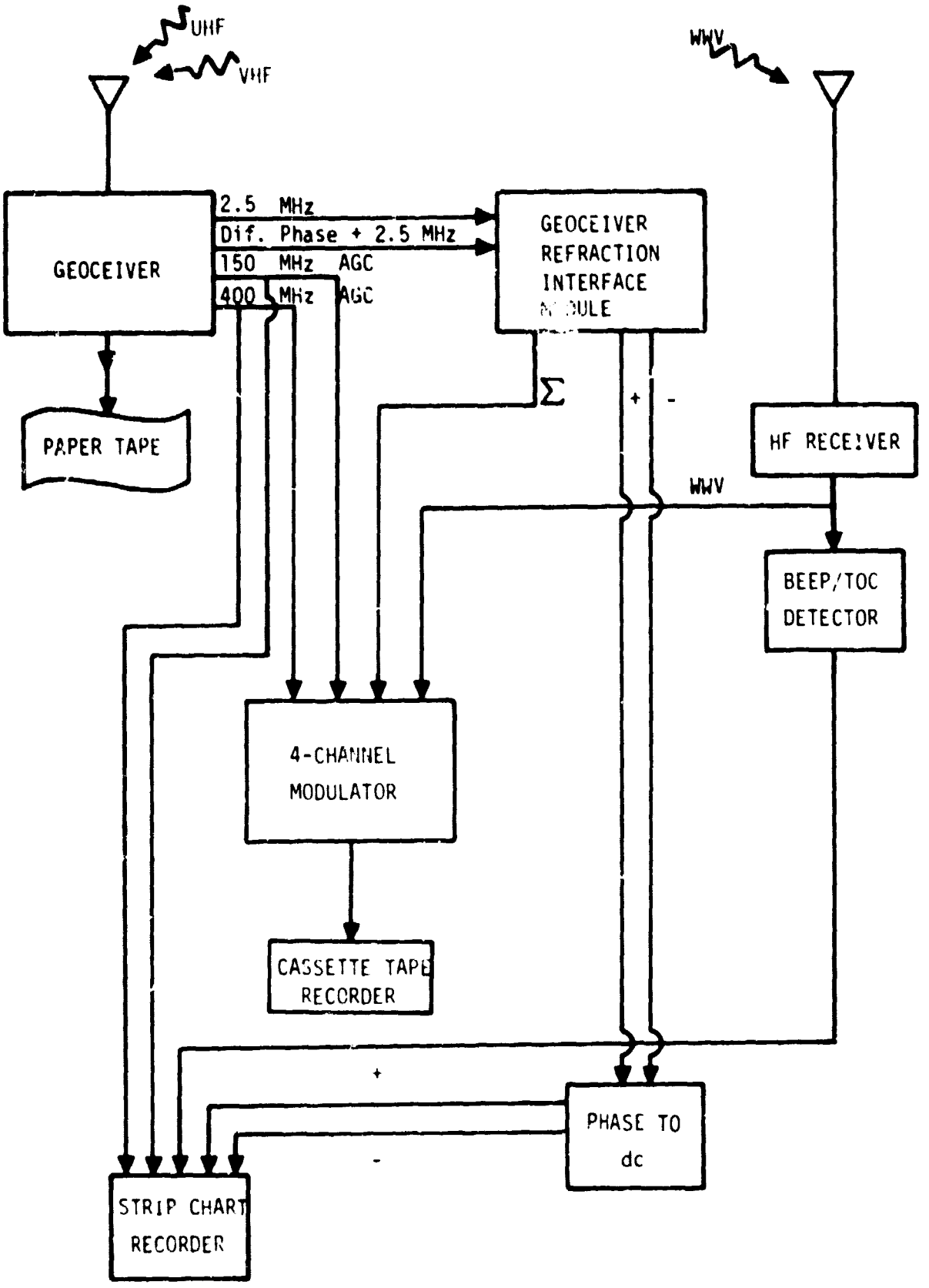

FIGURE 2

SYSTEM CONFIGURATION

AF-81-18

The RCC is a direct measure of the change in columnar electron content over the counting interval as shown in the appendix. However, the time resolution is not adequate for a detailed examination of ionospheric turbulence. Accordingly, the analog signal on the 2.5 MHz carrier and the 2.5 MHz carrier are brought out of the receiver and fed into a phase comparator which outputs a dc level proportional to the phase difference. This geoceiver refraction interface module outputs three signals: the positive phase (active when the data lead the reference), the negative phase (active when the data lag the reference), and a composite of the two. A history of the direction of the phase difference is maintained over several cycles and the sign of the difference signal followed through complete cycles. The output for a constant frequency difference would be a sawtooth on one of the separated channels and the composite. Inverting the sign of the frequency difference would change the output of the separated signals and the polarity of the composite signal. In addition to the phase data, the AGC voltages were brought out of the geoceiver.

These two AGC's, the composite phase signal, and the time signal from WWV were all recorded on a cassette tape recorder. The four channels were multiplexed with a unit built at ARL:UT. The WWV signal was directly recorded in the 0-1500 Hz band. The other signals were double sideband modulated on carriers at 3 kHz, 4.5 kHz, and 6 kHz, and the channels bandlimited to 200 Hz. A 9 kHz reference signal was also recorded. A complementary demodulator unit was also built by ARL:UT.

In addition to the data recorded on magnetic tape, strip charts were made for realtime system evaluation and as a backup. The AGC signals were directly recorded but, to save chart paper, the two separated phase channels were processed to produce a dc level proportional to the refraction frequency. This was done by high passing the signals at 1 kHz to isolate the sharp edges from switchbacks and then rectifying, low pass filtering, and amplifying the result. This gave a broad uncalibrated line on the chart recorder, which is an indication of refraction frequency.

As a further backup and to replace the primary tape recording system when it failed, the composite phase signal (marked Σ in Fig. 2) was directly recorded on a cassette tape recorder. This was done only during days 106-109.

As mentioned earlier, the modulator was damaged in shipment and never functioned satisfactorily during the experiment. An attempt was made to repair it in the field and testing showed it apparently was functioning. However, no data taken with it are recoverable without extremely extensive signal processing. Even then, the data would be highly degraded.

In addition to the magnetic tape problems, the 162 MHz preamplifier in the antenna failed during this experiment. A replacement unit was shipped from Defense Mapping Agency in Washington, DC, but it proved to have a defective 150 MHz preamplifier. A list of the dynamic ranges of the receiver with the various preamplifiers is shown in Table II. The original preamplifier was used for all 150/400 MHz data and the second replacement for 162/324 MHz data. Two 162/324 MHz passes were taken without preamplifiers in the interval prior to receipt of the second preamplifier. The dynamic range for these passes was reduced to about 10 dB.

TABLE II

DYNAMIC RANGE OF SYSTEM

Preamplifier	Dynamic Range (dB)			
	150 MHz	400 MHz	162 MHz	324 MHz
Original	25	33	-	-
Replacement I	5	35	-	29
Replacement II	21	35	15	29

III. OBSERVATIONS

The data collection took place between UT days 106 and 116, 1980, during which 13 heating passes were observed. Due to equipment problems, only ten of these passes were useful. Two of the ten were taken on the 162/324 MHz frequencies during an interval when no preamplifier was available for that frequency pair. Consequently, those two passes are of low quality. The first three heating passes were recorded on the auxiliary tape system, and high spatial resolution of electron content variation is available for these passes. Strip chart data are available on all passes.

A list of the useful data passes is given in Table III. This table contains the satellite number in the DMA numbering system, the nominal rise time in UT, geometric parameters, ionospheric parameters, and receiving site. The geometric quantities are illustrated in Fig. 3. As the satellite moves, the line of sight will sweep north or south according to the direction of satellite motion. The receiving sites were chosen so that the LOS cuts through the beam of the Platteville heater as shown in Fig. 3. The time of first and last contact with a geometric cone 11.5° in angle are listed in Table III. In addition, several quantities are given for the time when the LOS passed directly over the heater. These include the time, the altitude of the LOS as it enters the cone (side closest to the receiver), the altitude of the beam when it exits the cone, and the elevation angle.

The ionospheric parameters listed were taken from ionograms made at Boulder. The values were interpolated to satellite rise time from hourly ionograms. H_{min} is the virtual height of the base of the F region. This should be within 10 km of the true height as there were very few electrons in lower layers during the night.

TABLE III

GEOMETRIC AND IONOSPHERIC PARAMETERS OF HEATING PASSES

PASS	SAT.	DAY	RISE	FIRST CONTACT	LAST CONTACT	CLOSEST TO CENTER				F REGION H_{min}	F_0F_2	LOCATION
						TIME	ALT. IN	ALT. OUT	ELEV.			
1	93	106	4:18	4:26:53	4:27:20	4:27:06	323	540	69	230	7.5	Sterling
2	60	108	6:50	6:59:17	6:59:57	6:59:37	114	280	78	300	6.5	Loveland
3	68	109	11:02	11:11:19	11:12:06	11:11:43	88	163	73	280	5.6	Loveland
4	60	112	6:56	7:04:29	7:04:56	7:04:42	217	299	60	290	7.2	Sterling
5	93	113	3:57	4:06:11	4:06:37	4:06:24	228	319	61	250	8.2	Sterling
6	83	113	5:56	6:04:38	6:04:55	6:04:47	138	167	46	260	7.5	Sterling
7	83	114	5:41	5:49:42	5:50:03	5:50:52	218	385	72	280	6.9	Fort Morgan
8	60	114	6:58	7:07:13	7:07:38	7:07:25	104	131	52	310	6.4	Fort Morgan
9	83	115	5:26	5:34:37	5:34:55	5:34:47	105	167	68	280	6.5	Boulder
10	93	116	3:13	3:27:27	3:27:54	3:27:41	121	210	63	240	7.3	Boulder

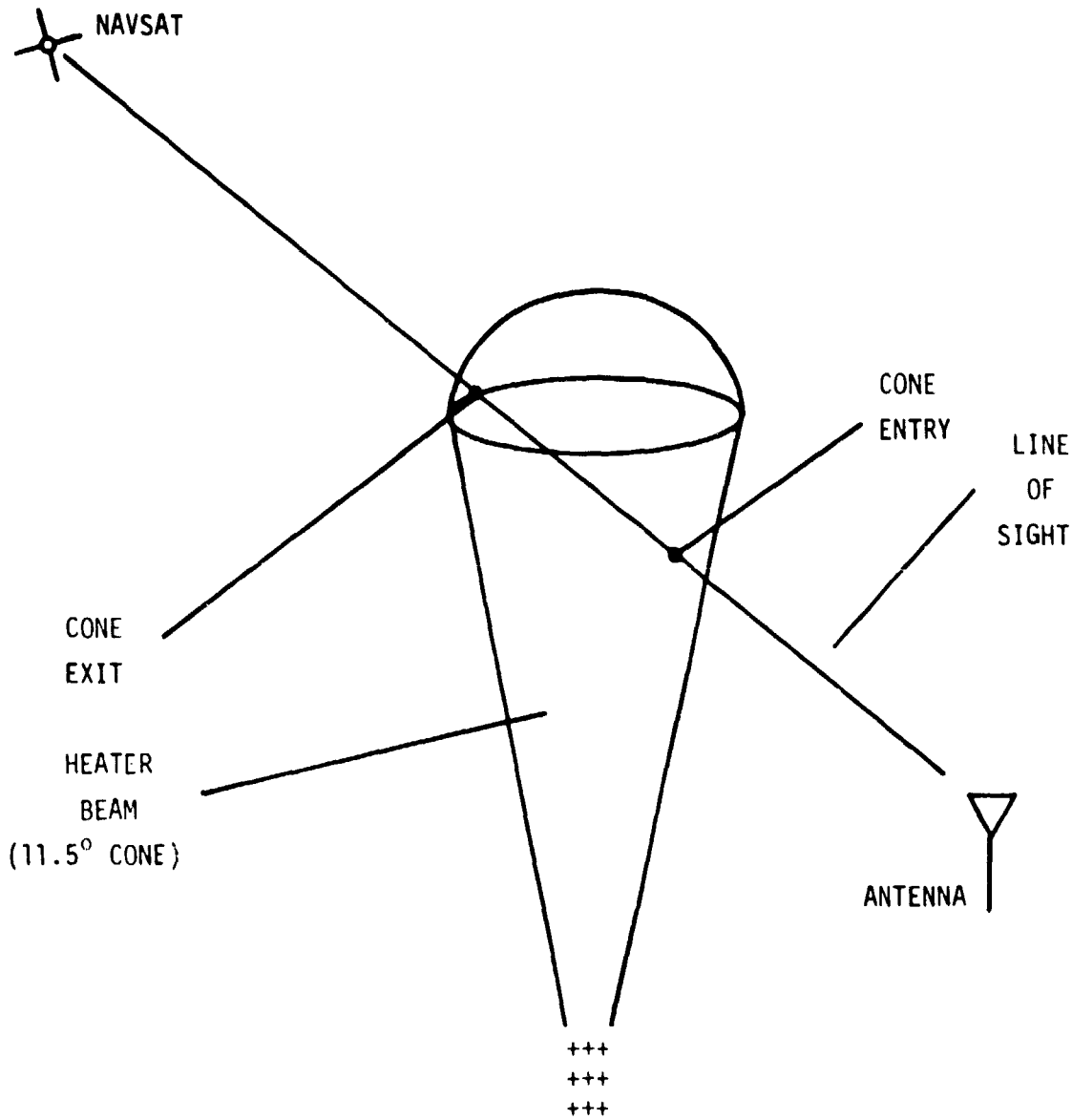

FIGURE 3
EXPERIMENTAL GEOMETRY

A. Low Time Resolution Data

The paper tape data and the chart recorder data contain the only usable information for passes 4-10. The paper tape data have a time resolution of 10 sec and contain accurate columnar electron content (N_c) measurements but no amplitude data (except for the absence of data indicating loss of lock). The strip charts contain calibrated amplitude data and uncalibrated electron content data. Both of these electron content data can give only crude qualitative information such as the sign of $\dot{N}_c$ and whether or not it is very noisy.

In this section, a series of graphs present the low resolution data for each heating pass. Included are

1. geometry,
2. amplitude from strip charts,
3. paper tape data, and
4. PSL Tranet II data, if taken.

The geometry graphs display three quantities as a function of time: the minimum distance from the LOS to the vertical line above the heater, the altitude at which the LOS enters the cone, and the altitude at which the LOS exits the cone. The time scale begins about 50 sec prior to the LOS crossing over the heater. As an additional time reference, UT minutes are also marked on these graphs. The amplitude graphs are presented on one or two pages with up to three segments per page. The time of beam crossing is given in the legend and the first and last contact times are marked on the figures.

The last two graphs present the rate of change of the electron columnar content ($\dot{N}_c$). The first of these presents the paper tape data in an ARL:UT standard format, usually at a 10 sec grain. The top graph in these figures is $\dot{N}_c$ in units of TECU/sec. The zero of the time scales is given in the legend. The lower graph in these figures shows the location of the LOS in the ionosphere. For this purpose, the position along the LOS at an altitude of 350 km has been used. The ionospheric longitude will be essentially horizontal due to the 90° inclination of the orbit.

It is also marked with a small triangle at the setting end. The last graph type in each set presents the PSL Tranet II data. These $\dot{N}_c$ data were taken with equipment which counts the change in N_c over 1 sec intervals. A large spike or long flat area in these data usually indicates a momentary or extended loss of lock, respectively. The PSL data were acquired for most, but not all, of the heating passes, and therefore this graph may be missing from some data sets.

There are several natural and instrumental effects which show up in the amplitude records. First, the ionosphere to the north of the observing sites often had naturally occurring turbulence at night. This caused scintillations on the northern portion of some passes. Most passes set in the north, placing these scintillations at the end of the passes. The variations on 150 MHz are larger than those on 400 MHz during natural scintillations.

In addition to scintillations, there will be amplitude variations due to the Faraday effect. This causes the plane of polarization of a linearly polarized signal to rotate by an angle proportional to the columnar electron content times the projection of $\vec{B}$ (the magnetic field of the earth) on the LOS. The NAVSATs and geodetic satellites were designed to emit circularly polarized signals to circumvent this effect. However, all emit elliptically polarized radiation, some with high axial ratios, and the direction of the major axis will rotate in this case. The receiving antenna is a short vertical stub, causing the received amplitude to vary as the semimajor axis of the elliptically polarized radiation changes its angle. This causes shallow nulls with long periods (minutes) as the moving LOS changes its N_c. This effect is most pronounced on the 150 MHz signals and varies from satellite to satellite depending on the specific antenna.

The short vertical antenna would have a dipole beam pattern with a large null above and below were it not for a ground plane. The geoceiver has a bent artificial ground plane which almost suppresses the overhead null. Because some passes acquired data at high elevation angles, the

beam pattern was measured by monitoring three passes, one with a maximum elevation angle of 88°, one of 89°, and one of 72°. For the first two passes the antenna was in the standard position. For the last, the antenna was tilted toward the satellite at TCA. The 400 MHz signal lost lock only on the 72° pass and the 150 MHz signal lost lock near TCA on the 72° and 89° passes.

Finally, the 150 MHz AGC voltage occasionally makes very rapid 2 dB step changes. These occur irregularly and infrequently; there may be one or two in a pass and then none for several passes. The cause of these steps in the 150 MHz AGC voltage is unknown. However, they are very distinctive and will not be confused with propagation effects.

1. Pass of Satellite 93, Day 106, 0418 UT

This pass was observed from Sterling, CO. The heater was turned on about 10 min prior to the LOS passing through the beam on this and all other passes. Therefore any instabilities should have been fully developed prior to the probing of the heated region.

The geometry for a direct probing of the heated region was very favorable on this pass, as seen in Fig. 4. The LOS traversed the beam over an altitude range of 300-580 km. The F region began at 230 km during this pass and had a F_0F_2 of 7.5 MHz. The heating frequency was 1.3 times the peak plasma frequency.

The amplitude record in Fig. 5 shows a small scintillation on 150 MHz beginning at 4:25:10 UT and an abrupt drop of 5 dB at 4:26:40. Although it is likely that the scintillation was caused by the heater, neither of these features is unique to heating passes. There is a TEC variation beginning at 4:25:17, which is unusual for this latitude and corresponds to these amplitude variations.

This pass rose in the south and set in the north. Near the northern end of the pass, there are very heavy scintillations on the

FIGURE 4

HEATER - LINE OF SIGHT GEOMETRY

Satellite 93 Day 106 Zero Time 4:26:17 UT

AE-81-20(a)

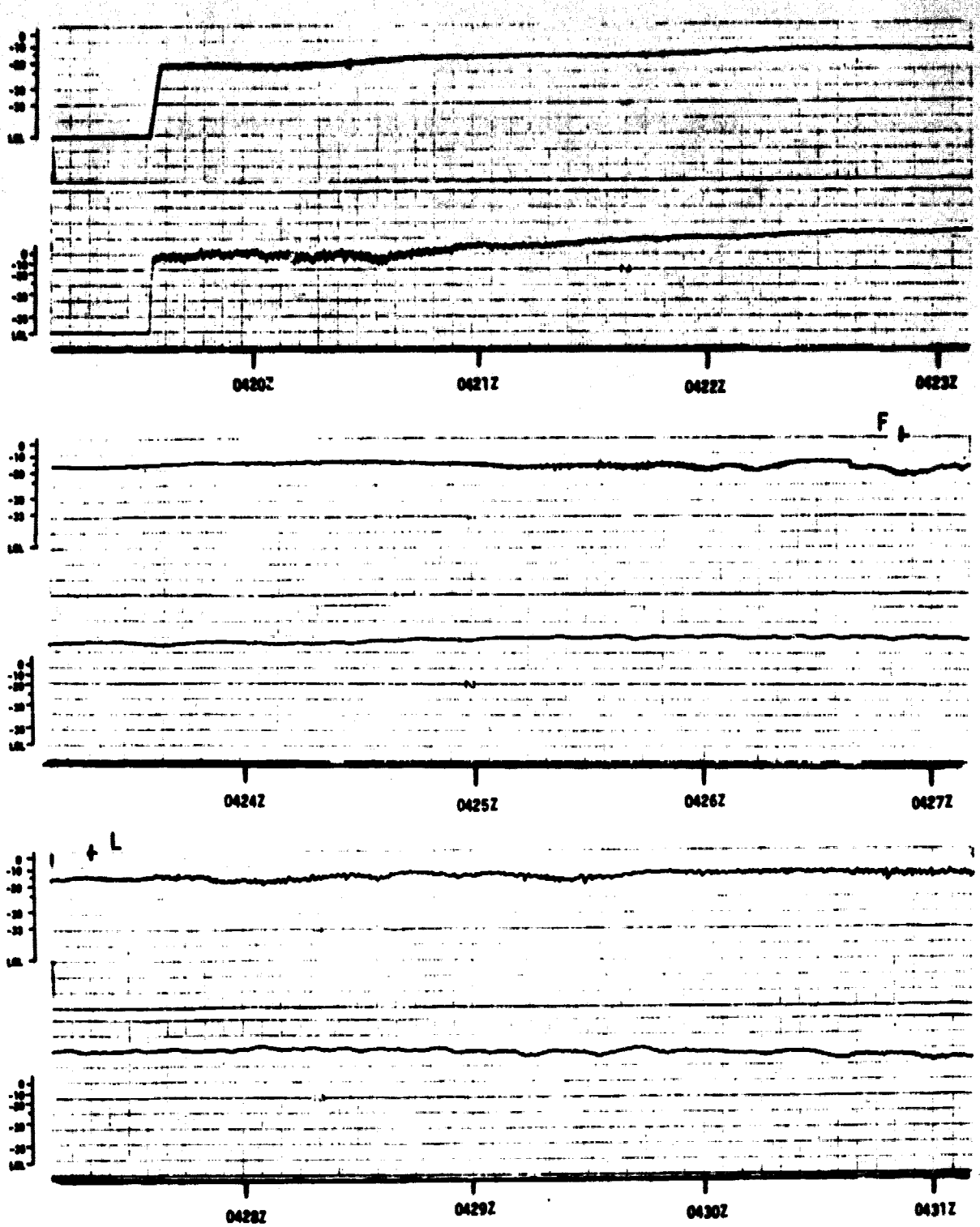

FIGURE 5

AMPLITUDE versus TIME OF NAVSAT PASS

Upper Trace 150 MHz Lower Trace 400 MHz

Day 106 Satellite 93 Rise 4:18

Line of Sight Crosses Above Transmitter at 4:27:06 AE-81-20(b)

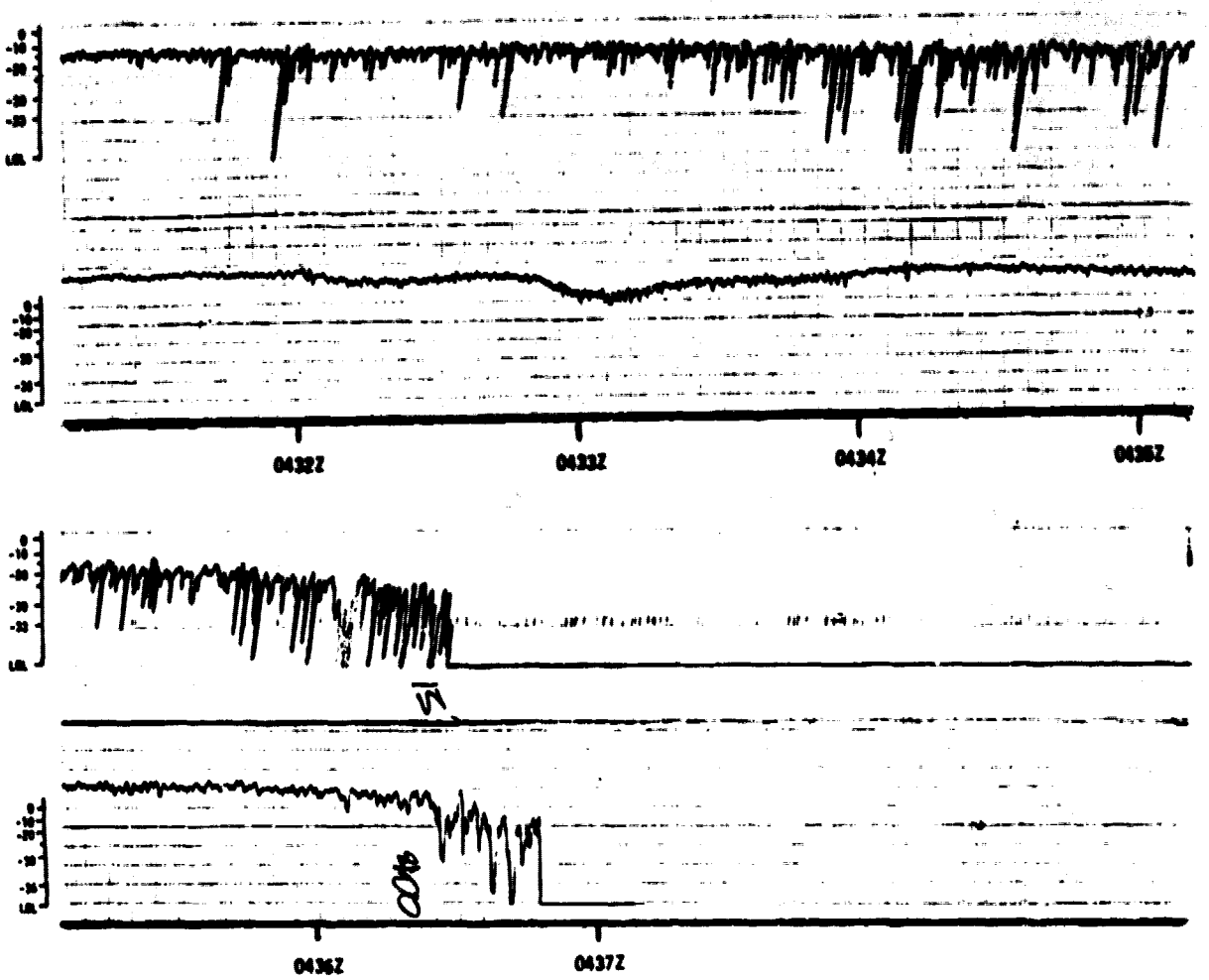

FIGURE 5 (cont'd)

AMPLITUDE versus TIME OF NAVSAT PASS

Upper trace 150 MHz Lower Trace 400 MHz

Day 106 Satellite 93 Rise 4:18

Line of Sight Crosses Above Transmitter at 4:27:06

150 MHz channel (over 25 dB) and 15 dB variations on the 400 MHz channel. These variations were caused by naturally occurring scintillations to the north of the station. They form a good basis for comparison of natural to heater induced effects.

The paper tape data, shown in Fig. 6, give a rough picture of the rate of change of electron columnar content as the LOS swept from south to north. For a uniform shell ionosphere, these data would show an S shaped curve. The value of $\dot{N}_c$ at rise would have been some negative value which would slowly move toward zero as the elevation angle increased and the distance through the ionosphere shortened. Near the time of closest approach (TCA), the slope would have increased and $\dot{N}_c$ would go through zero at TCA. After that, the reverse process would have occurred.

In this case, the shape has been greatly distorted by the variation of electron density with latitude. From the beginning to about second 100, the loss rate is considerably higher than in the following 200 sec. During the first 100 sec, this pass has sampled the northern edge of the northern equatorial electron peak. Note that after the TCA, when $\dot{N}_c$ would be positive for a uniform shell, it goes negative. This indicates a large latitudinal gradient which causes more electrons to be lost from the LOS than are gained by the increase in path length through the ionosphere.

The LOS crosses the beam between seconds 437 and 464 on this time scale. The points at 420 to 440, just prior to beam entrance, show some irregularity. However, the resolution is insufficient to determine any details or even to definitely associate this variation with the heater. The variations later in the pass, during the scintillations, are much more erratic. Note also that the 350 sec point, which corresponds to a counting interval of 4:25:16 - 4:25:26, is below the line of adjacent points; this corresponds to the amplitude irregularity mentioned earlier. These features will be examined in more detail in the section on magnetic tape data.

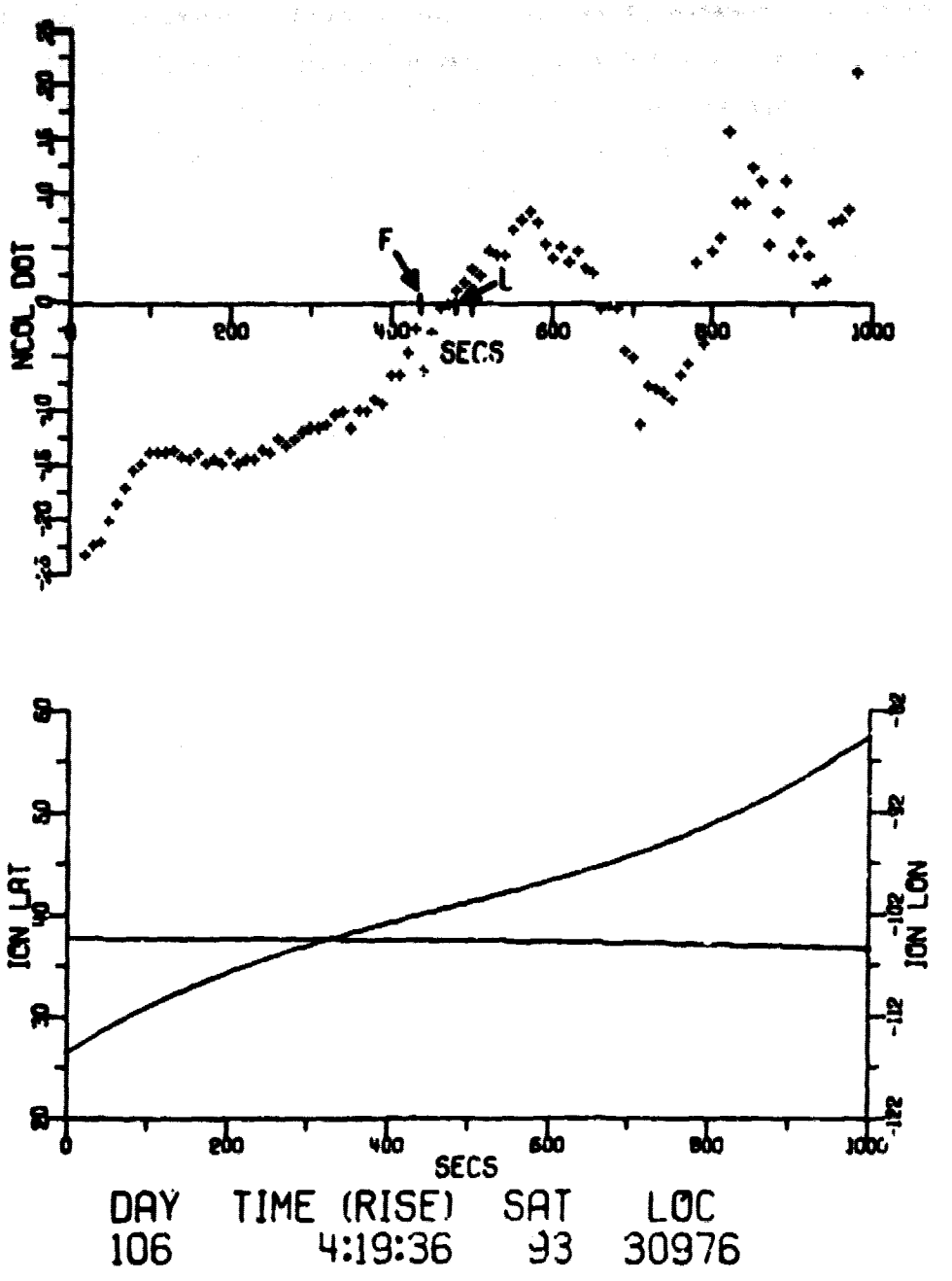

FIGURE 6

PAPER TAPE DATA OF N_c DOT

It is expected that any irregularities formed by the heating would be elongated along the magnetic field. Therefore, the angle between the LOS and $\vec{B}$ will determine how effective a given irregularity is in disrupting the transmissions. The B field points down and northward. Accordingly, the LOS will come closest to lining up with B during the southern half of the pass. For this pass, ψ, the angle between $\vec{B}$ and the LOS, had a minimum of 12° at 4:26:20.

This pass was tracked by the Tranet II at PSL. The observed $\dot{N}_c$, shown in Fig. 7, covers an area shifted to the south of the data acquired in Colorado. One sees the maximum of the northern equatorial anomaly clearly defined at about 90 sec into this pass. This pass sets south of the region of scintillations observed in Colorado.

The satellite passed essentially overhead at PSL and was abreast of and 218 km to the west of the heater at 4:27:34. There is a step in the PSL TECU data at second 805 (04:29:15 UT) which may have been caused by the heater. At this time, the LOS was 230 km due west and abreast of the heater at an altitude of 620 km. This is a step of 3.6×10^{-2} TECU/sec, about one-fourth of the total loss rate at this time. This isolated step is quite unusual, and did not occur on any of the 26 non-heating background passes observed at PSL.

2. Pass of Satellite 60, Day 108, 0650 UT

This pass was observed from Loveland, CO. As shown in Fig. 1, Loveland is just outside the geometric beam at an altitude of 300 km. The geometry graph in Fig. 8 shows that the LOS for this pass entered the beam low and became essentially aligned with it over a large altitude range at exit. The Loveland passes are therefore very sensitive probes of the irregularities. Unfortunately, these irregularities were so strong that, on this pass, the receiver lost lock at first contact with the beam and no phase (i.e., $\dot{N}_c$) information within the beam was acquired.

FIGURE 7

$\dot{N}_c$ DATA FROM LAS CRUCES, NEW MEXICO

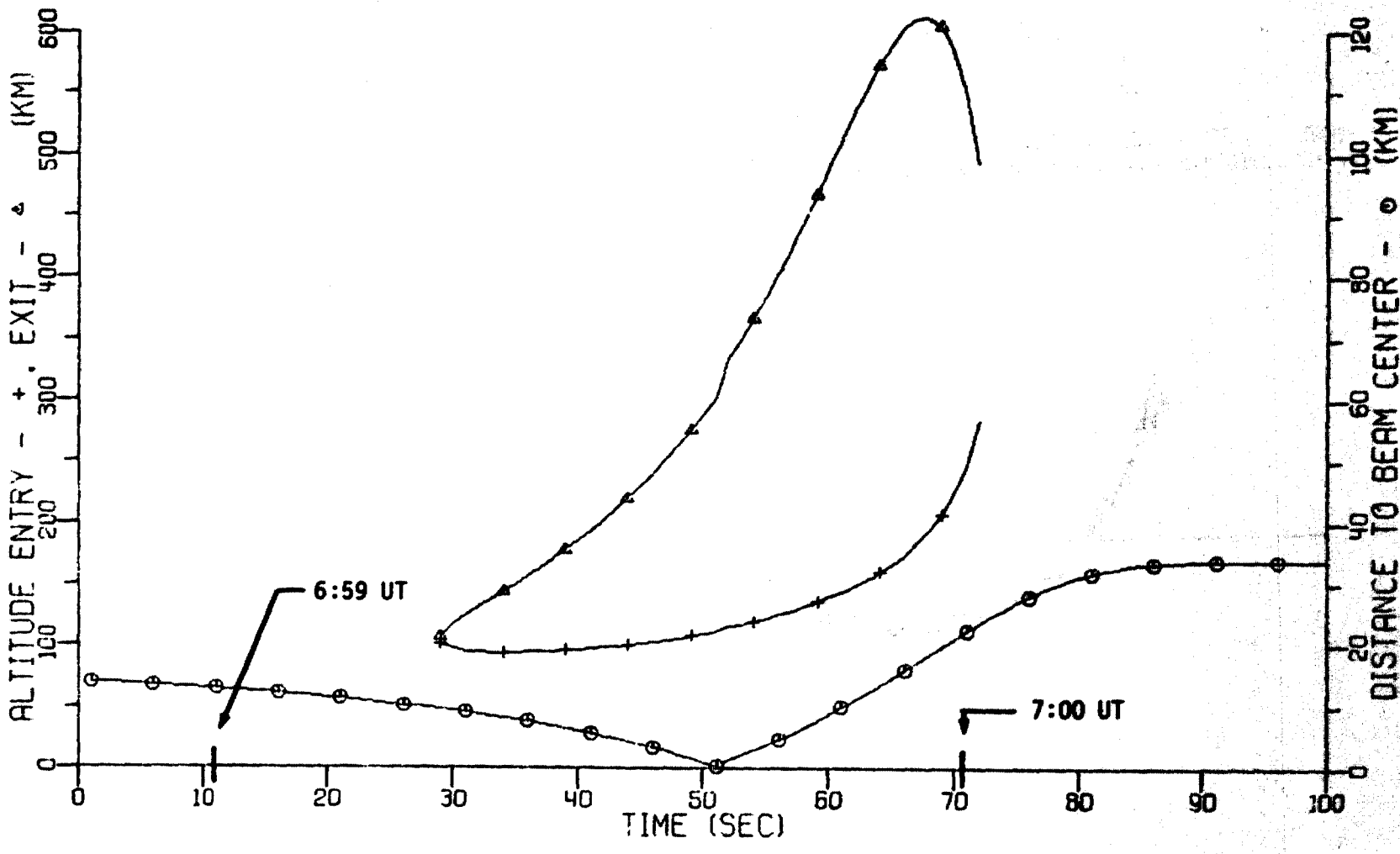

FIGURE 8

HEATER - LINE OF SIGHT GEOMETRY

Satellite 60 Day 108 Zero Time 6:58:49 UT

The amplitude recorded in Fig. 9 shows several features prior to the massive dropout at first contact. The 150 MHz channel had some long period fades which occur often with some NAVSATs. These fades are due to the Faraday rotation occasionally causing the major axis of the elliptically polarized satellite signal to be perpendicular to the vertical antenna. Of more relevance is the 400 MHz variation, which begins at about 6:58:35 UT and culminates in the loss of lock (LOL) at 6:59:15. The LOL on the 150 MHz channel was due to the 400 MHz dropout. The 150 MHz always loses lock when the 400 MHz is not locked for over a second or so because the 400 MHz Doppler is used in the 150 MHz phase loop.

The exact time of reacquisition is a function of the operator although the signal must, of course, be strong enough to be tracked. After the signal was reacquired, both signals were attenuated from their preencounter levels.

The paper tape data for this pass are shown in Fig. 10. The blank region around 500 sec corresponds to the dropout. The last point prior to the dropout contains data taken during very deep and rapid 400 MHz fades and therefore is highly contaminated with multipath and other inaccuracies.

The Tranet II TEC data are shown in Fig. 11. In this case, the PSL LOS actually passed through the beam in the upper ionosphere. At 07:00:10, the LOS made first contact with the beam at an altitude of 1000 km. It made last contact at 07:03:00 at an altitude of 460 km. The large spike on Fig. 11 occurs just as the LOS enters the beam. It is impossible to tell from the available data if this is a true phase measurement implying an N_c change of 0.3 TECU, or if it is due to an amplitude dropout of less than 1 sec. The second phase spike occurs just as the LOS leaves the cone. It appears that the heating has had some effect on these PSL observations.

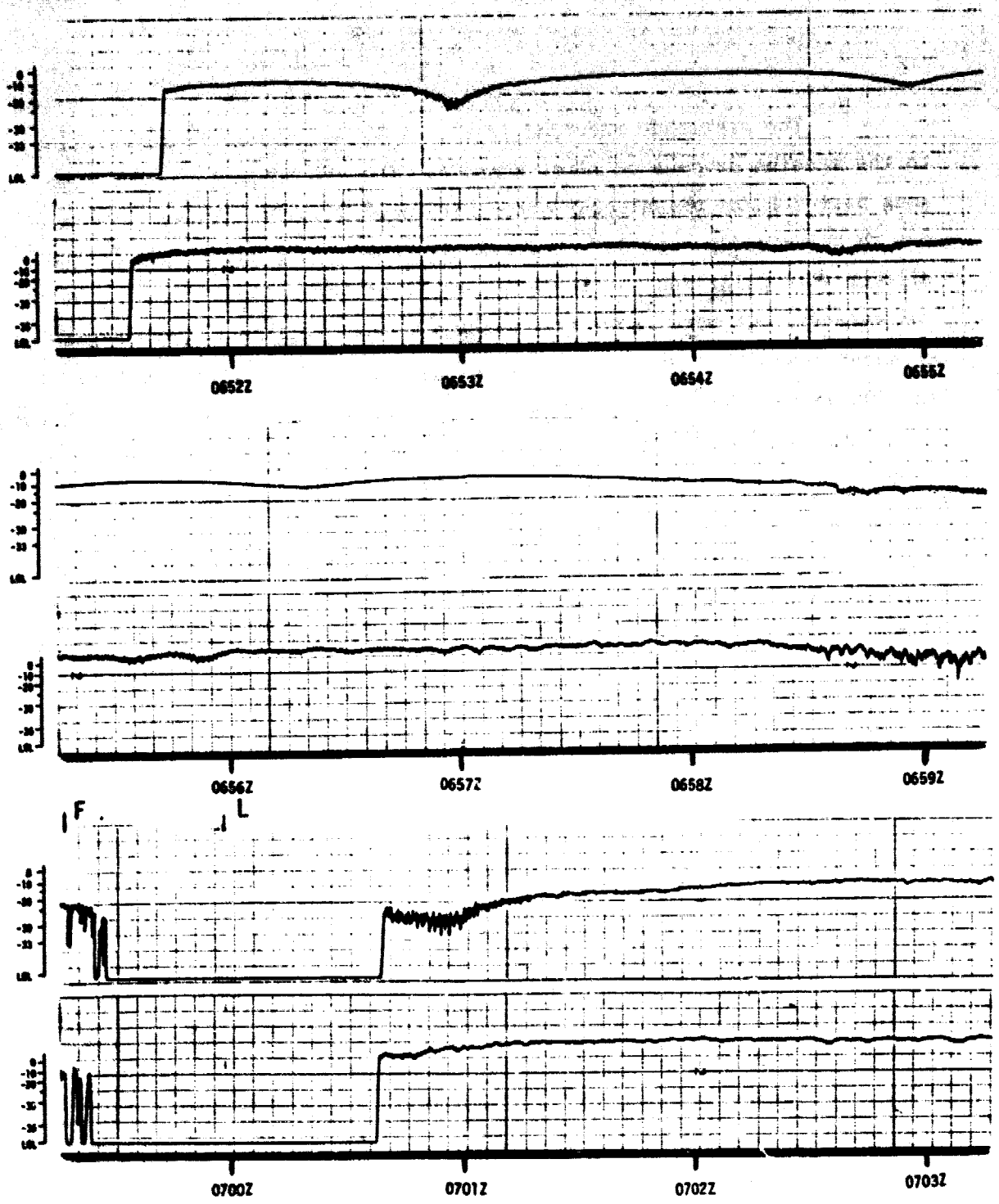

FIGURE 9

AMPLITUDE versus TIME OF NAVSAT PASS

Upper Trace 150 MHz Lower Trace 400 MHz

Day 108 Satellite 60 Rise 6:50 UT

Line of Sight Crosses Above Transmitter at 6:59:37 UT

AE-81-25

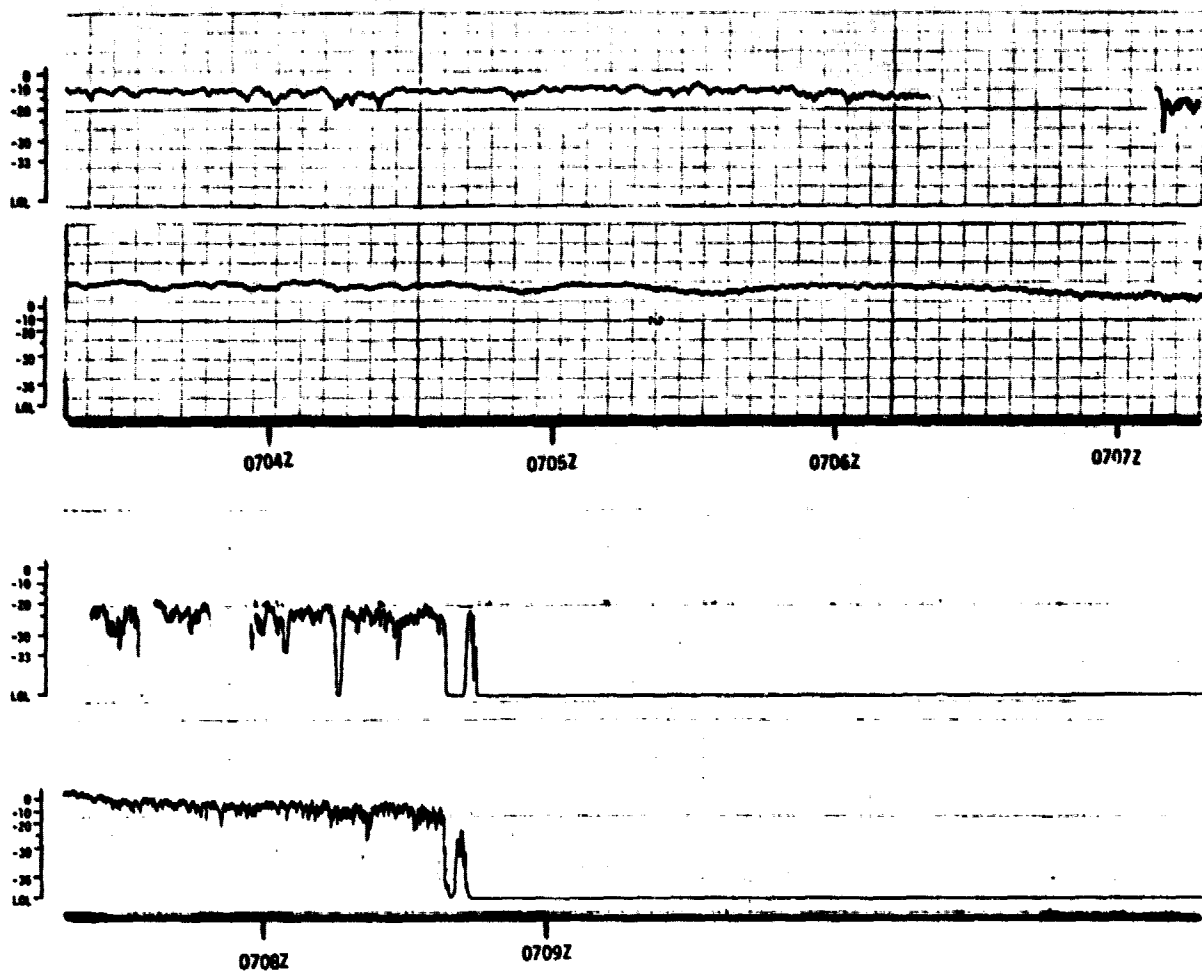

FIGURE 9 (cont'd)

AMPLITUDE versus TIME OF NAVSAT PASS

Upper Trace 150 MHz Lower Trace 400 MHz

Day 108 Satellite 60 Rise 6:50 UT

Line of Sight Crosses Above Transmitter at 6:59:37 UT

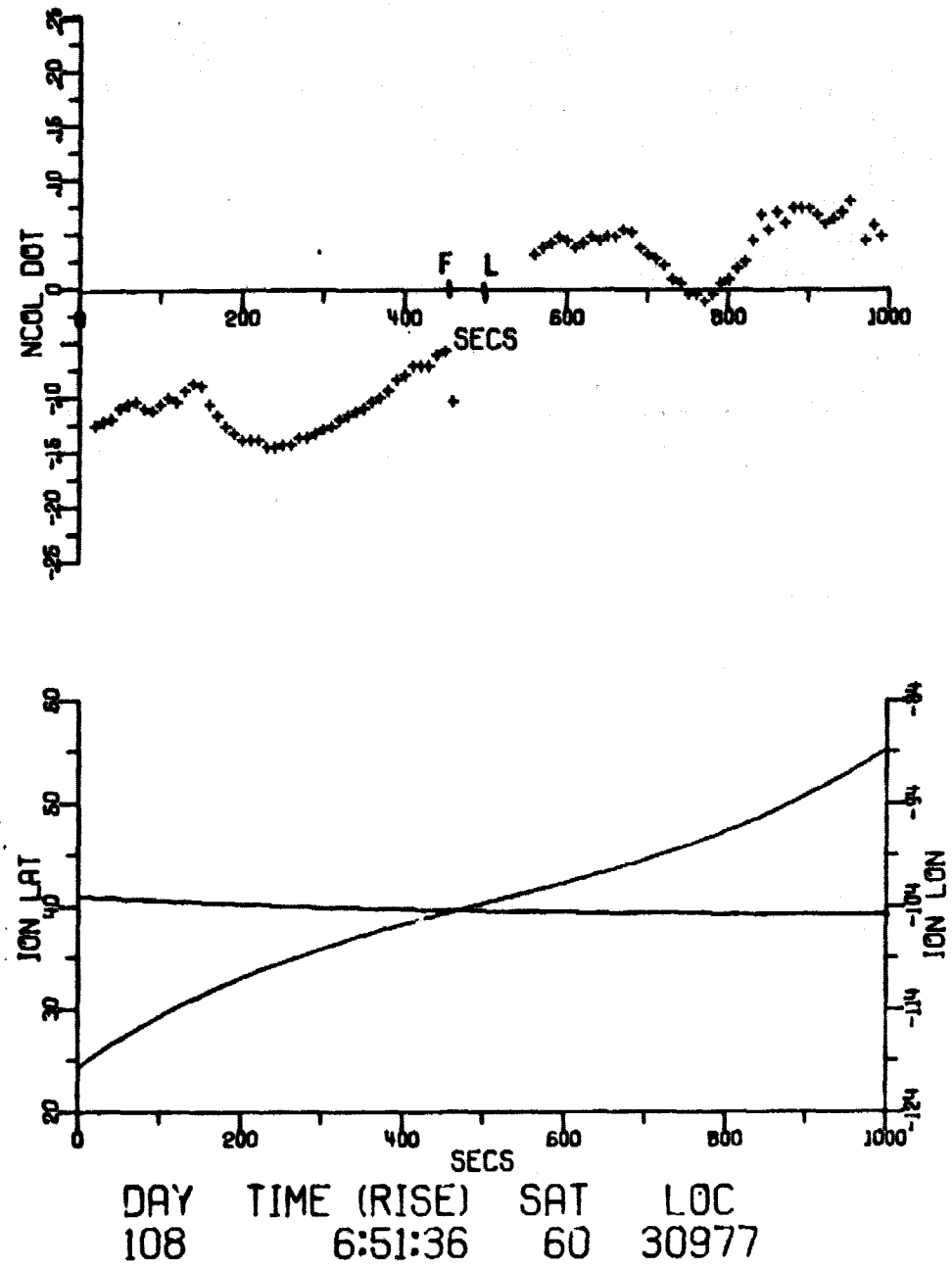

FIGURE 10

PAPER TAPE DATA OF N_c DOT

AE-81-26

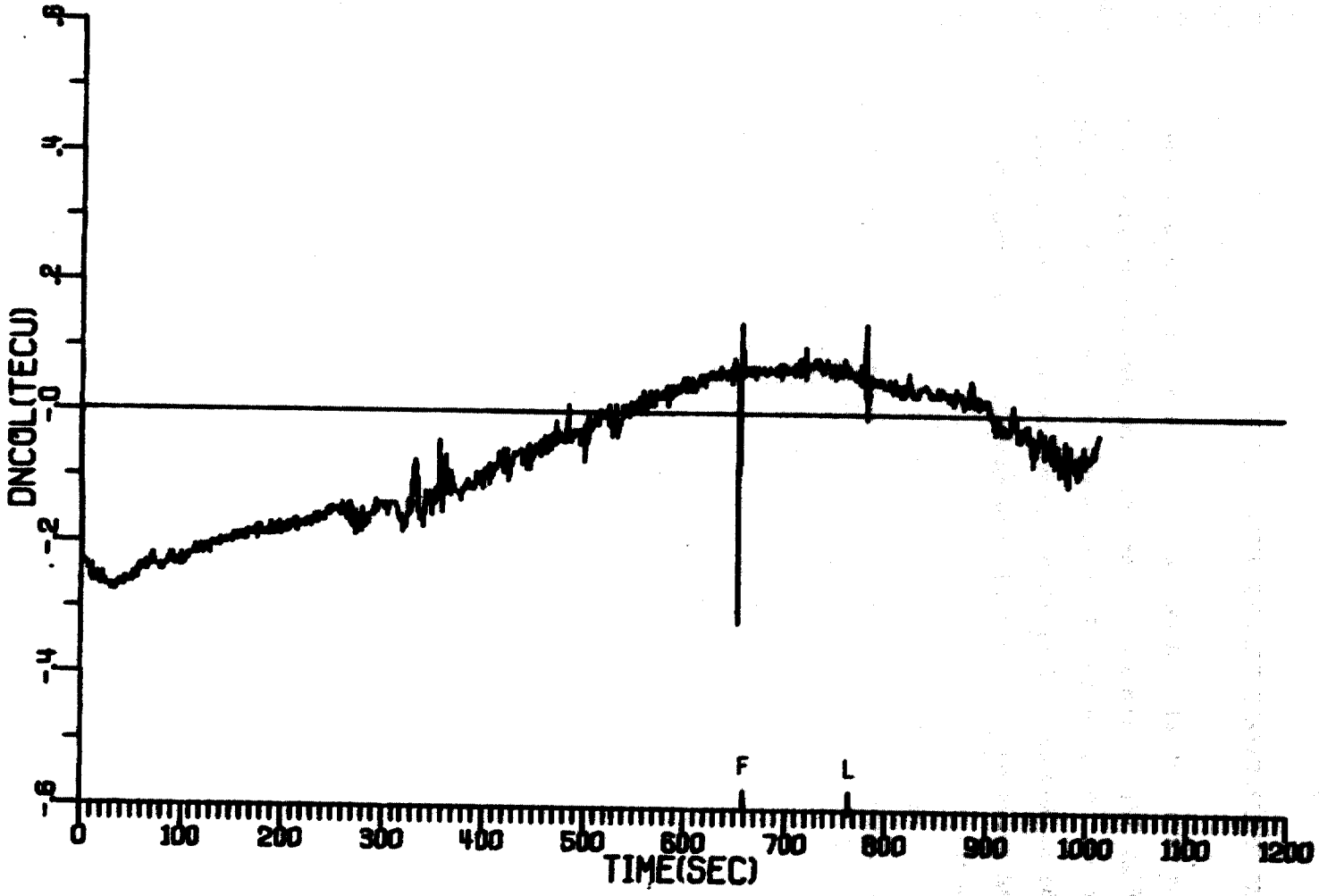

FIGURE 11

$\dot{N}_c$ DATA FROM LAS CRUCES, NEW MEXICO

3. Pass of Satellite 68, Day 109, 1102 UT

This pass was also observed at Loveland, CO. The geometry detailed in Fig. 12, is similar to the previous pass but at lower altitudes. Since the LOS is below the bottom of the F region, the effects should have been, and were, less than those observed on pass 2. One new phenomenon was observed, a deep amplitude null long before the LOS crossed the beam.

This phenomenon can be seen in Fig. 13 on the amplitude traces. At 11:08:12 there is a smooth null on the 150 MHz channel that is over 30 dB in depth and lasts about 35 sec. The dropout on 150 MHz just after this smooth null is due to the 400 MHz dropout. Although the pen on this recorder clogged just prior to beam encounter, it functioned reasonably well through the beam crossing, but the 150 MHz AGC had to be switched to another channel soon afterwards. The LOL on the 150 MHz channel at 11:12:14 was caused by the 400 MHz LOL.

The 400 MHz channel was noisy during the entire first (southern) half of the pass. As with the 150 MHz signal, this led to a total LOL twice, first at 11:08:23 and again at 11:08:40. Neither of these occurred at the same time as the 150 MHz dropout. These amplitude variations may be due to multipath interference from field aligned irregularities. The general geometry for this is correct; a mirror lined up with the B field at an altitude of 300 km over the heater would reflect the satellite signal down and to the west, i.e., toward the station. After passing to the north of the station, the reflected signal would be reflected into back space from such a mirror. The amplitude was much smoother after TCA, supporting this thesis; and the scallops prior to contact could be interpreted as a Lloyd's mirror phenomenon also supporting this idea. An alignment between the B field and the LOS does not appear to account for these dropouts, as the minimum angle between the two occurred at 11:11:10, 2 min after the first dropout. The angle was 16° at that time.

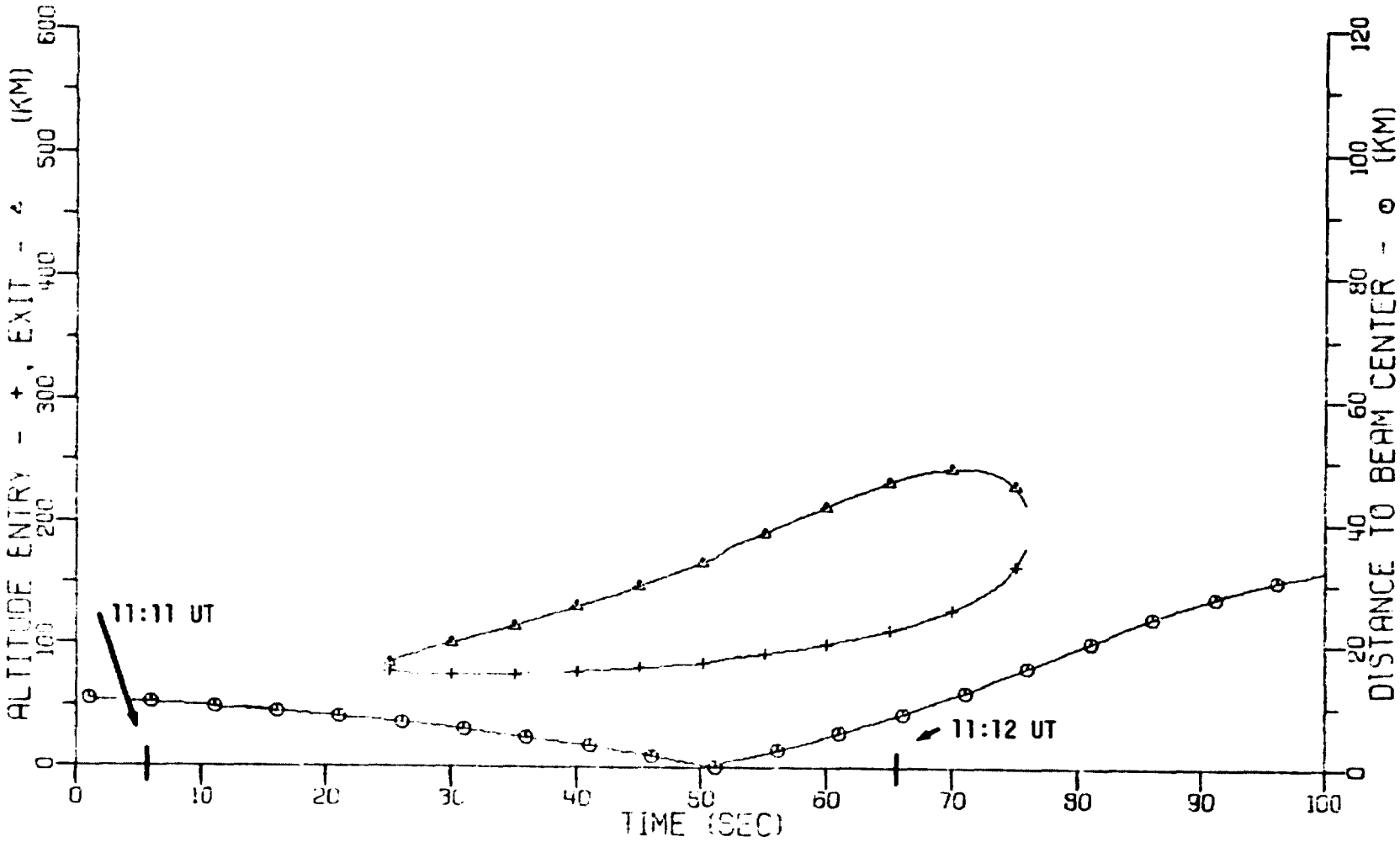

AE-81-28

FIGURE 12

HEATER - LINE OF SIGHT GEOMETRY

Satellite 68 Day 109 Zero Time 11:10:54 UT

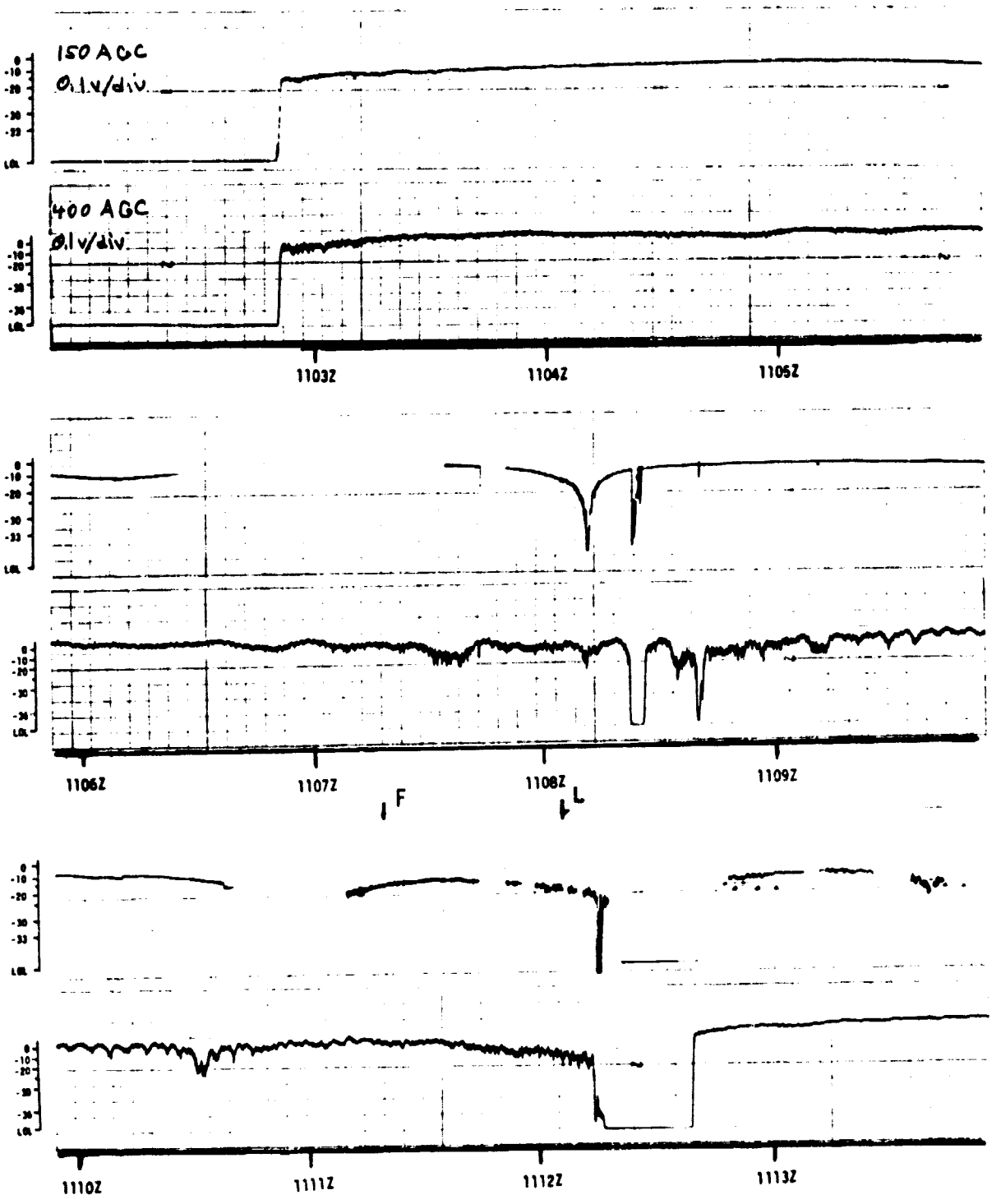

FIGURE 13

AMPLITUDE versus TIME OF NAVSAT PASS

Upper Trace 150 MHz Lower Trace 400 MHz

Day 109 Satellite 68 Rise 11:02 UT

Line of Sight Crosses Above Transmitter at 11:11:43 UT

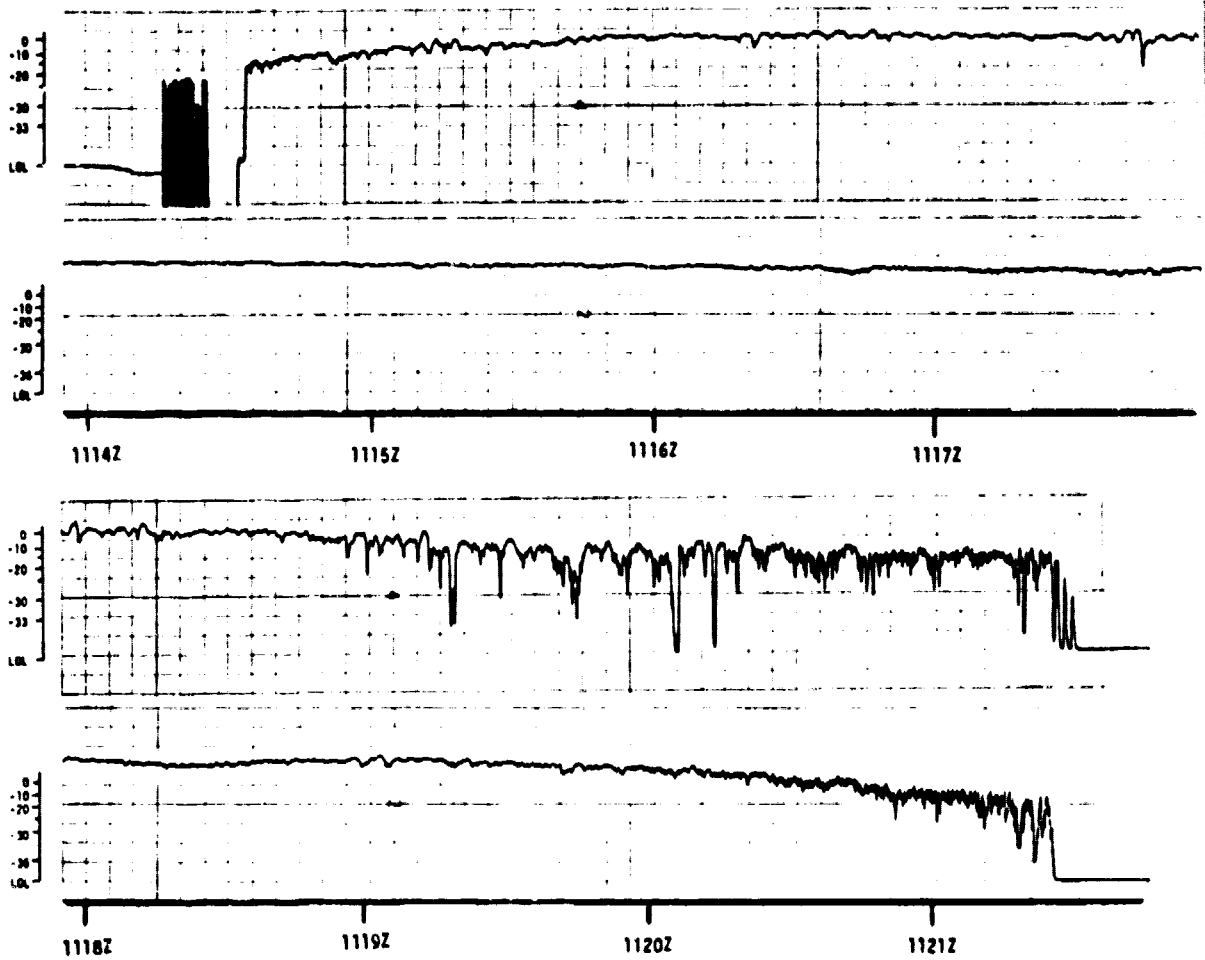

FIGURE 13 (cont'd)

AMPLITUDE versus TIME OF NAVSAT PASS

Upper Trace 150 MHz Lower Trace 400 MHz

Day 109 Satellite 68 Rise 11:02 UT

Line of Sight Crosses Above Transmitter at 11:11:43 UT

AE-81-29(b)

Both signals kept lock as the LOS passed through the beam. Just after this, at 11:12:14, the 400 MHz receiver lost lock almost at TCA, dropping out the 150 MHz with it. The elevation angle was 78° at the time of the dropout.

The paper tape data for this pass are shown in Fig. 14. There is little to note at this resolution concerning the data taken when the LOS was within the cone. This pass was recorded on the auxiliary tape system, and the high resolution phase data will be discussed later. There is no PSL data available for this pass.

4. Pass of Satellite 60, Day 112, 0656 UT

The geometry shown in Fig. 15 indicates that this pass just barely entered the ionosphere as the LOS passed through the beam. The LOS was most closely aligned with $\vec{B}$ at 7:04:10 when the angle was 21°.

The amplitude record in Fig. 16 shows several of the features of the previous passes. The 150 MHz signal had several Faraday nulls prior to beam encounter, a step attenuation within the beam, and some scintillations of about 10 dB on the end of the pass, which occurred to the north. The 150 MHz signal appears to be at a lower plateau 9 dB below the rest of the pass from first contact till 7:05:55. The 400 MHz signal was affected much more than the 150 MHz signal. Several 20 dB fades occurred from 1 min before first contact until 2 min after last contact. The 35 dB dip at 7:02:55 comes just prior to the B field LOS minimum angle.

The paper tape data (Fig. 17) are the only calibrated TEC measurements on this pass. There is a slowing down of $\dot{N}_c$ through the region of contact. If this is interpreted as a depletion, N_c will be only 0.05 TECU below the ambient level. This is consistent with previous heating passes and a major depletion within the beam given the low altitude involved. It is also consistent with a minor N_c variation along the LOS beyond the beam at a higher altitude.

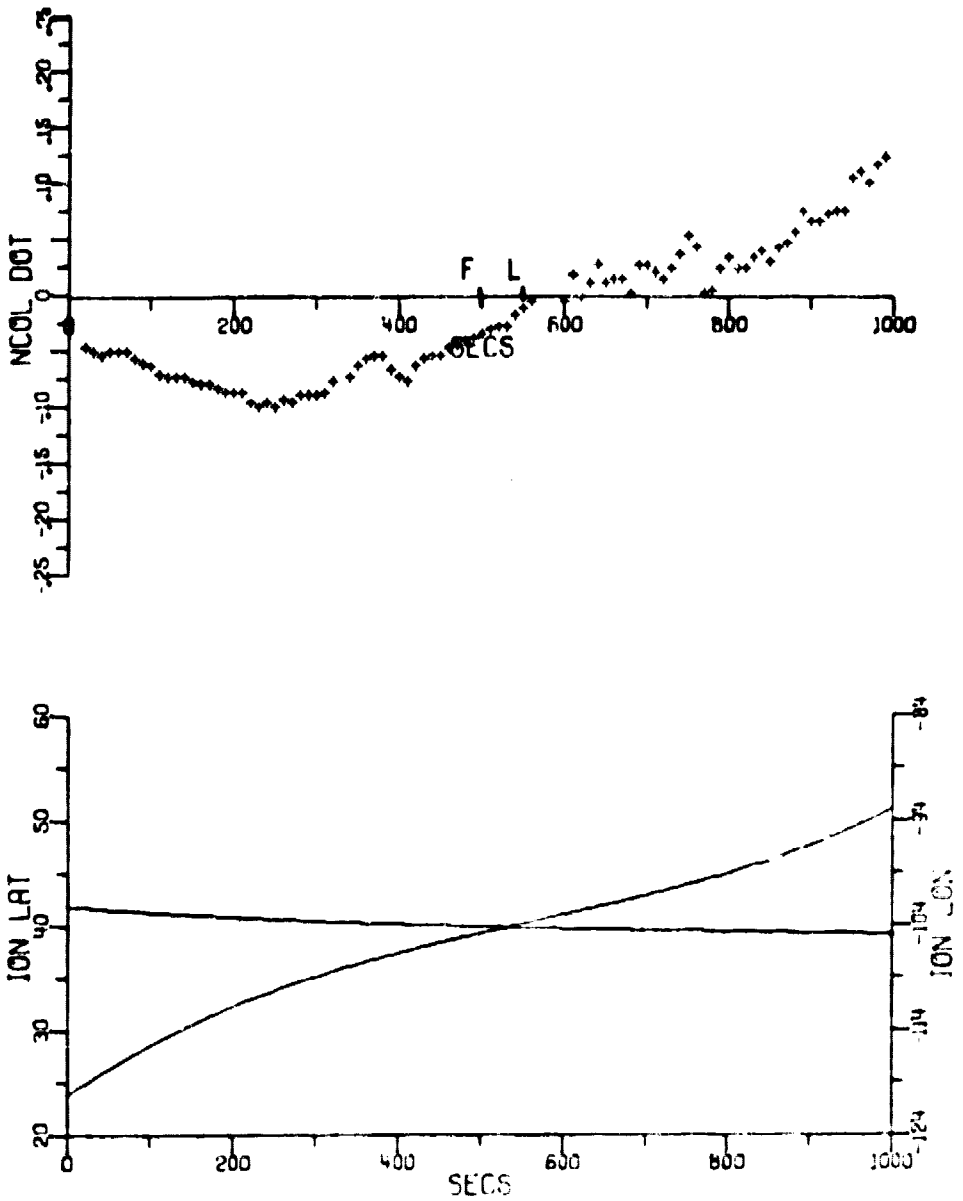

FIGURE 14

PAPER TAPE DATA OF N_c DOT

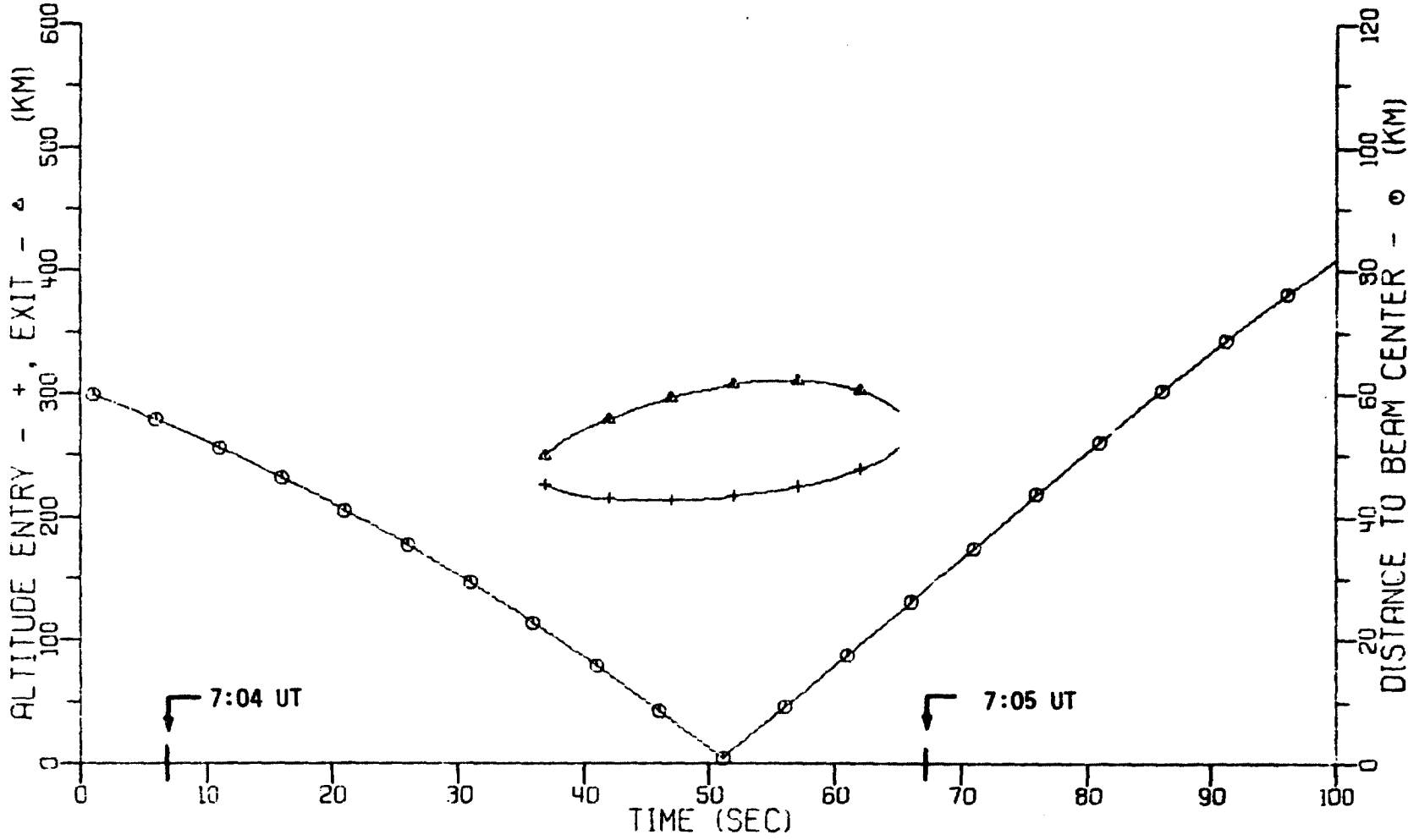

FIGURE 15

HEATER - LINE OF SIGHT GEOMETRY

Satellite 60 Day 112 Zero Time 7:03:53 UT

AE-81-31

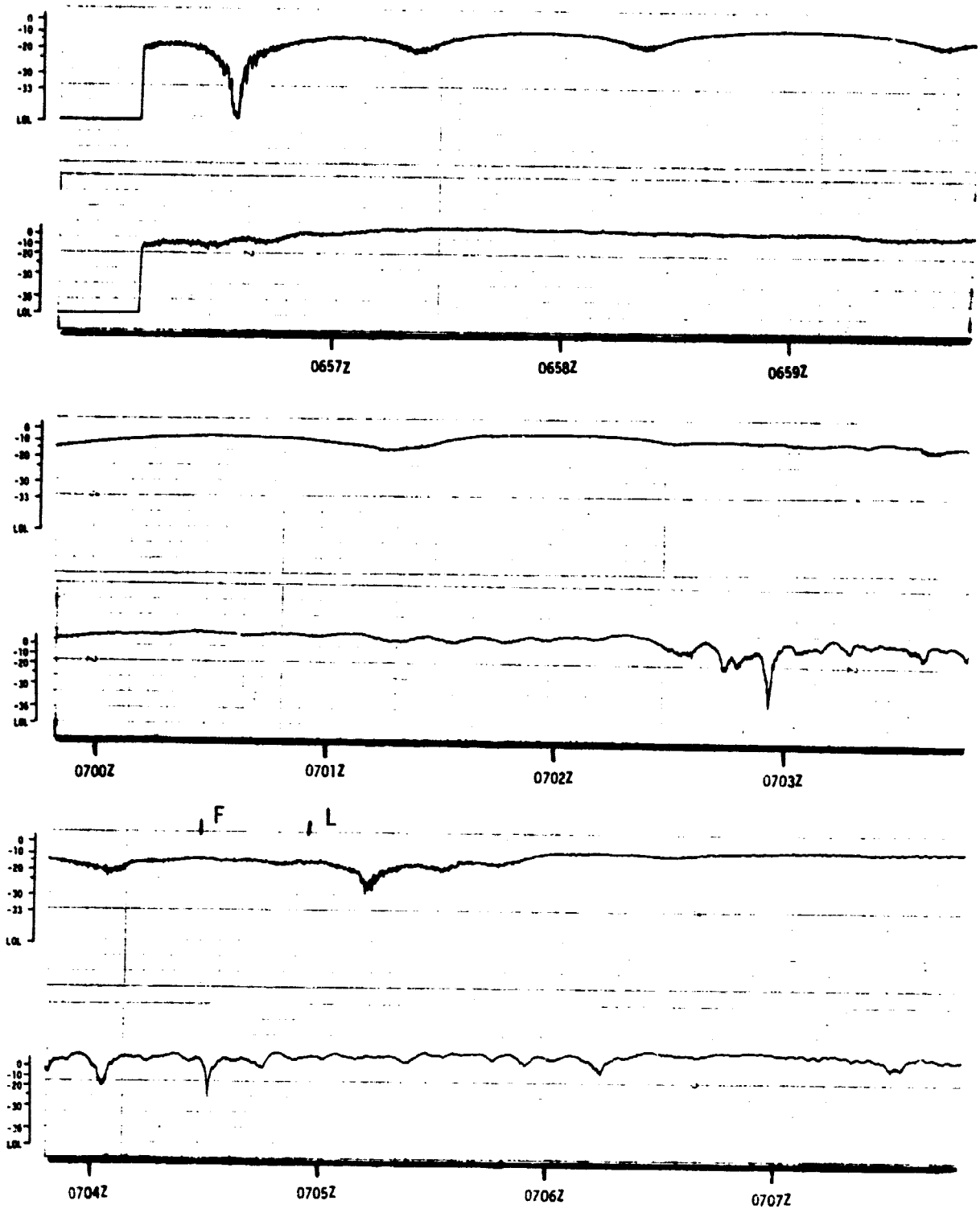

FIGURE 16

AMPLITUDE versus TIME OF NAVSAT PASS

Upper Trace 150 MHz Lower Trace 400 MHz

Day 112 Satellite 60 Rise 6:56 UT

Line of Sight Crosses Above Transmitter at 7:04:42 UT

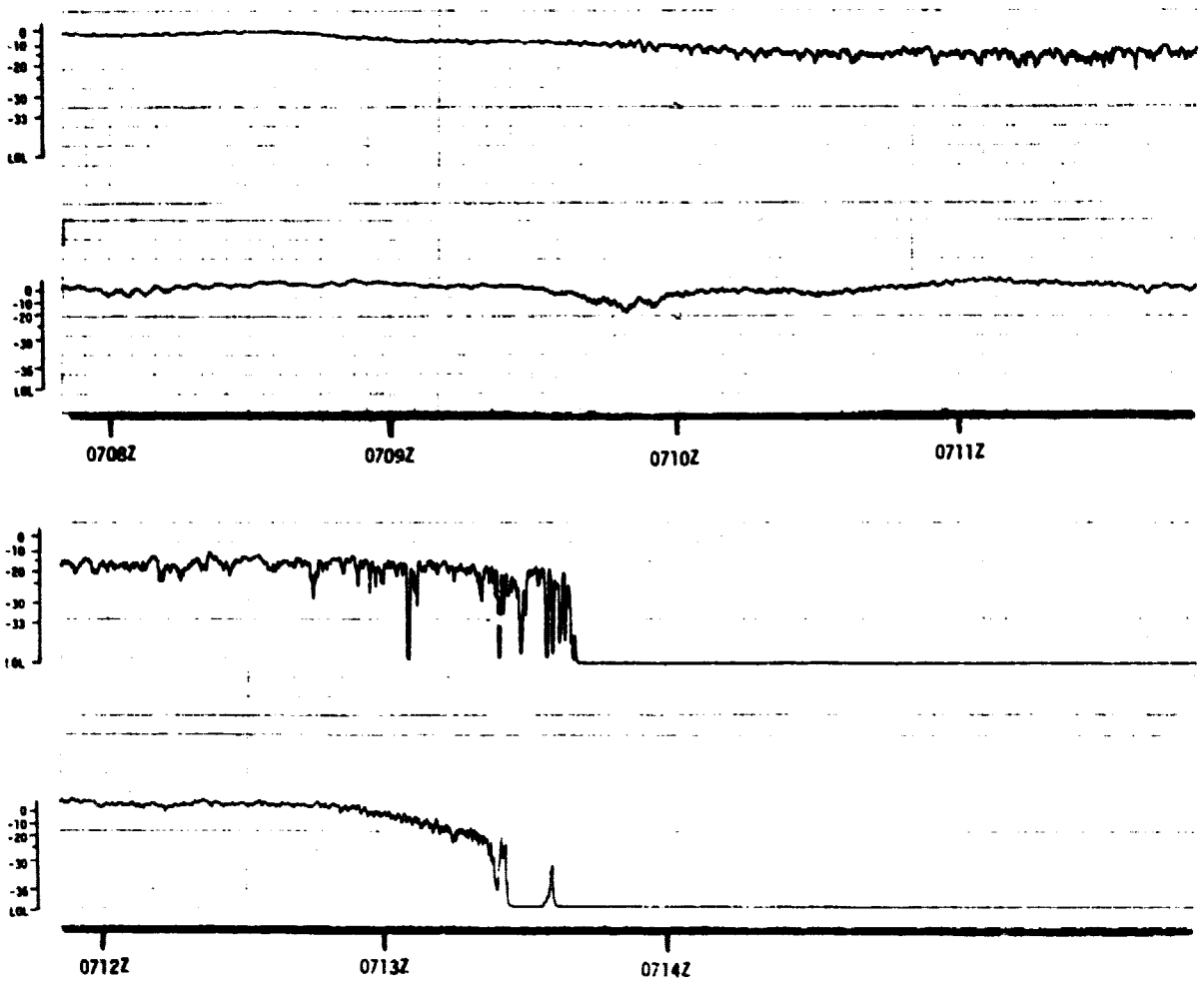

FIGURE 16 (cont'd)

AMPLITUDE versus TIME OF NAVSAT PASS

Upper Trace 150 MHz Lower Trace 400 MHz

Day 112 Satellite 60 Rise 6:56 UT

Line of Sight Crosses Above Transmitter at 7:04:42 UT

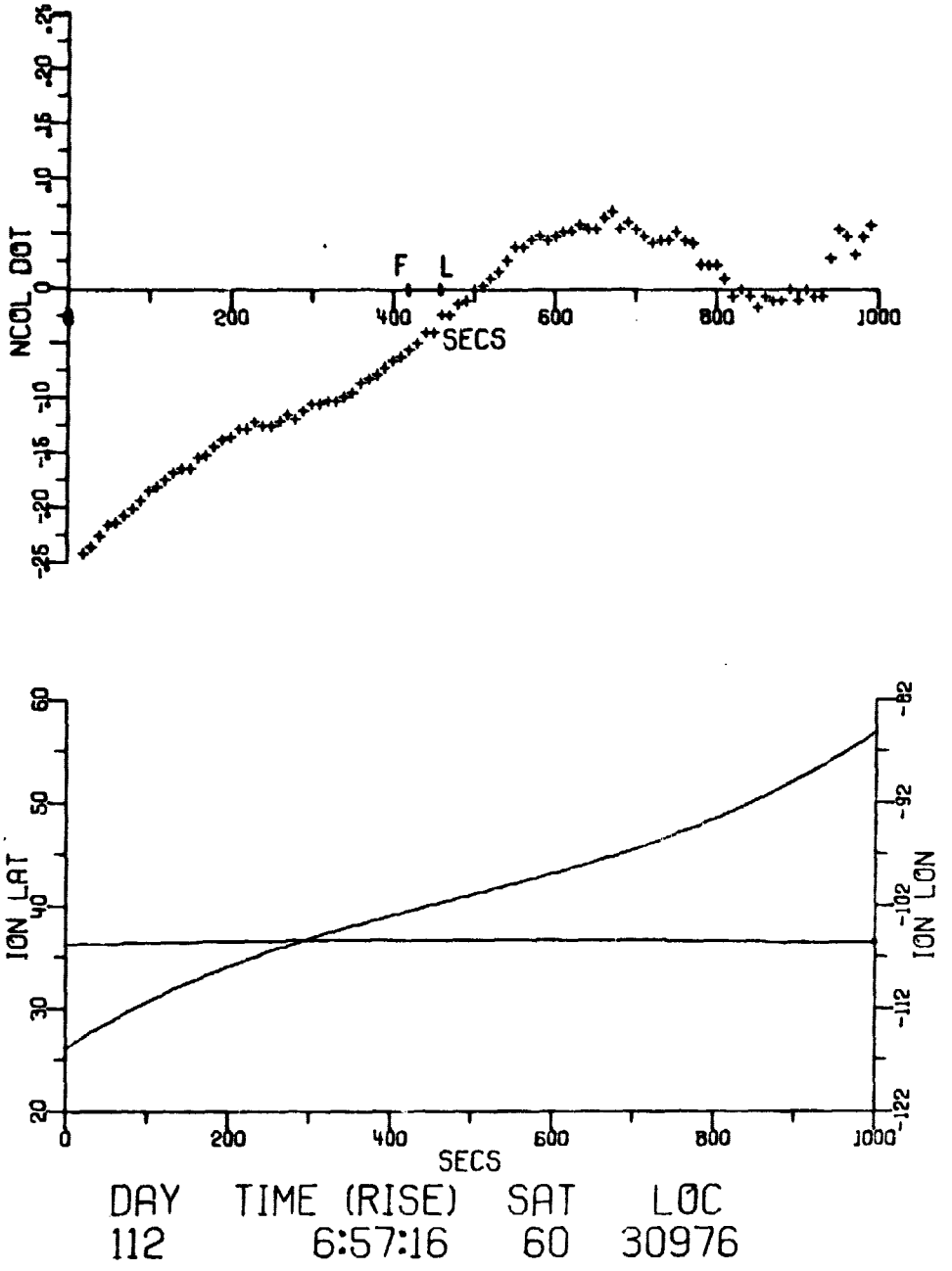

FIGURE 17

PAPER TAPE DATA OF N_c DOT

AE-81-33

5. Pass of Satellite 93, Day 113, 0357 UT

The LOS passed through the beam well into the ionosphere as shown in Fig. 18. The amplitudes (Fig. 19) did not vary greatly, although the Faraday null, which occurs within the beam, is broadened and more irregular than the previous ones. The paper tape data for the pass were taken at a 30 sec grain and are not shown. The Tranet II data, shown in Fig. 20, show no indication of the heating. As seen from PSL, this pass was slightly to the west and therefore away from Platteville. The spikes are typical of Tranet II data and indicate a short amplitude fluctuation.

6. Pass of Satellite 83, Day 113, 0556 UT

This and the next pass were taken without a preamplifier. The receiver maintained lock on both 162 MHz and 324 MHz through the beam crossing, which was at a low altitude and below the ionosphere. The geometry is given in Fig. 21 and amplitude data in Fig. 22. There is a LOL over 2 min after beam crossing; it is to the north and probably unrelated to the heating. The paper tape data (Fig. 23) show only a slight irregularity in the region of beam crossing.

7. Pass of Satellite 83, Day 114, 0541 UT

This pass south to north was also made without a preamplifier. In this case, the LOS passed through the beam high in the ionosphere (see Fig. 24). The amplitude charts (Fig. 25) show a sharp null on 162 MHz just after beam crossing that probably was associated with the heater beam. The paper tape data (Fig. 26) show several small variations including a small jump in $\dot{N}_c$ at first contact.

The lack of large fluctuations on 324 MHz is probably the most significant fact about the last two passes. Even without a preamplifier, these passes crossed the beam in the ionosphere with little trouble.

FIGURE 18

HEATER - LINE OF SIGHT GEOMETRY

Satellite 93 Day 113 Zero Time 4:05:35 UT

AE-81-

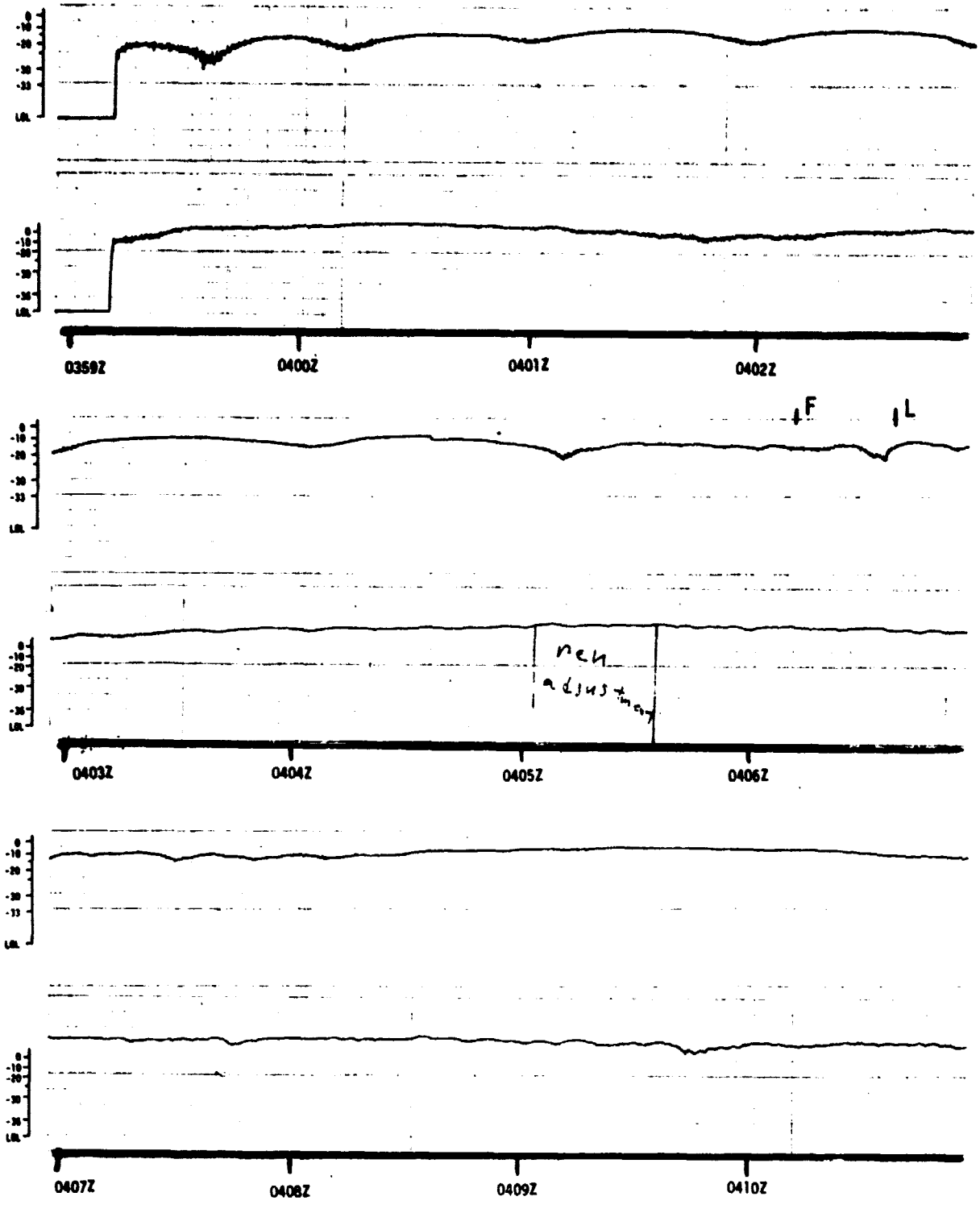

FIGURE 19

AMPLITUDE versus TIME OF NAVSAT PASS

Upper Trace 150 MHz Lower Trace 400 MHz

Day 113 Satellite 93 Rise 3:57 UT

Line of Sight Crosses Above Transmitter at 4:06:24 UT

AE-81-35(a)

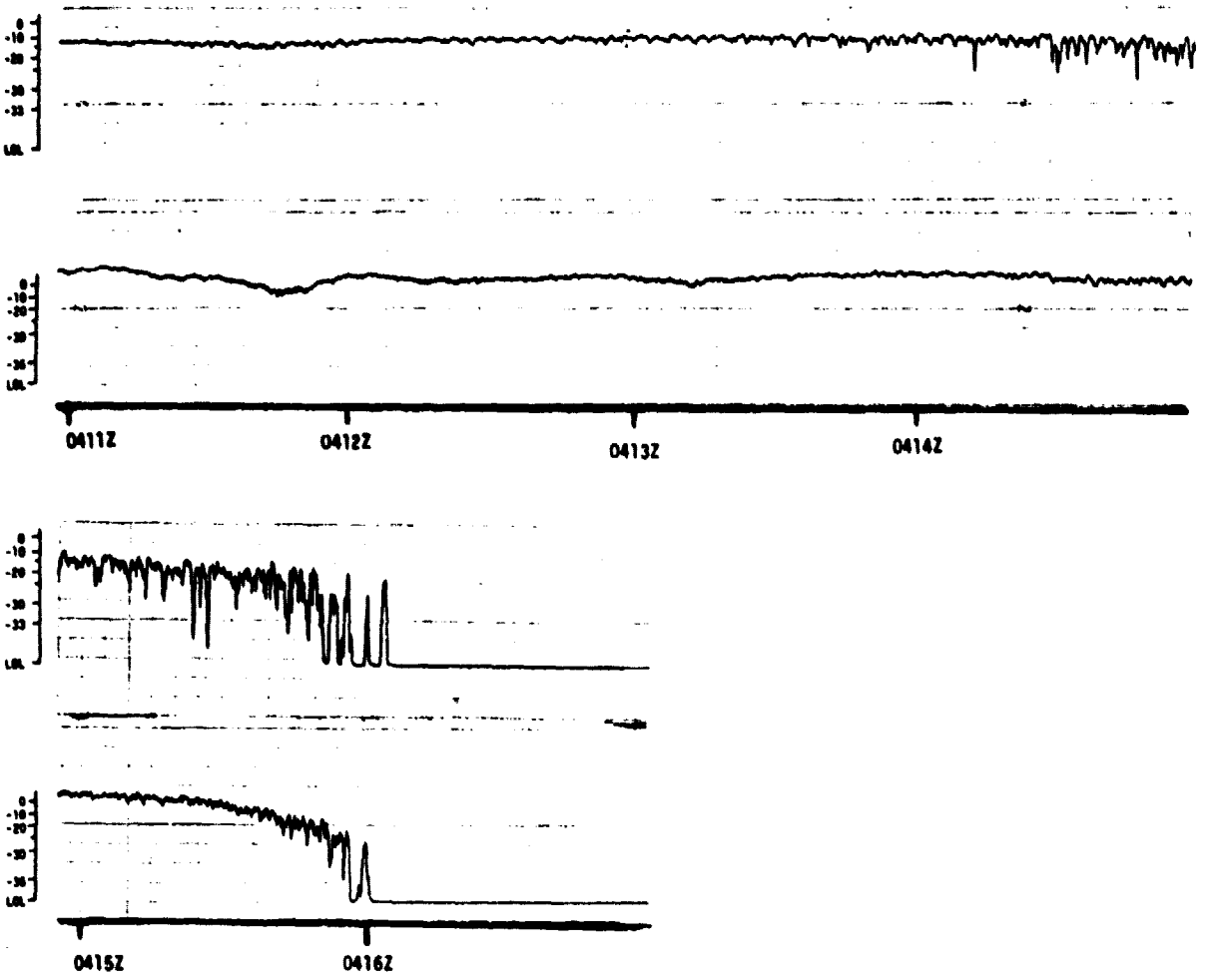

FIGURE 19 (cont'd)

AMPLITUDE versus TIME OF NAVSAT PASS

Upper Trace 150 MHz Lower Trace 400 MHz

Day 113 Satellite 93 Rise 3:57 UT

Line of Sight Crosses Above Transmitter at 4:06:24 UT

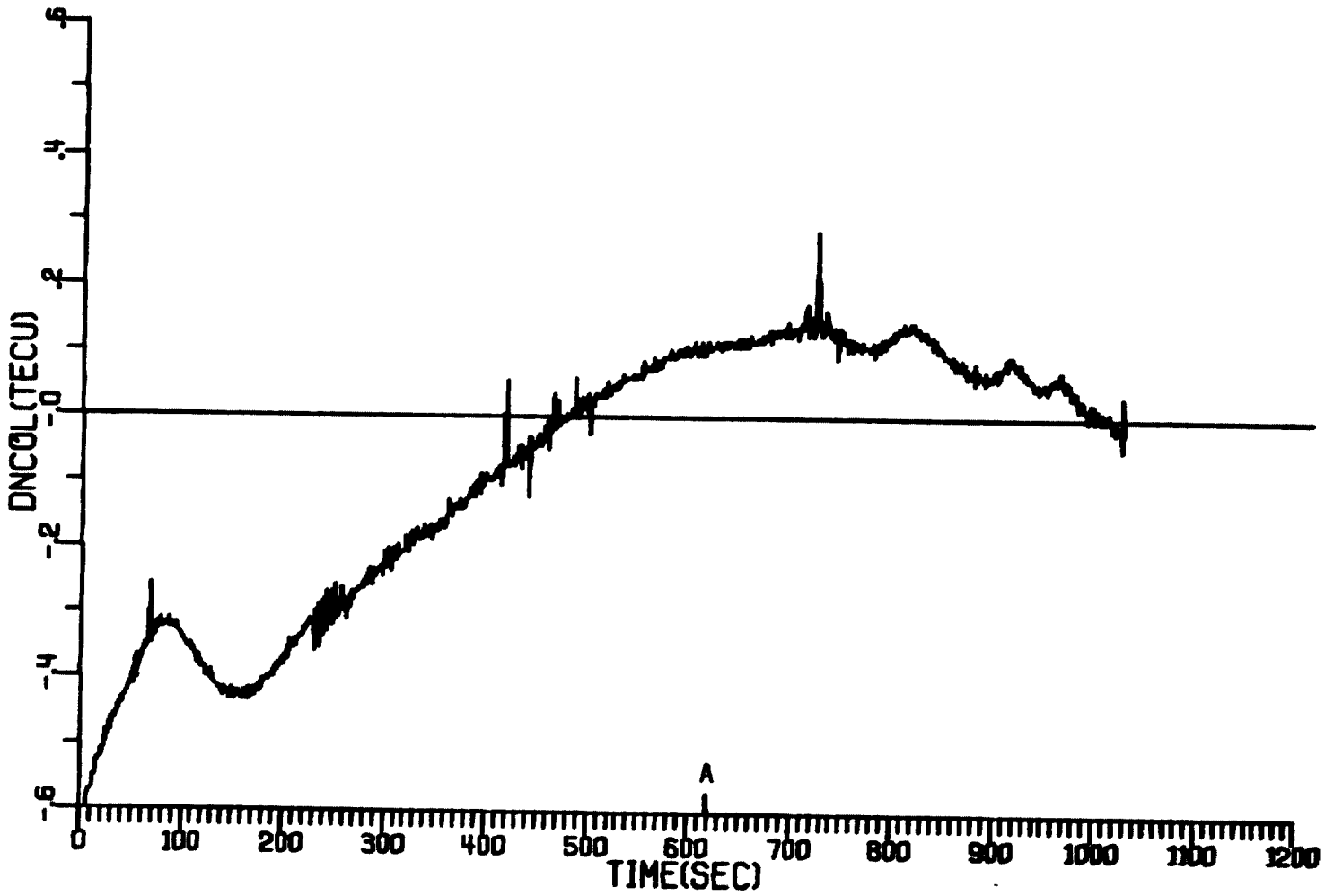

UT 3:56:41, DAY 113, YR 1980, STA 513, SAT 93

FIGURE 20

$\dot{N}_c$ DATA FROM LAS CRUCES, NEW MEXICO

FIGURE 21

HEATER - LINE OF SIGHT GEOMETRY

AE-81-37

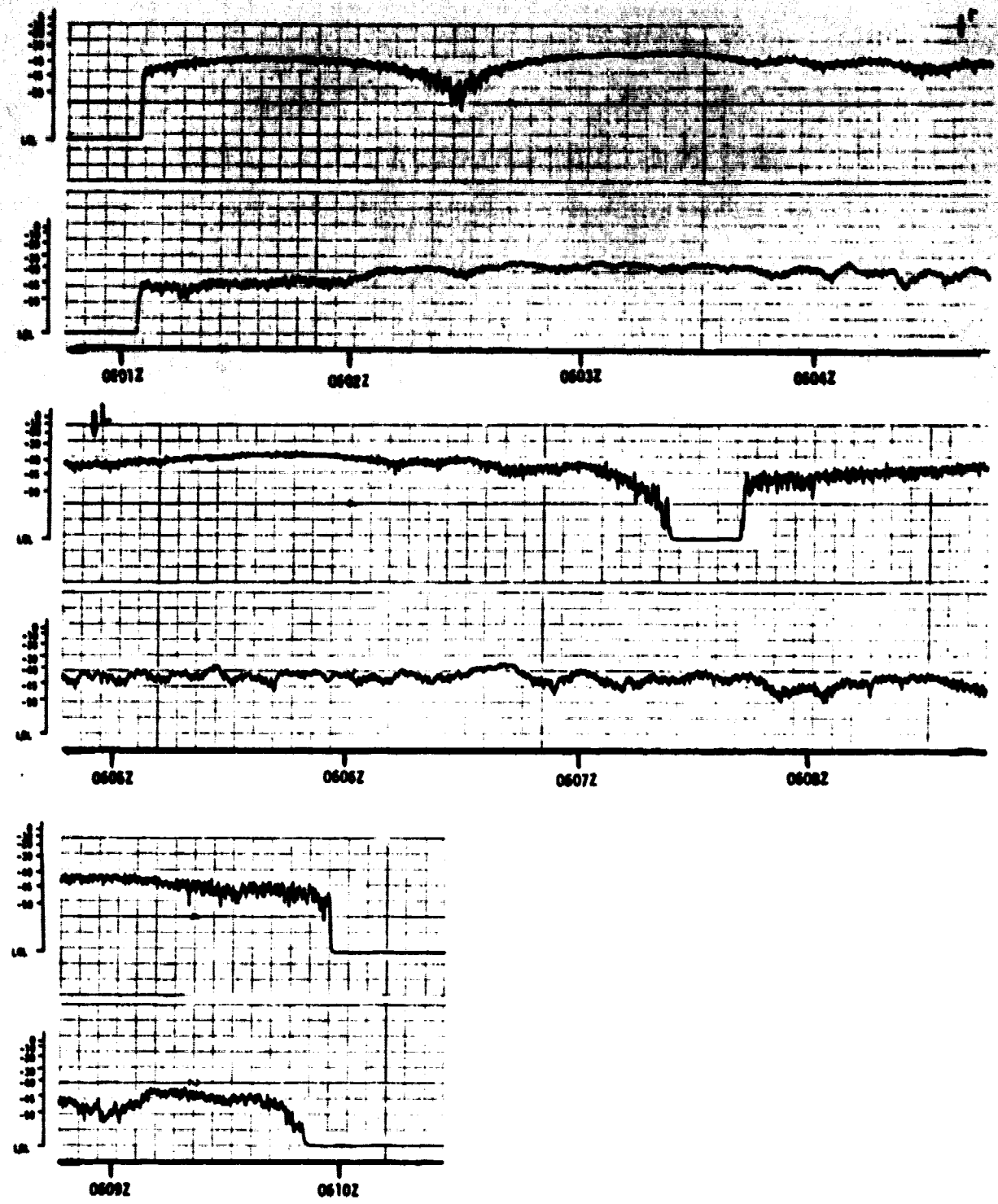

FIGURE 22

AMPLITUDE versus TIME OF NAVSAT PASS

Upper Trace 162 MHz Lower Trace 324 MHz

Day 113 Satellite 83 Rise 5:56 UT

Line of Sight Crosses Above Transmitter at 6:04:49 UT

AE-81-38

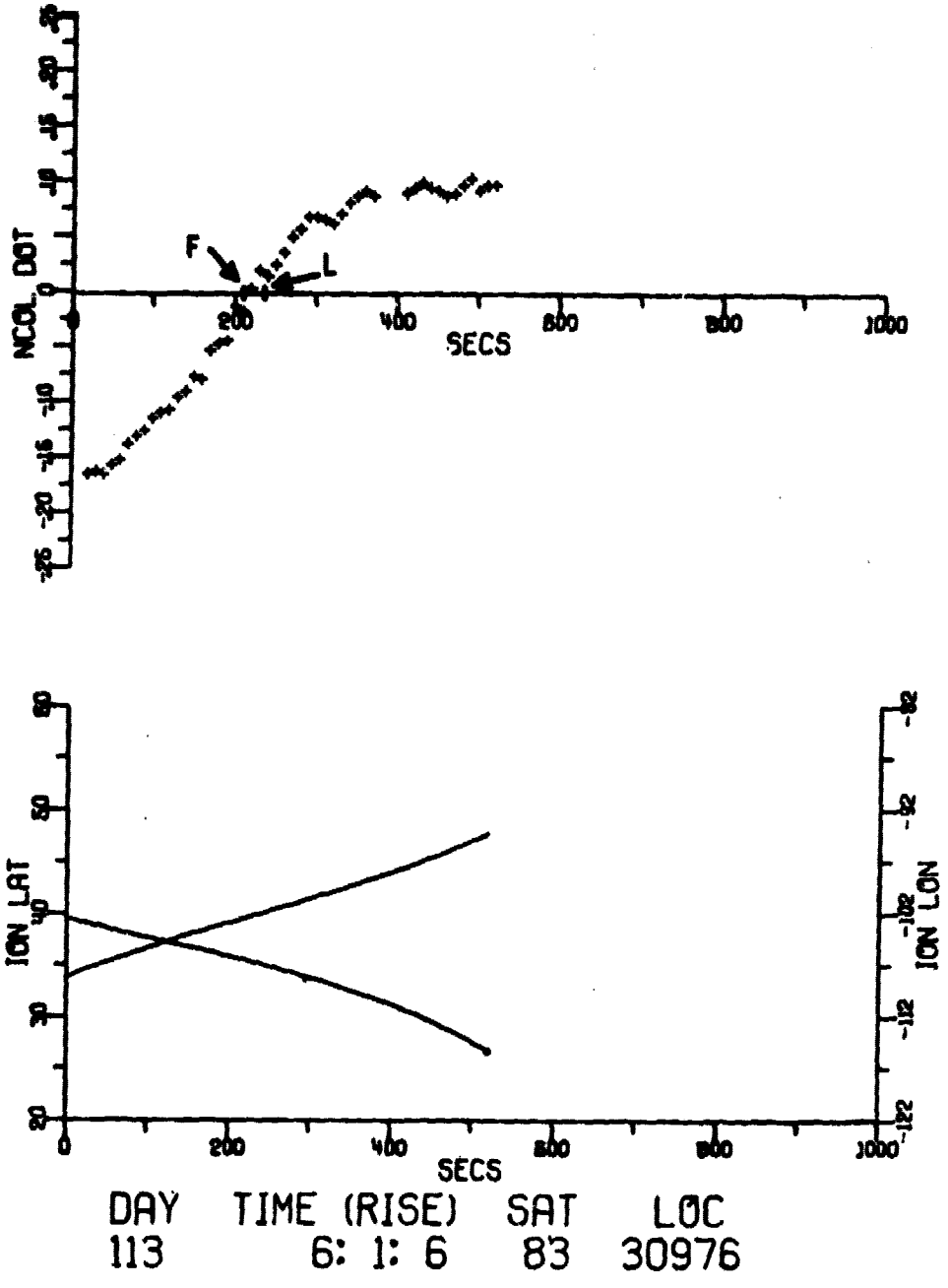

FIGURE 23

PAPER TAPE DATA OF N_c DOT

FIGURE 24

HEATER - LINE OF SIGHT GEOMETRY

Satellite 83 Day 114 Zero Time 5:49:04 UT

AE-81-40

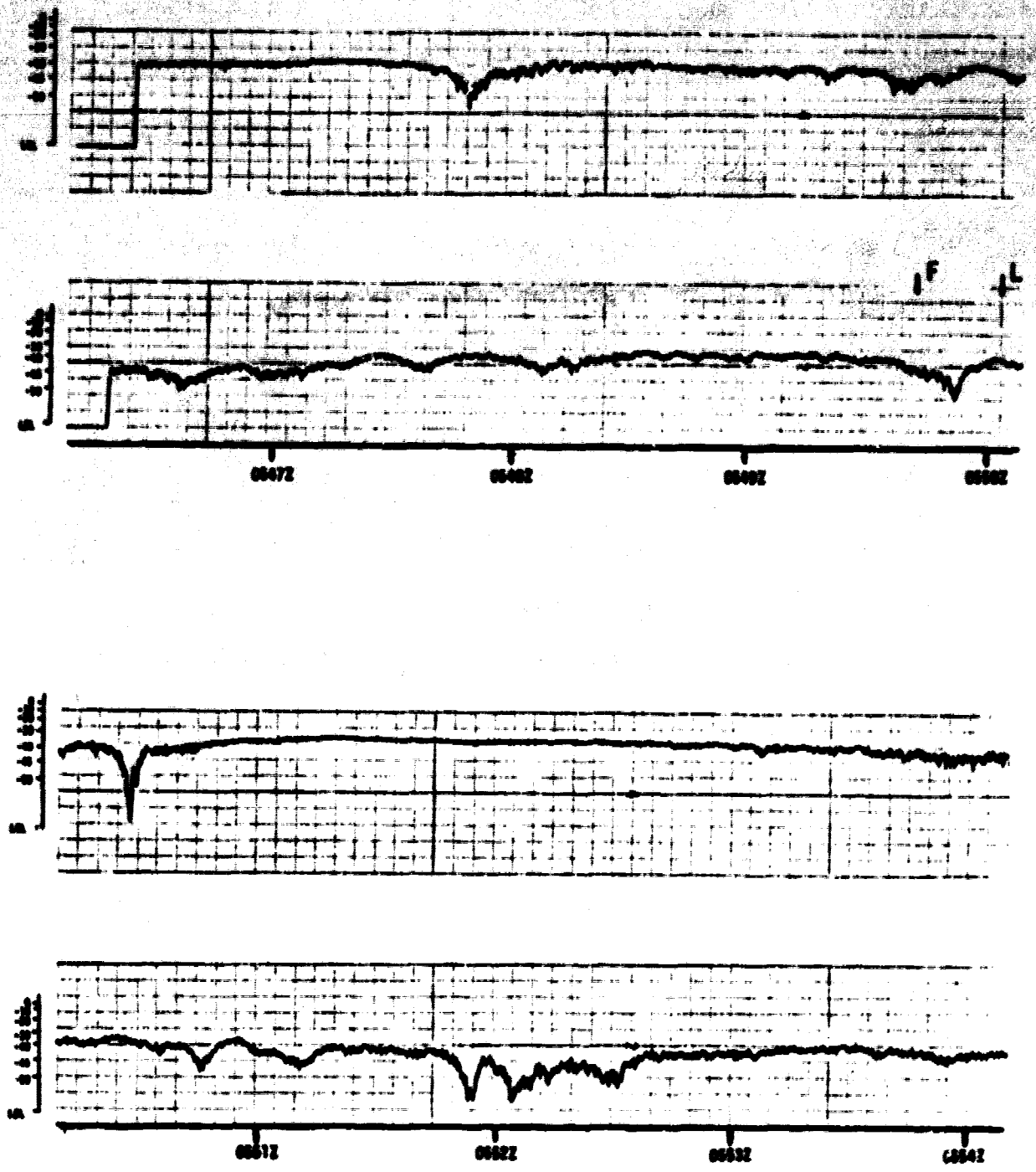

FIGURE 25

AMPLITUDE versus TIME OF NAVSAT PASS

Upper Trace 162 MHz Lower Trace 324 MHz

Day 114 Satellite 83 Rise 5:41 UT

Line of Sight Crosses Above Transmitter at 5:49:54 UT

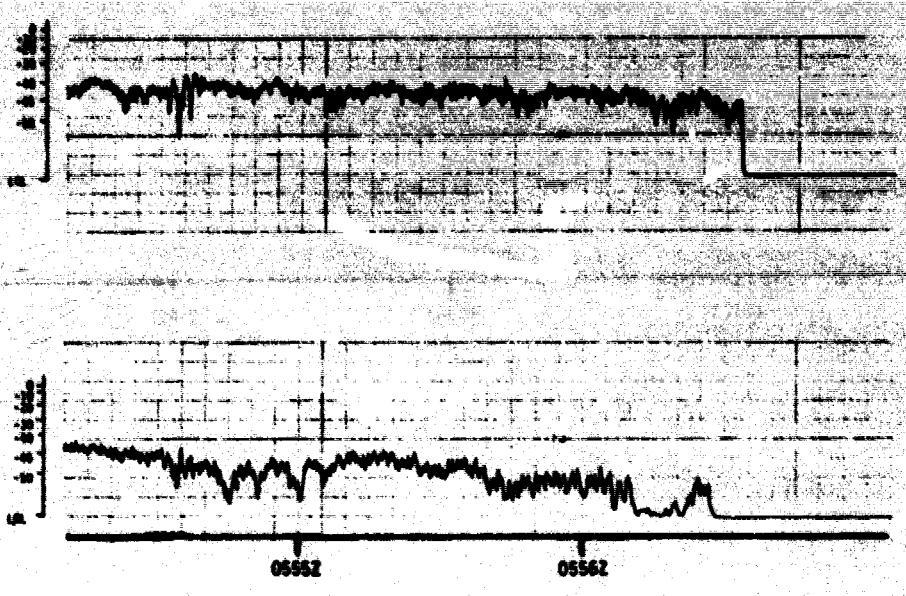

FIGURE 25 (cont'd)

AMPLITUDE versus TIME OF NAVSAT PASS

Upper Trace 162 MHz Lower Trace 324 MHz

Day 114 Satellite 83 Rise 5:41 UT

Line of Sight Crosses Above Transmitter at 5:49:54 UT

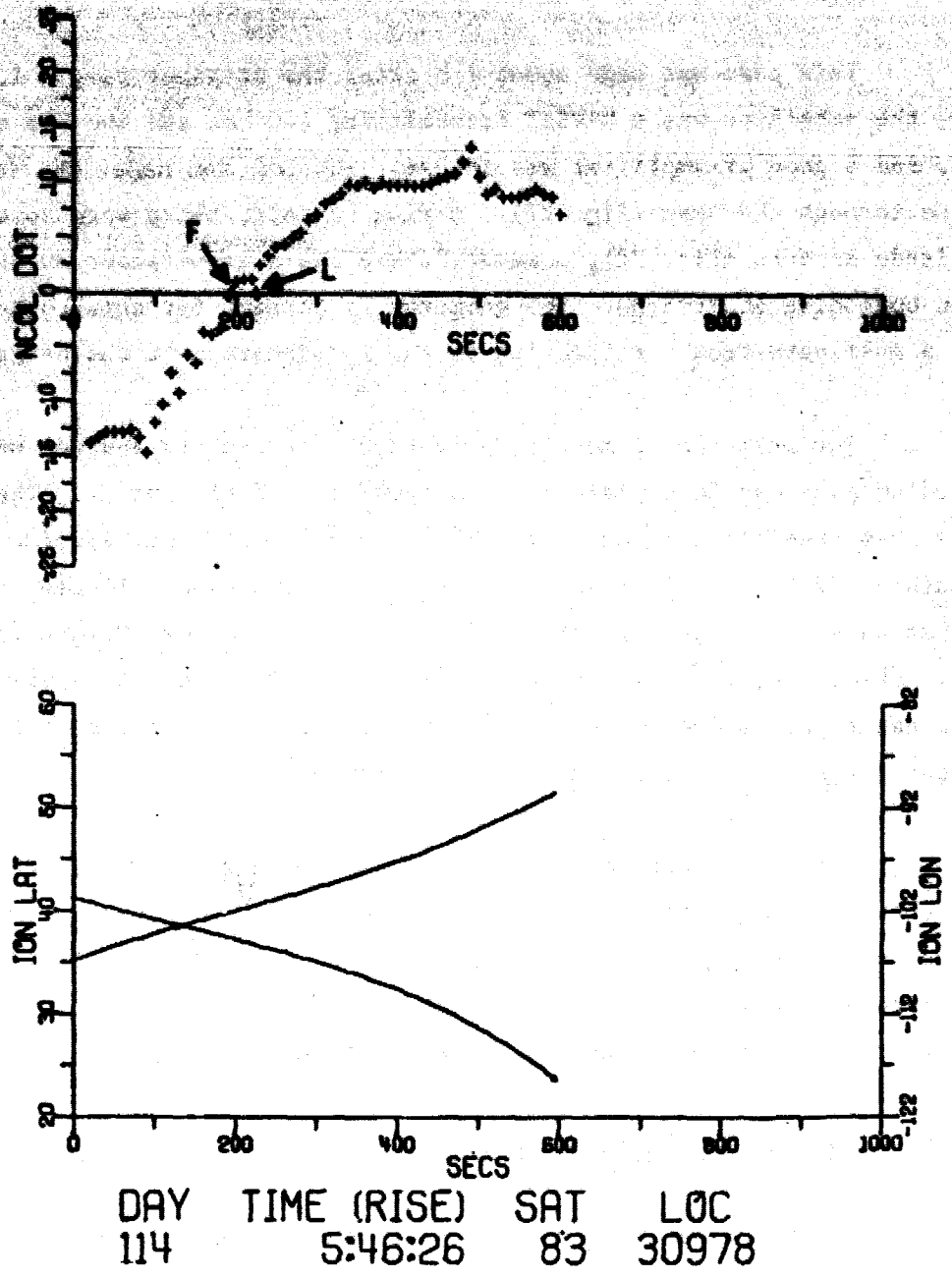

FIGURE 26

PAPER TAPE DATA OF N_c DOT

8. Pass of Satellite 60, Day 114, 0658 UT

This pass was made about 1 h after the previous pass. In this case, the satellite was a NAVSAT transmitting 150 MHz and 400 MHz signals, and a good preamplifier was in use. The LOS ran under the ionosphere through the beam (Fig. 27). During contact, there were no major amplitude effects (Fig. 28); however, there was a significant 30 dB variation beginning at 7:05:30. The geometry is correct for this to have been a multipath from a reflection in the ionosphere over the heater.

The presence of multipath on this pass and its absence on the preceding pass can be explained by the geometry of the passes. The previous pass rose at an azimuth of 146° and moved northwest, setting at an azimuth of 324°. A mirror above Platteville would have reflected signals of that pass to the west prior to TCA and not toward Fort Morgan in the east. After TCA, the signals would have been reflected into space. In the present pass (rise azimuth 190°, set azimuth 355°), the heater was between the satellite and the receiver throughout.

The paper tape data (Fig. 29) show considerable turbulence after TCA, when the satellite was in the north, but no significant variations during beam crossing. The Tranet II LOS did not cross the beam as the satellite was west of the station. The satellite was due west of the heater at the time marked on the Tranet II data in Fig. 30.

9. Pass of Satellite 83, Day 115, 0526 UT

The LOS from this pass went through the beam below the ionosphere (Fig. 31). The pass rose at an azimuth of 137° and set at 327° prior to TCA. Thus it had a favorable geometry for multipath interference. However, the amplitude records (Fig. 32) show no evidence of multipath. The strip charts are the only available data on this pass.

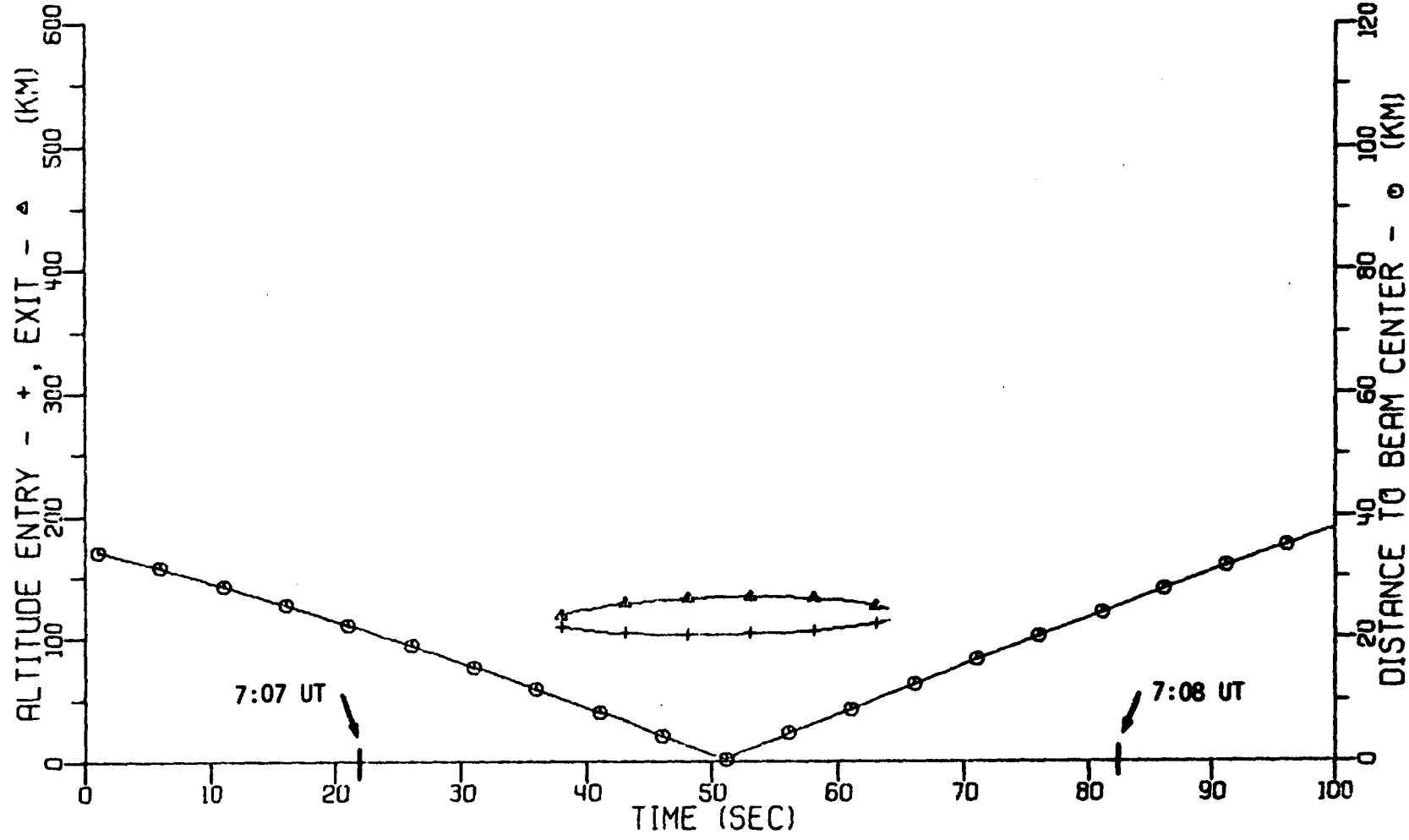

FIGURE 27

HEATER - LINE OF SIGHT GEOMETRY

Satellite 60 Day 114 Zero Time 7:06:37 UT

AE-81-43

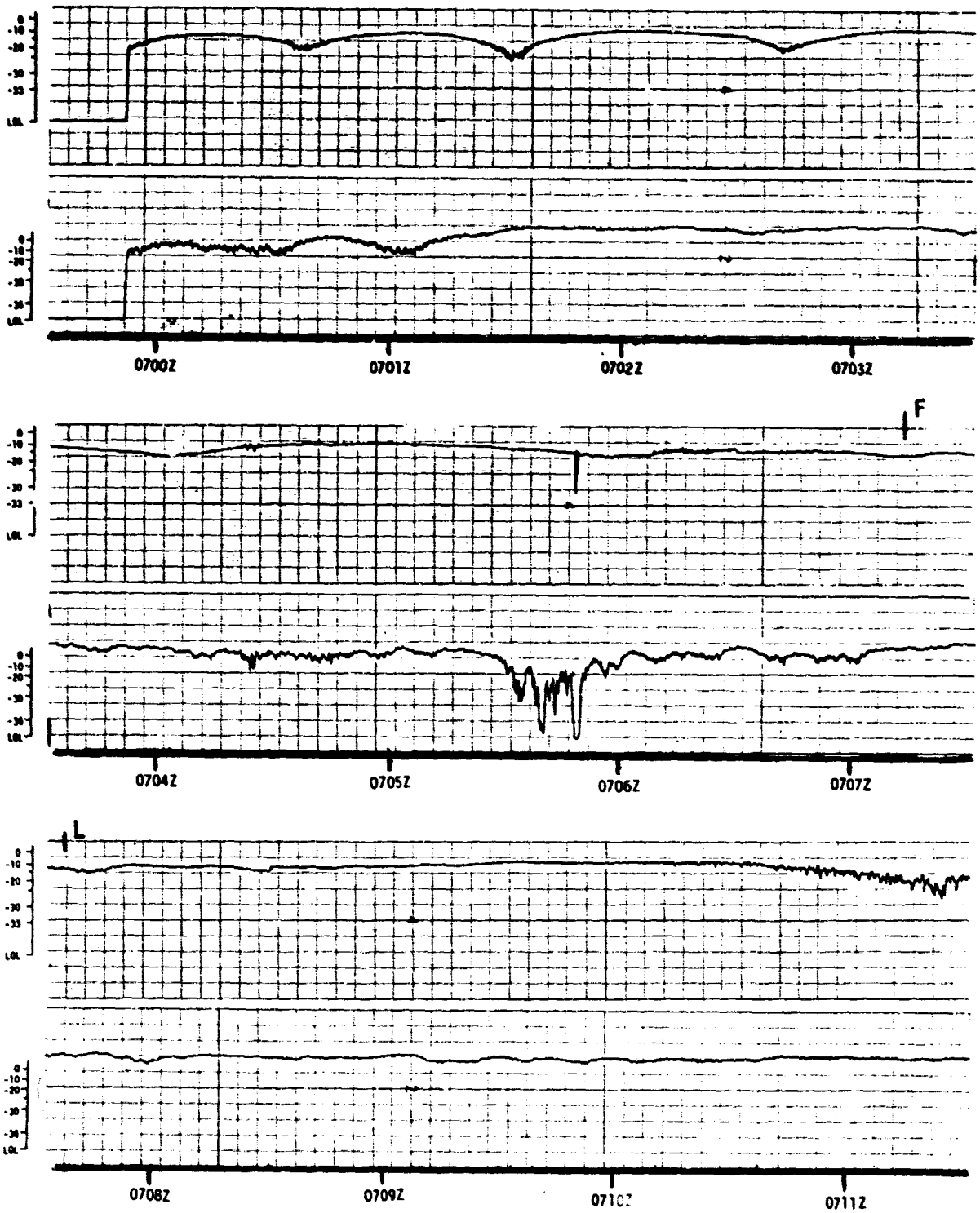

FIGURE 28

AMPLITUDE versus TIME OF NAVSAT PASS

Upper Trace 150 MHz Lower Trace 400 MHz

Day 114 Satellite 60 Rise 6:58 UT

Line of Sight Crosses Above Transmitter at 7:07:25 UT AE-81-44(a)

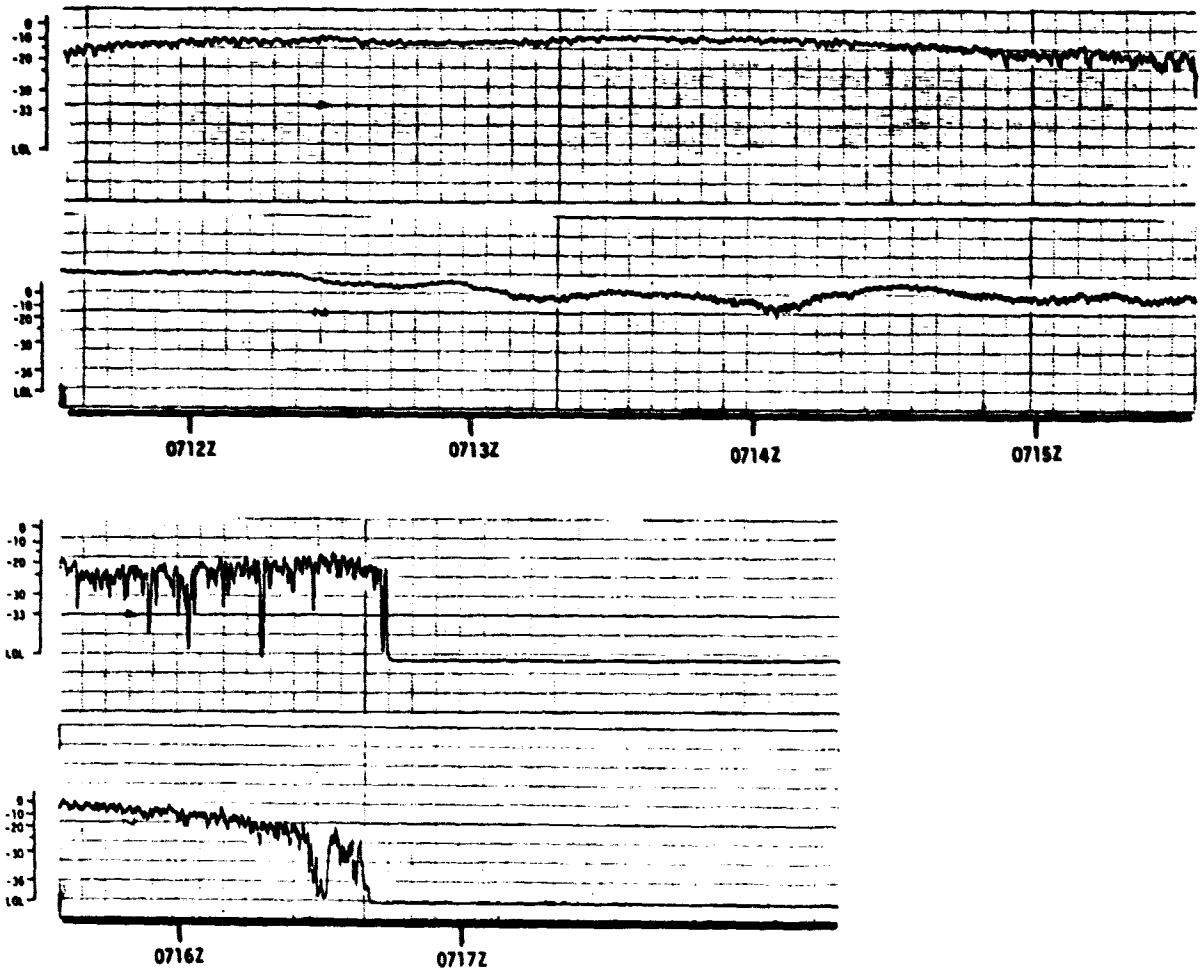

FIGURE 28 (cont'd)

AMPLITUDE versus TIME OF NAVSAT PASS

Upper Trace 150 MHz Lower Trace 400 MHz

Day 114 Satellite 60 Rise 6:58 UT

Line of Sight Crosses Above Transmitter at 7:07:25 UT

AE-81-44(b)

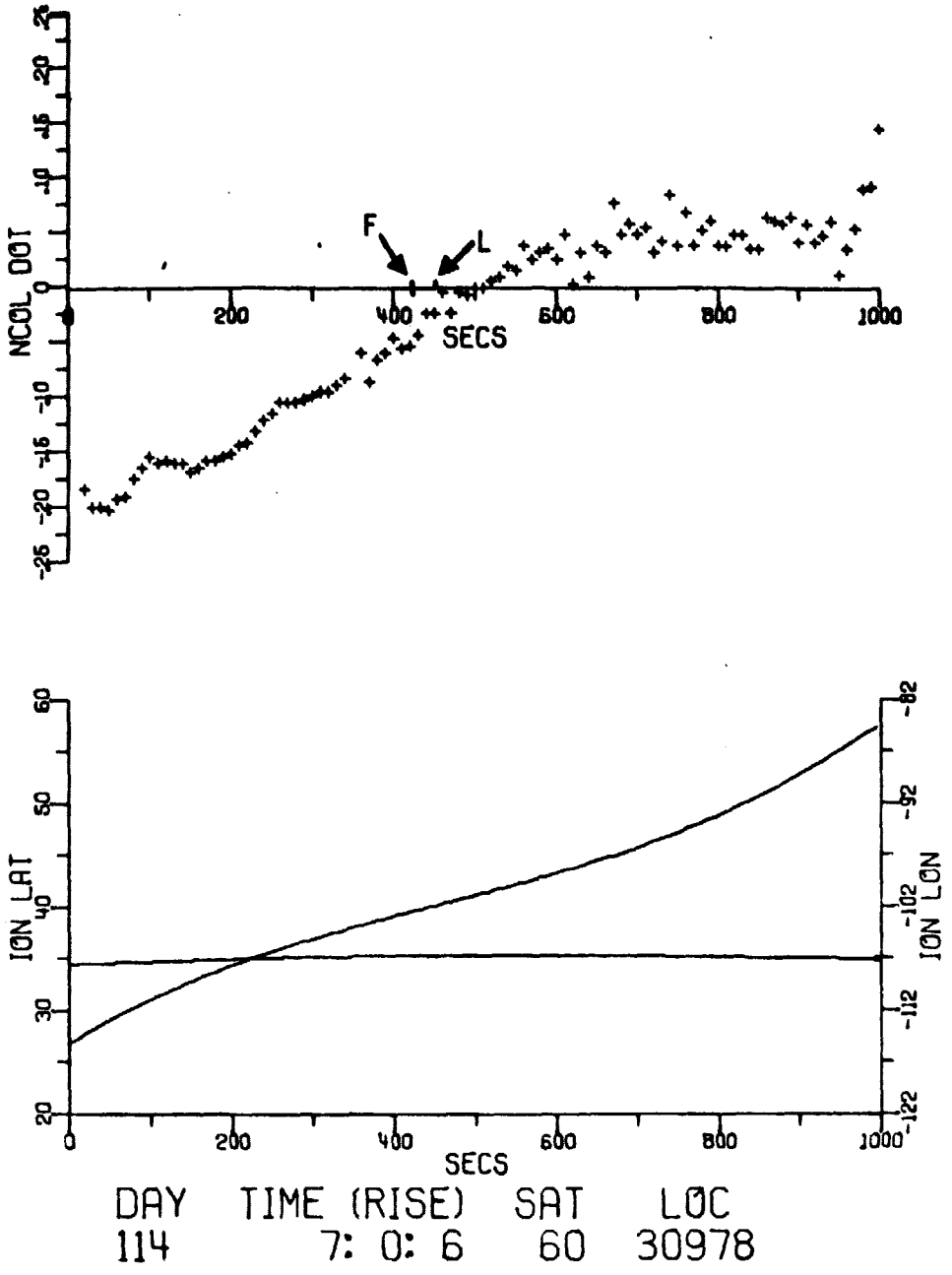

FIGURE 29

PAPER TAPE DATA OF N_c DOT

AE-81-45

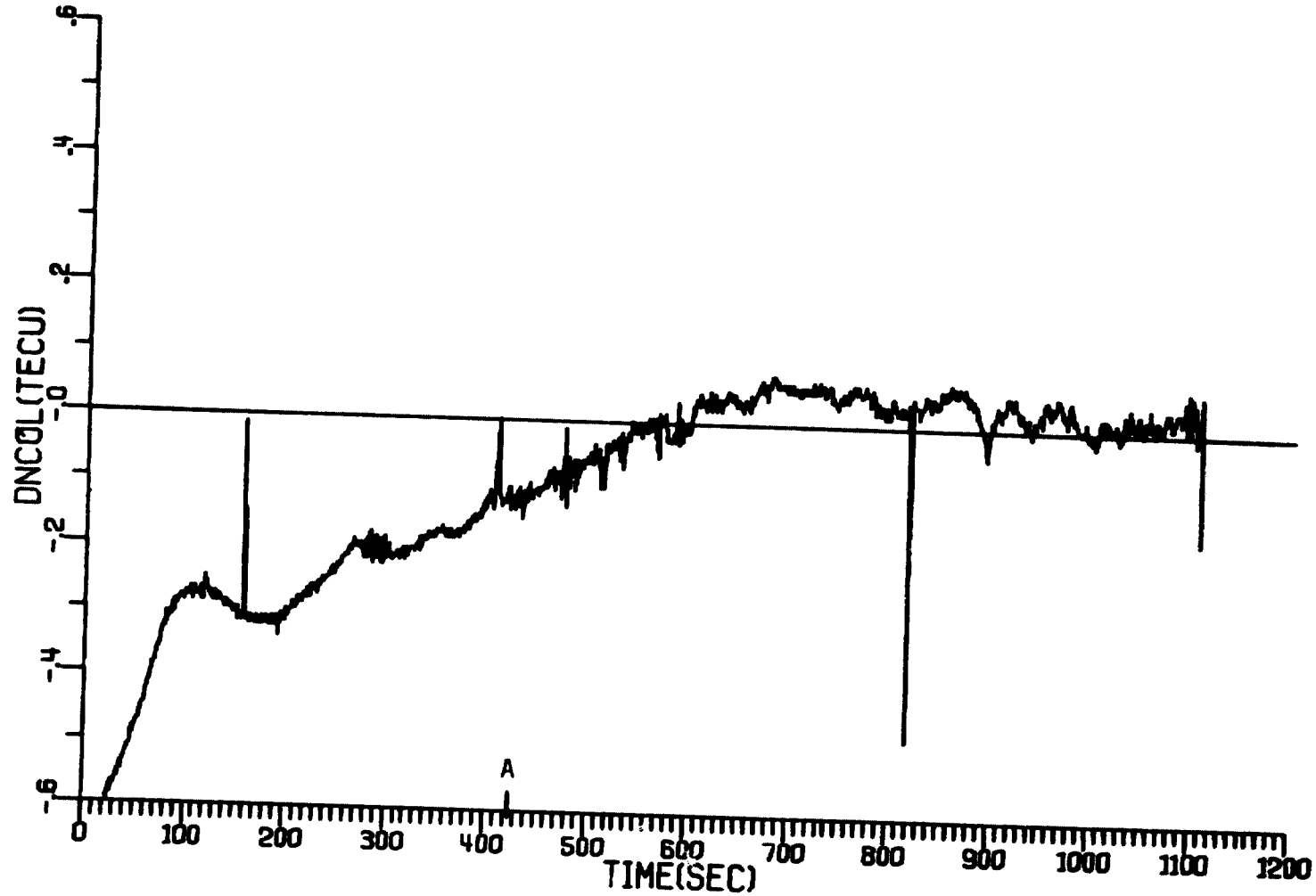

UT 6:56:17, DAY 114, YR 1980, STA 513, SAT 60

FIGURE 30

$\dot{N}_c$ DATA FROM LAS CRUCES, NEW MEXICO

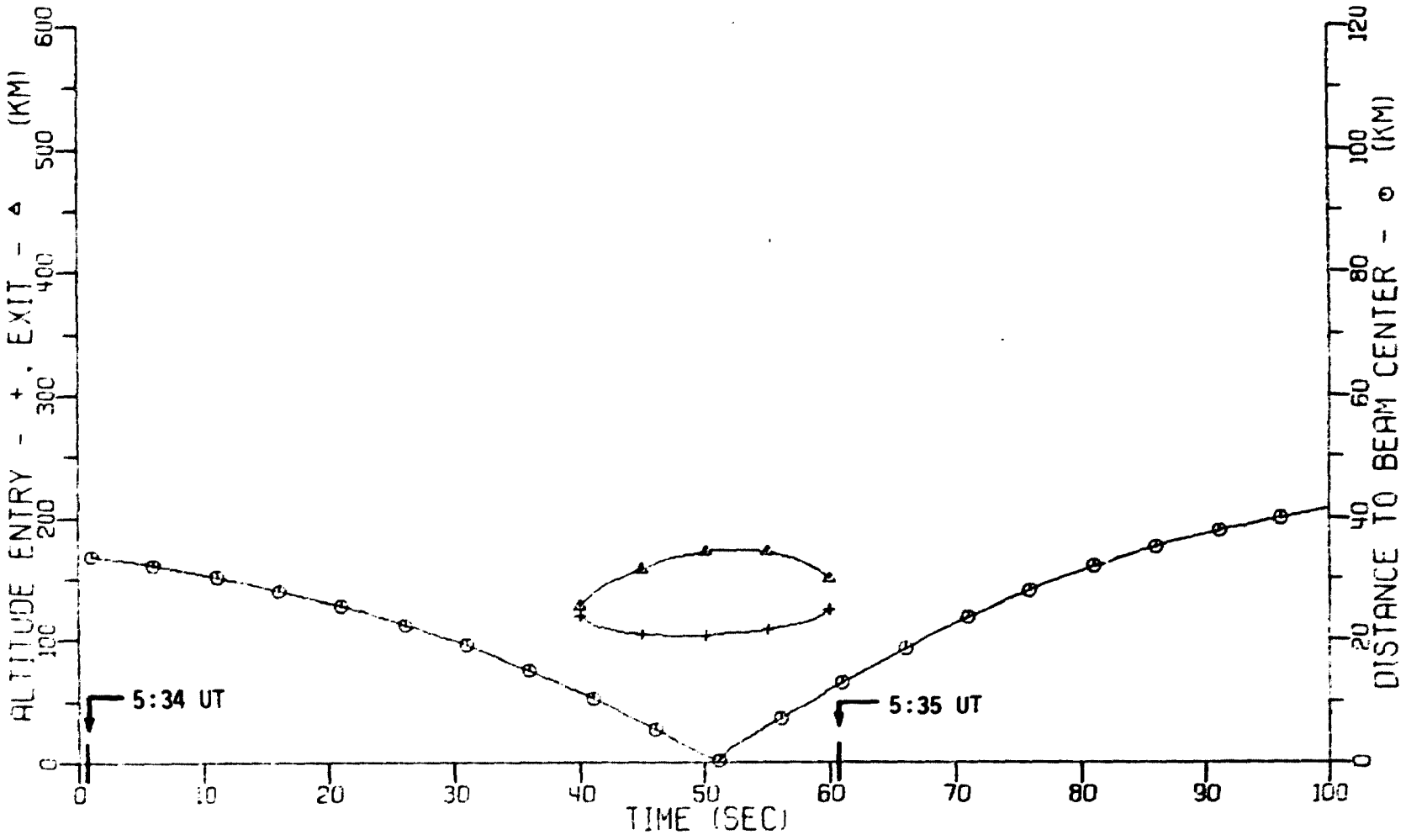

FIGURE 31

HEATER - LINE OF SIGHT GEOMETRY

Satellite 83 Day 115 Zero Time 5:33:59 UT

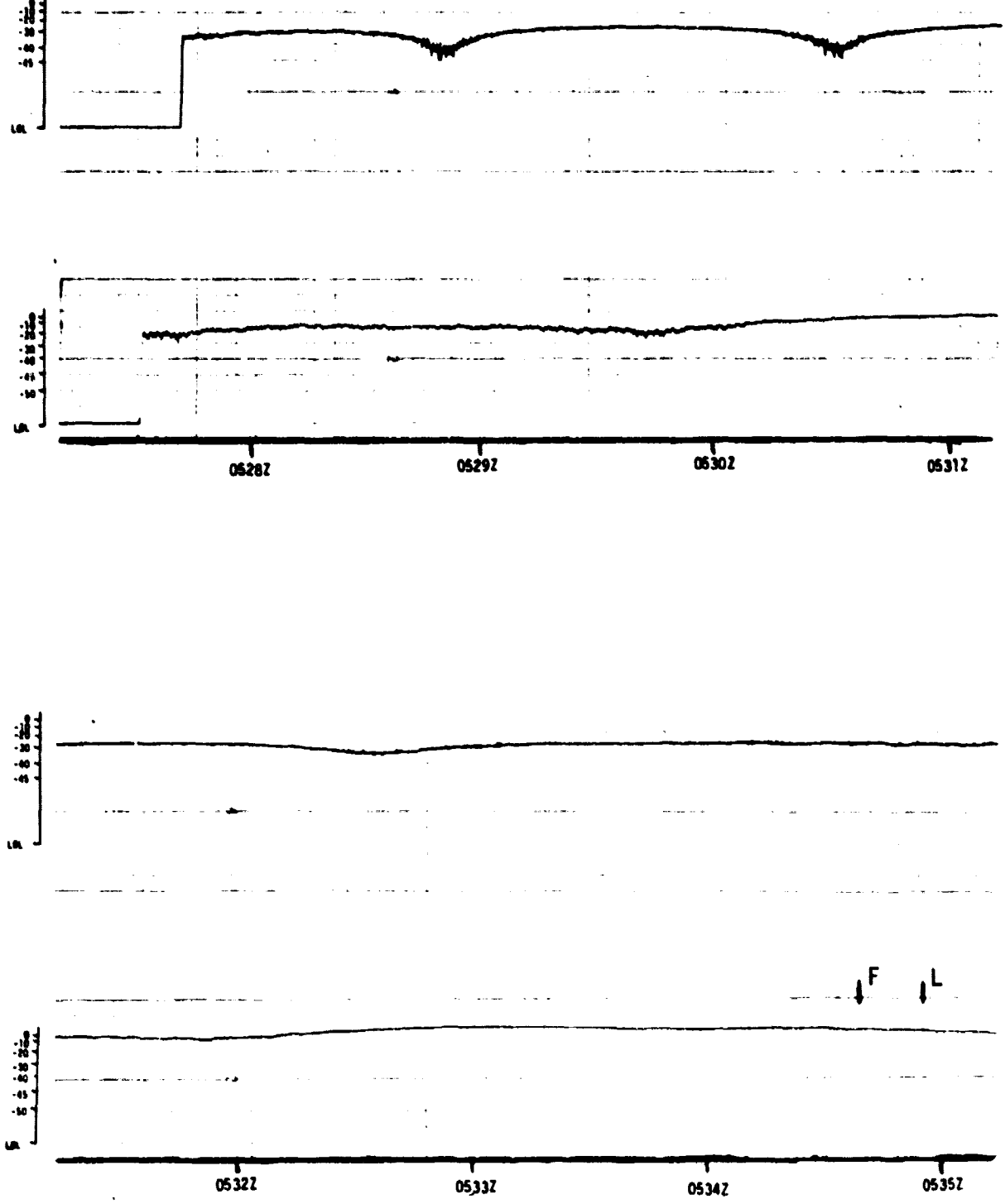

FIGURE 32

AMPLITUDE versus TIME OF NAVSAT PASS

Upper Trace 162 MHz Lower Trace 324 MHz

Day 115 Satellite 83 Rise 5:26 UT

Line of Sight Crosses Above Transmitter at 5:34:47 UT AE-81-48(a)

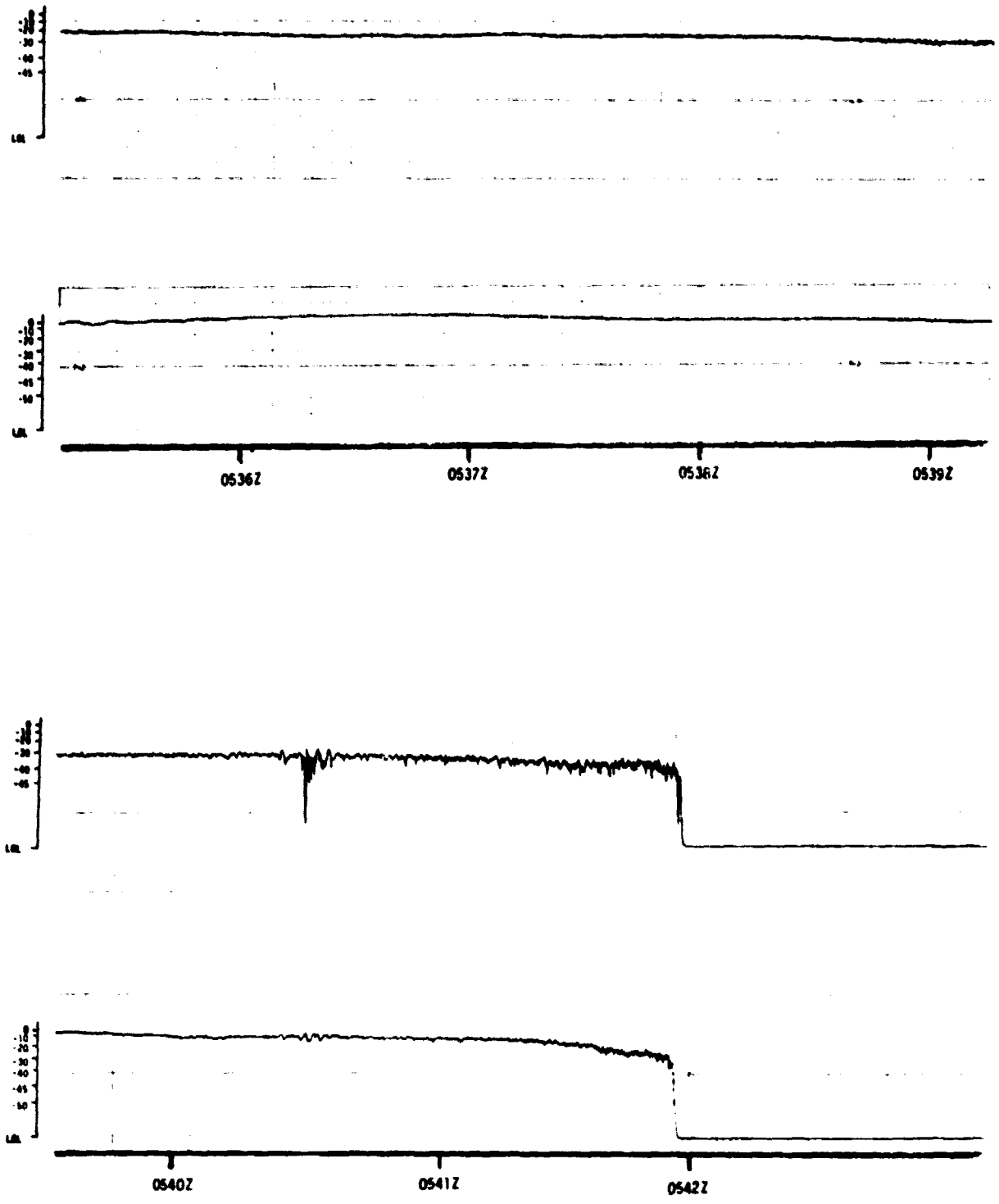

FIGURE 32 (cont'd)

AMPLITUDE versus TIME OF NAVSAT PASS

Upper Trace 162 MHz Lower Trace 324 MHz

Day 115 Satellite 83 Rise 5:26 UT

Line of Sight Crosses Above Transmitter at 5:34:47 UT

AE-81-48(b)

10. Pass of Satellite 93, Day 116, 0327 UT

The LOS passed through the beam just below the bottom of the ionosphere, which was at 240 km (Fig. 33). The geometry for multipath from beam area turbulence was favorable prior to TCA. The amplitude record (Fig. 34), however, shows no significant variations prior to or through beam encounter. There is a 10 dB variation on the 400 MHz signal 5 min after encounter, but this may be due to natural scintillations. The paper tape data (Fig. 35) show a very smooth pattern throughout the pass. The Tranet II data shows a similar picture (Fig. 36).

B. High Resolution Data

On the first three heating passes and several background passes, the auxiliary tape system was employed. This system was initially used on the first heating pass due to failure of the 4-channel modulator. The modulator was damaged in shipment and field repairs were not complete till the evening of day 107. In order to record some high resolution data, the composite signal (marked Σ on Fig. 2) was run directly into a cassette tape recorder. To establish time marks, the plug to the tape recorder was momentarily pulled out on some WWV minute marks. A log of these events was kept for later reconstruction.

Because these are direct recordings (as opposed to FM), there is no response below a few hertz. The dc levels of the composite signal and the slower ramps are therefore not present. However, whenever the phase reached 360°, the voltage of the composite signal switched back to the center level very rapidly. This switchback provides a high frequency pop which was recorded and proved to have a very definite signature. The signal is a damped stretched sine wave with the direction of the first deflection indicating the sign of the switchback.

A set of signal processing programs was developed to retrieve these data. This process, diagrammed in Fig. 37, began with the digitization of the data at about 4 kHz. The switchbacks were then identified in these

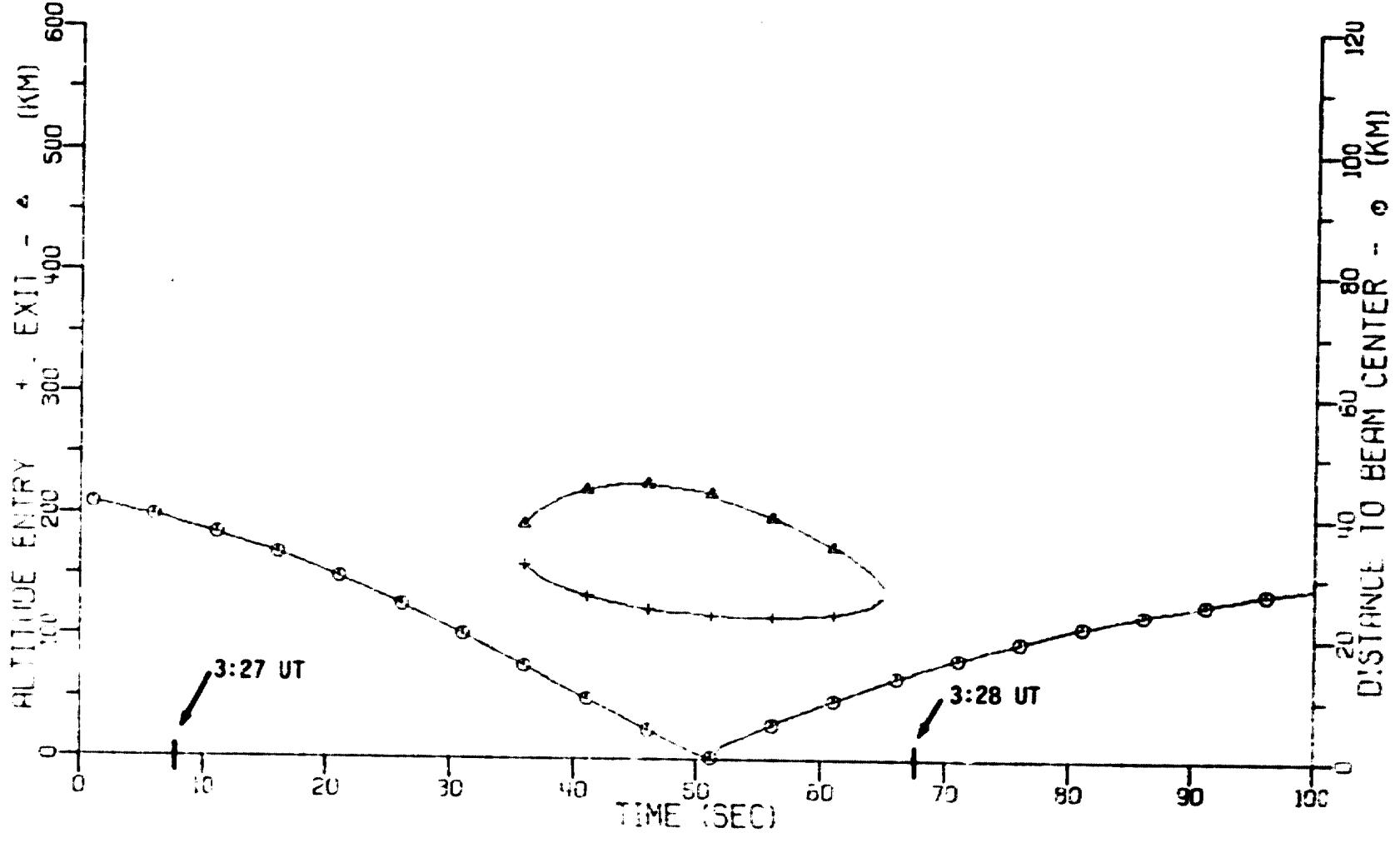

FIGURE 33

HEATER - LINE OF SIGHT GEOMETRY

Satellite 93 Day 116 Zero Time 3:26:52 UT

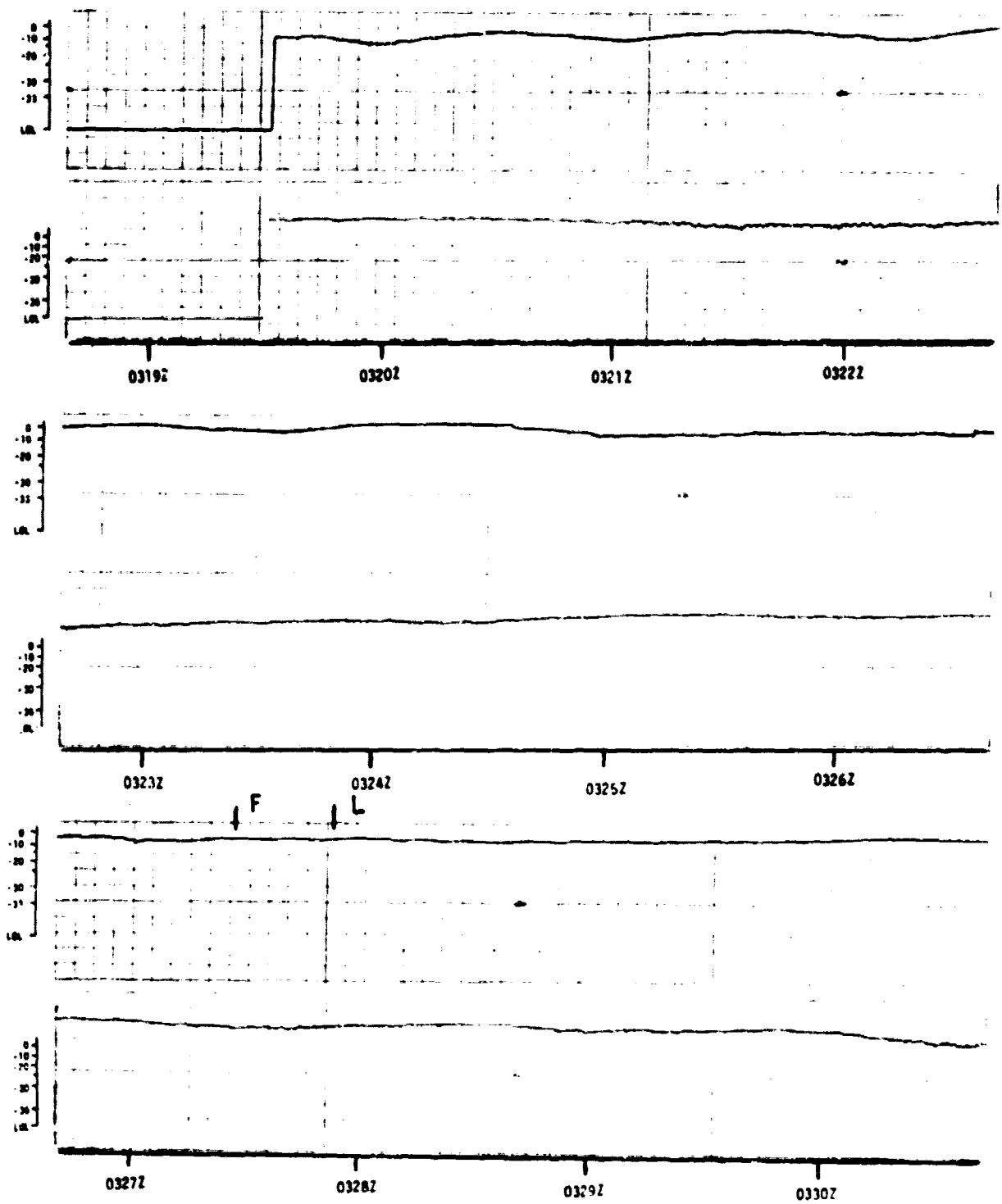

FIGURE 34

AMPLITUDE versus TIME OF NAVSAT PASS

Upper Trace 150 MHz Lower Trace 400 MHz

Day 116 Satellite 93 Rise 3:18 UT

Line of Sight Crosses Above Transmitter at 3:27:41 UT AE-91-50(a)

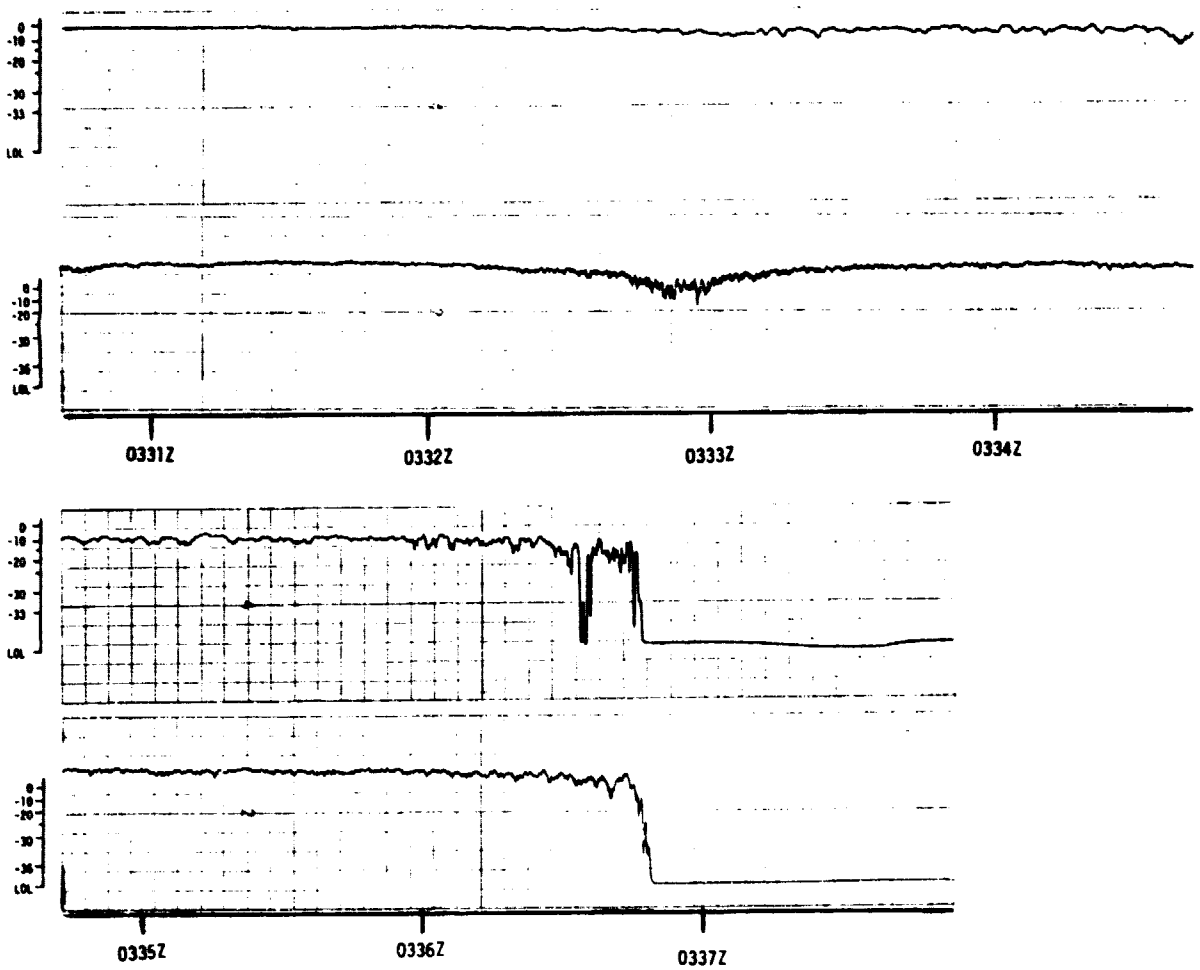

FIGURE 34 (cont'd)

AMPLITUDE versus TIME OF NAVSAT PASS

Upper Trace 150 MHz Lower Trace 400 MHz

Day 116 Satellite 93 Rise 3:18 UT

Line of Sight Crosses Above Transmitter at 3:27:41 UT

AE-81-50(b)

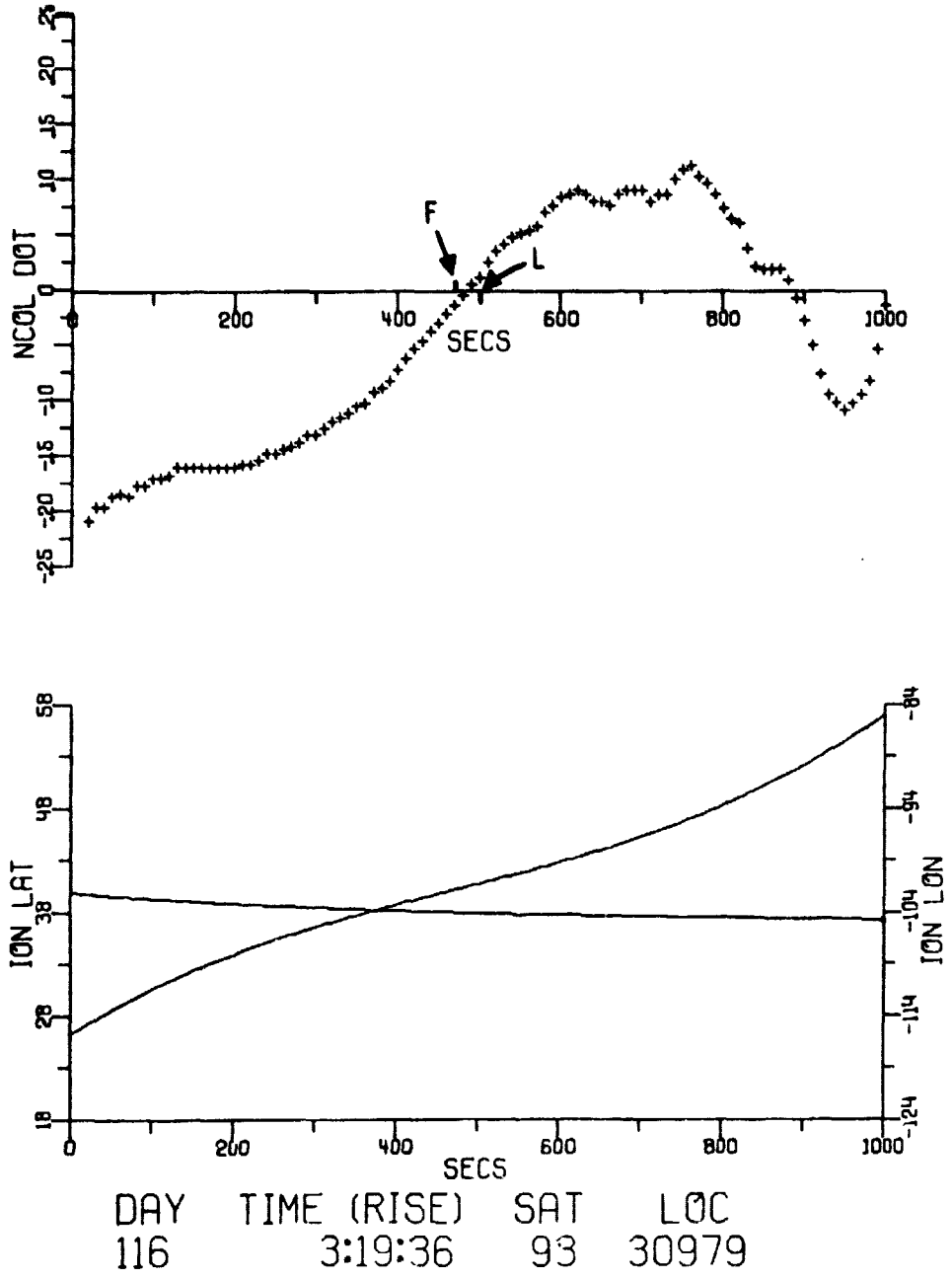

FIGURE 35

PAPER TAPE DATA OF N_c DOT

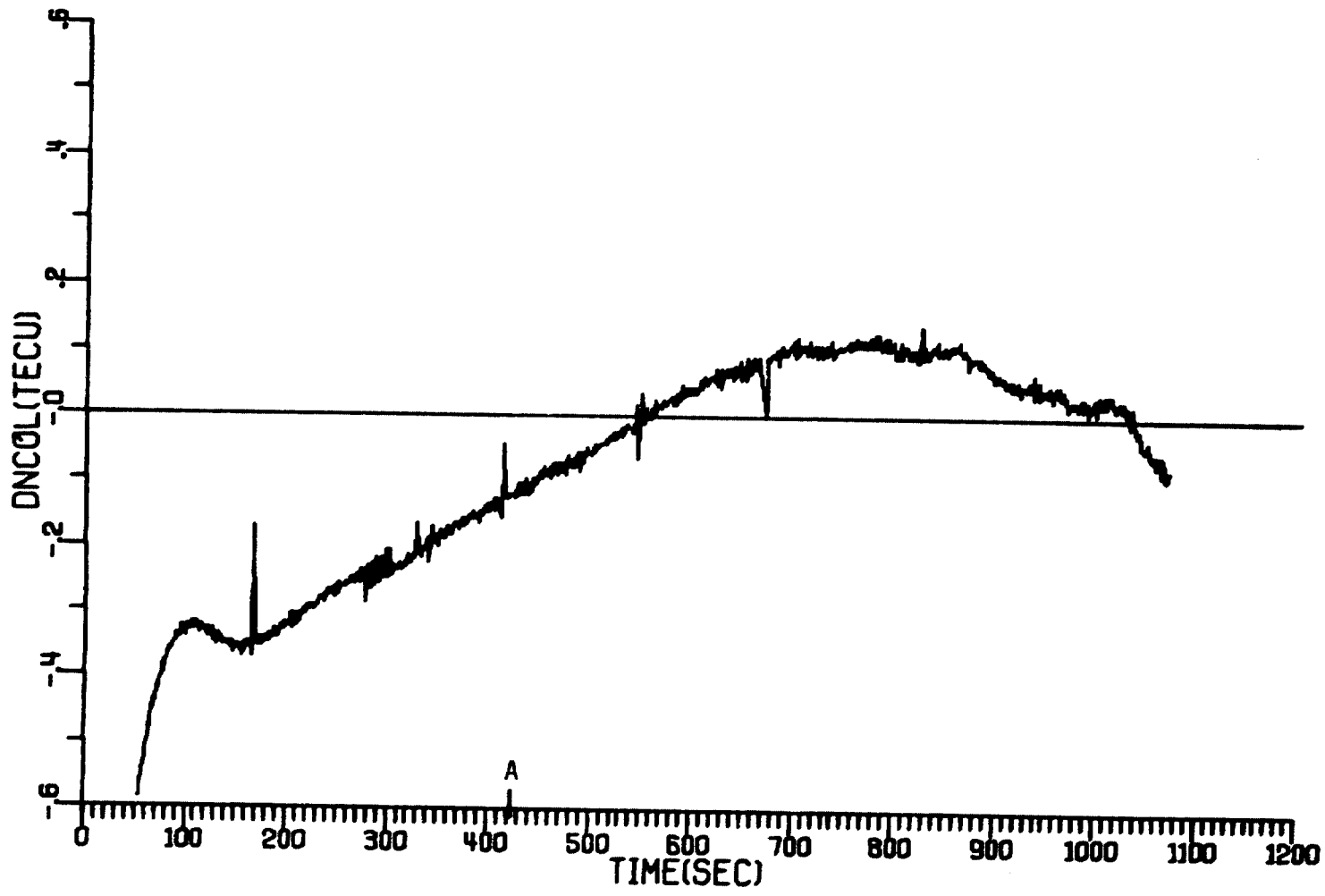

FIGURE 36

$\dot{N}_c$ DATA FROM LAS CRUCES, NEW MEXICO

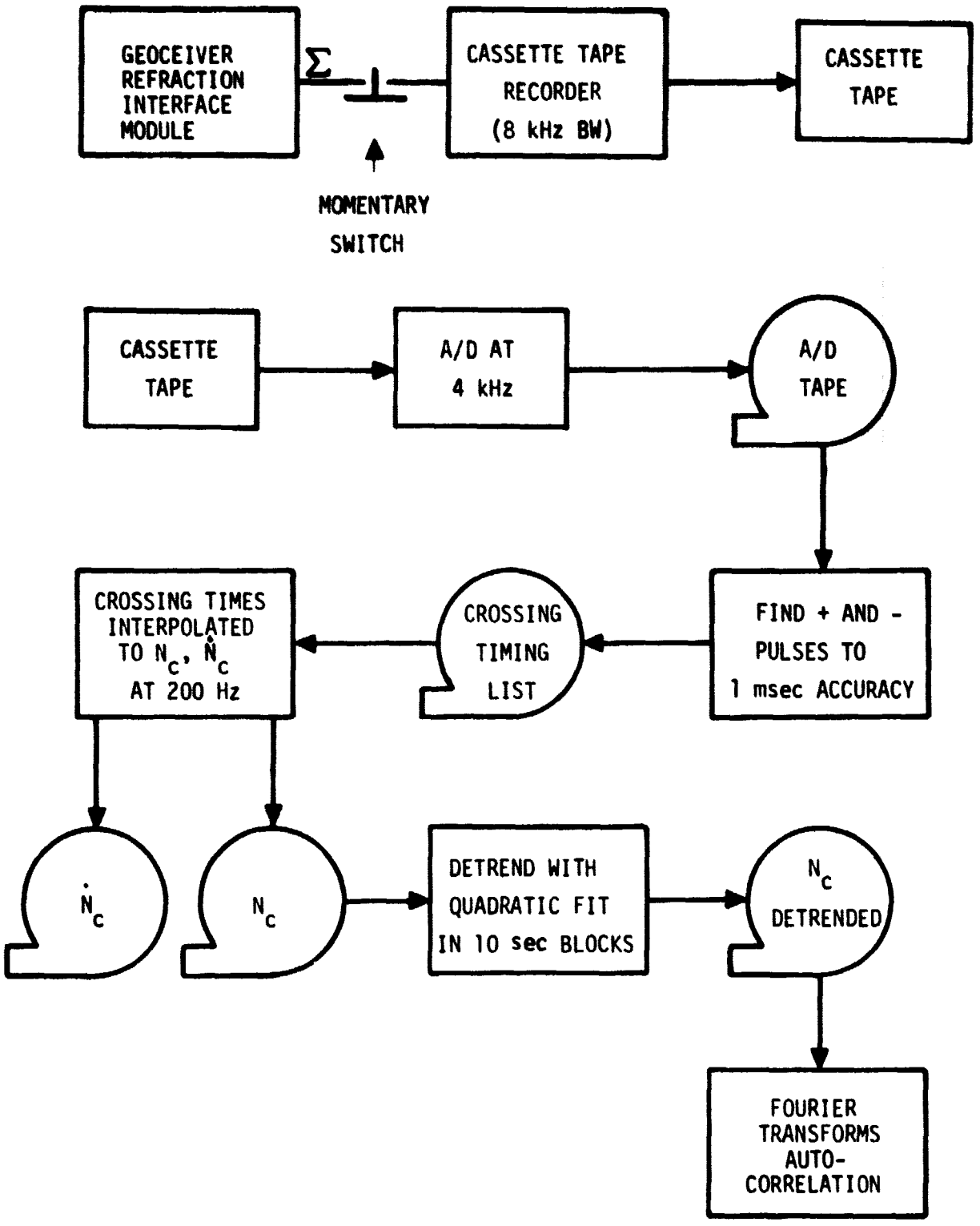

FIGURE 37
AUXILIARY TAPE PROCESSING

data using the relative levels and locations of four peaks and the locations of five zero crossings. This procedure was found to have excellent noise immunity (which crosscorrelation didn't) and to be reasonably fast in execution. The output of this initial processor was a series of switchback times; these times were referred to the beginning of the digitizing and were all positive. The sign of the N_c change was given to the time, to avoid having another array carrying this information.

The times were accurate to 1 msec of time during digitizing. However, due to irregularities in the recording and playback cassette recorders, the accuracy in terms of time in the field was considerably less. With only the hand-produced data gaps as a reference, it is not possible to obtain a good estimate of the record/playback time irregularities. However, the timing points indicate that these irregularities were probably much smaller than 1 sec.

The time series was next converted to an evenly spaced time series at 200 Hz. This was done to facilitate processing with preexisting time series analysis programs. In this conversion, it was assumed that the rate of change was constant between two switchbacks at one count/ΔT, where ΔT is the time interval between counts. The highest count rates were at about 20 counts/sec. The assumption of constant rate of change between switchbacks is certainly not true and the frequency components above the counting rate are contaminated by this procedure.

Three times series were produced. One represented the counting rate and is proportional to the time rate of change of N_c. This is essentially the raw data, whereas the other two are integrated versions of the raw data. The first integrated time series begins at zero TECU and is continuously integrated throughout the pass. With the exception of a single additive integrated constant, this is the N_c curve. (There will be small errors due to the time marks but these are at known locations far from the beam crossings.) The third time series is a detrended version of the latter. A least squares fit quadratic was subtracted from the data in time segments 10 sec long. This will remove the effects of changing geometry and enhance the small scale, high frequency irregularities in spectra.

It should be noted that these procedures will affect the high frequency rolloff of the spectra. A straight line of non-zero slope has a spectrum that rolls off as 1/f. The non-detrended data are dominated by the large change over the interval and roll off as 1/f. Most of this energy is in the discontinuity between the first and last point (finite Fourier transforms represent the periodic repetition of the data). The effect of the endpoint discontinuity can be reduced somewhat by windowing, but the detrending does a better job. These procedures will leave a discontinuity in the slope in the detrended data wherever a switchback has occurred. Since a discontinuity in slope has a high frequency rolloff of $1/f^2$, this functional form is to be expected as a high frequency noise floor. Real effects may rise above this floor, of course.

1. Pass of Satellite 93, Day 106, 0418 UT

The geometry for this pass and a detailed discussion of the chart recorder data are given in Section III.A.1. This pass cut through the heater beam well within the ionosphere and, as observed from the Sterling site, the beam crossing came just prior to TCA. There were only minor amplitude variations prior to and during beam crossing. Toward the end of the pass, there were intense natural scintillations in the north.

The $\dot{N}_c$ time series from the auxiliary tape for this pass is shown in Fig. 38. There were additional problems with equipment during this pass which are indicated in this figure. The cassette occasionally jammed and stopped three times as indicated in Fig. 38. The scallops early in the pass are probably due to slippage of the tape on the capstan. After this pass, both the brand of tape and the cassette recorder were changed to avoid a repetition of these problems. The integral of this $\dot{N}_c$ data over 10 sec periods gives the paper tape data as expected.

The $\dot{N}_c$ data show a fairly constant rate (ignoring the scallops) up to about second 340. The minor amplitude scintillations seen on the chart recordings occurred just after this time. The $\dot{N}_c$ data also show

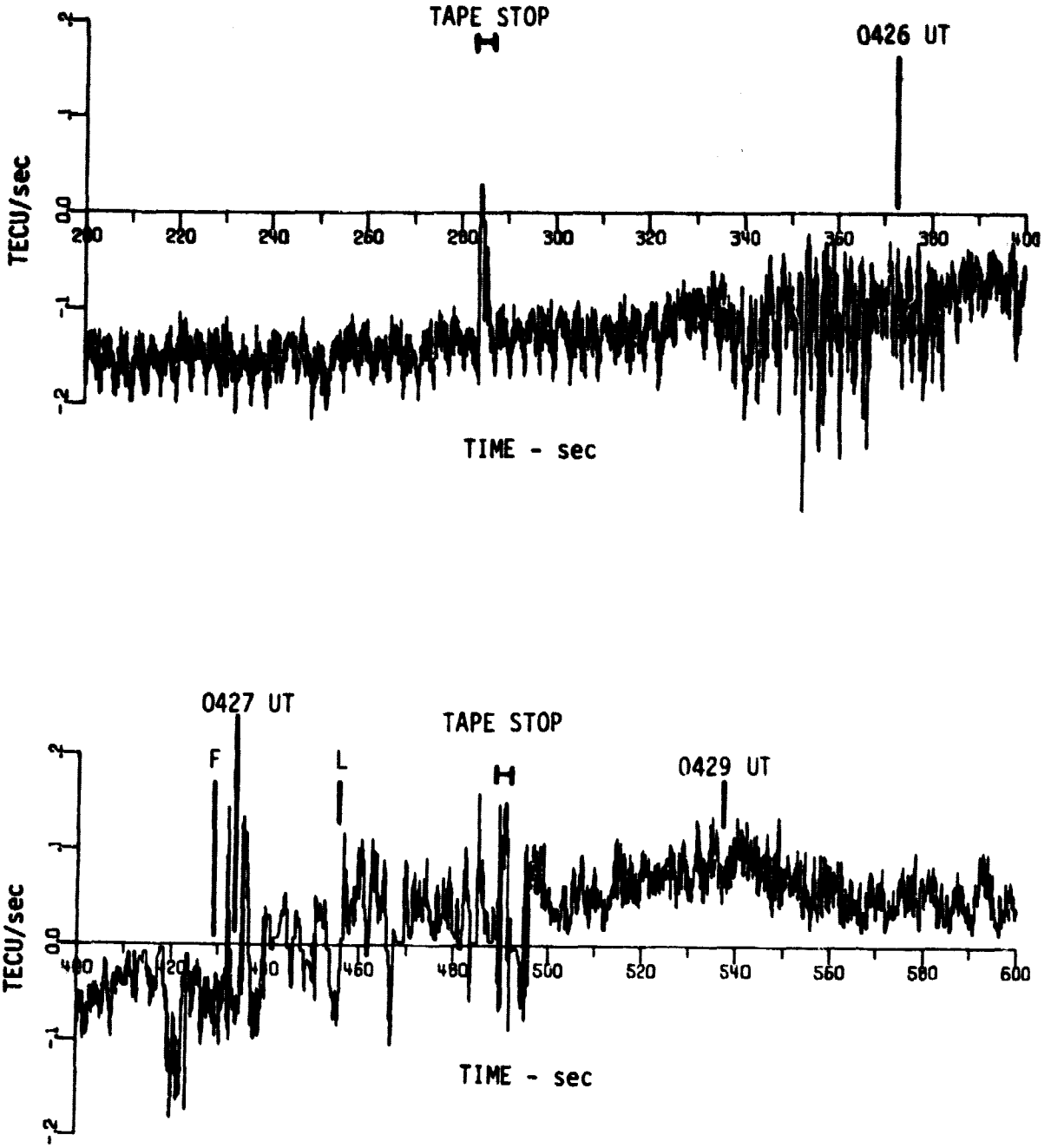

FIGURE 38

$\dot{N}_c$ versus TIME FROM AUXILIARY TAPE SYSTEM

Satellite 93 Day 106 Rise 04:18 UT

AE-81-54(a)

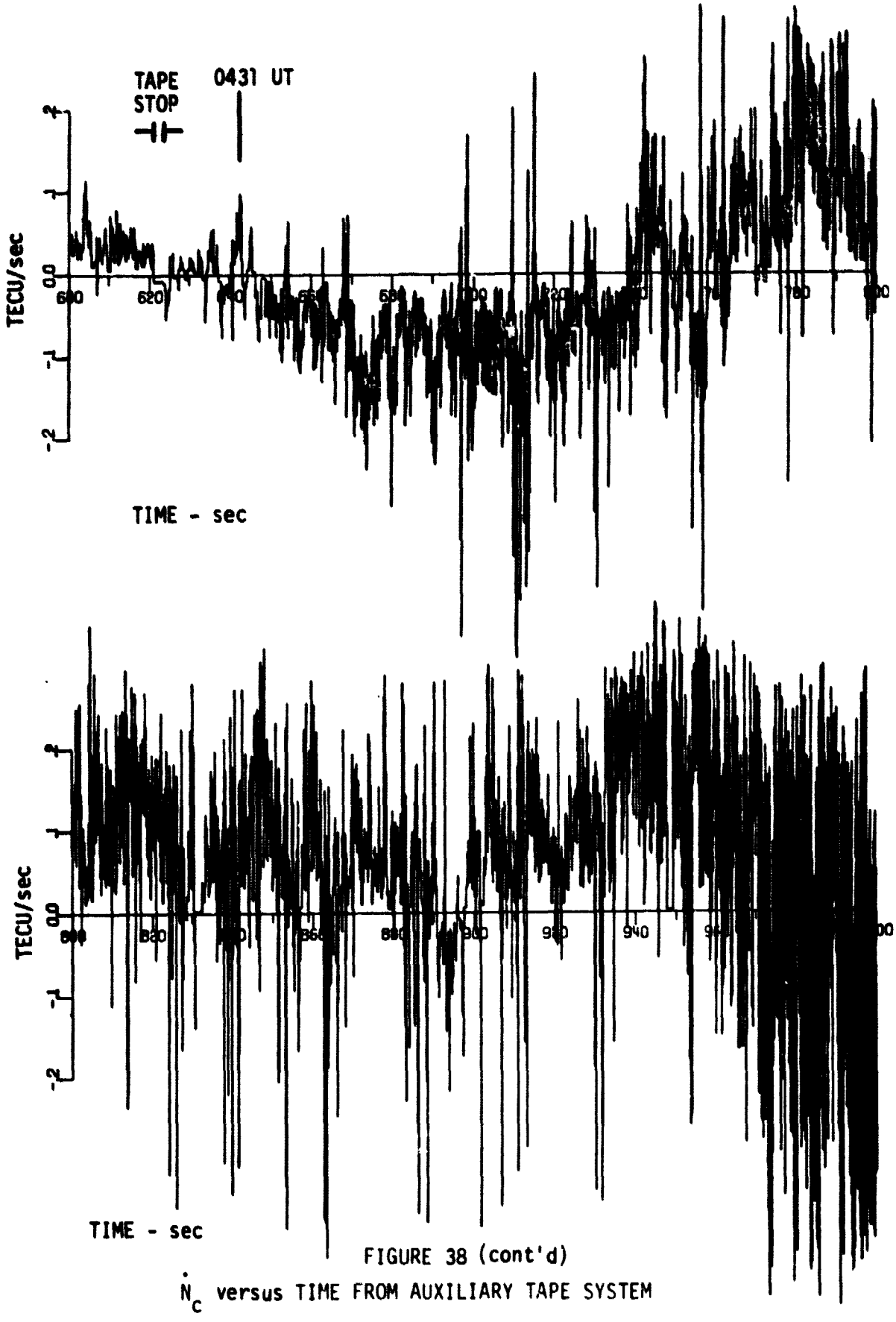

FIGURE 38 (cont'd)

$\dot{N}_c$ versus TIME FROM AUXILIARY TAPE SYSTEM

Satellite 93 Day 106 Rise 04:18 UT

AE-81-54(b)

several large jumps around the time of beam contact. Late in the pass, $\dot{N}_c$ becomes extremely erratic during the era of intense natural scintillations.

An expanded view of $\dot{N}_c$ through the beam crossing time is given in Fig. 39. Just prior (southward) to beam entry, there is a region of $\dot{N}_c$ which is about 0.1 TECU/sec lower than the surrounding region. This corresponds to a sharp break in the slope of N_c versus time and can be seen in Fig. 40, a detailed view of N_c during beam crossing. This area of the pass is near TCA when the N_c curve should show a minimum. A circle matching the curve prior to the beam entry has been extended across the central area to approximate the undisturbed ionosphere. The area between this dotted curve and the measured data represents a depletion. This difference is shown in the lower half of Fig. 40. The depletion was about 0.75 TECU in depth and 65 sec wide. The LOS was moving with a horizontal velocity of 2.4 km/sec at 350 km through this region; this implies that the depletion extended over a north-south region of 160 km.

There are regions of varying slopes in the depletion, but due to the approximate nature of the baseline curve, only rough values can be obtained. The beginning of the depletion has a slope of about 1.7×10^{-2} TECU/km, while the slope at the end of the depletion is about one-half this value. The total depth of the depletion corresponds to 0.4 cycles at 2.45 GHz, or an increased phase range of 5 cm. The beginning and ending slopes can be considered optical wedges bending the beam inward. The beginning slope in phase path length/horizontal distance is 5 cm/35 km, or 1.4×10^{-6}. This is the deflection angle in radians and corresponds to about 10^{-4} deg. The deflection from the ending slope would be about half this value.

The rough lens shape of the depletion will cause inward focusing; the radius of curvature was measured to be over 3.0×10^{7} km at 2.45 GHz. This effect will therefore be negligible.

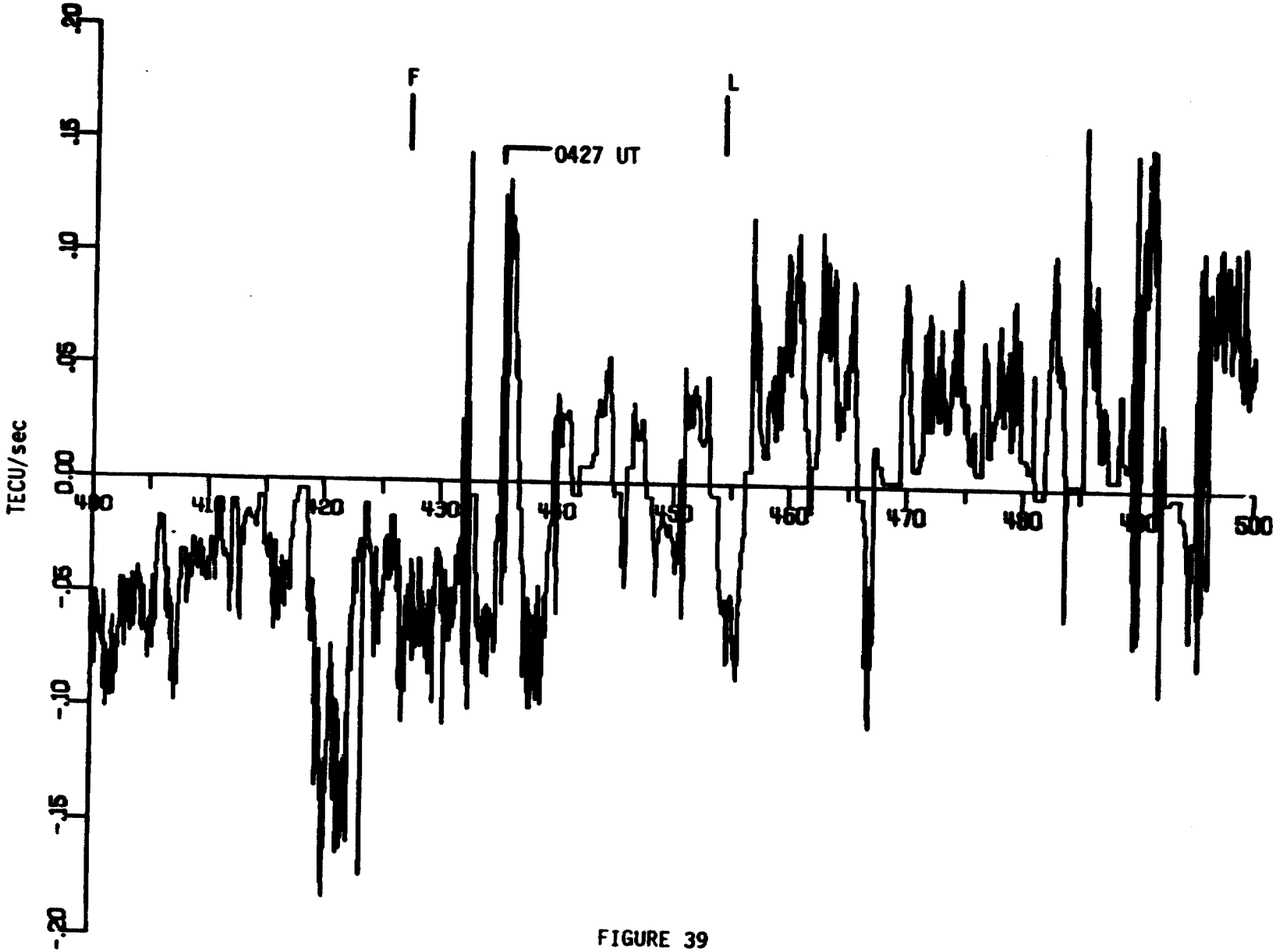

FIGURE 39

EXPANDED VIEW OF $\dot{N}_c$ versus TIME AROUND BEAM CROSSING

Satellite 93 Day 106 Rise 04:18 UT

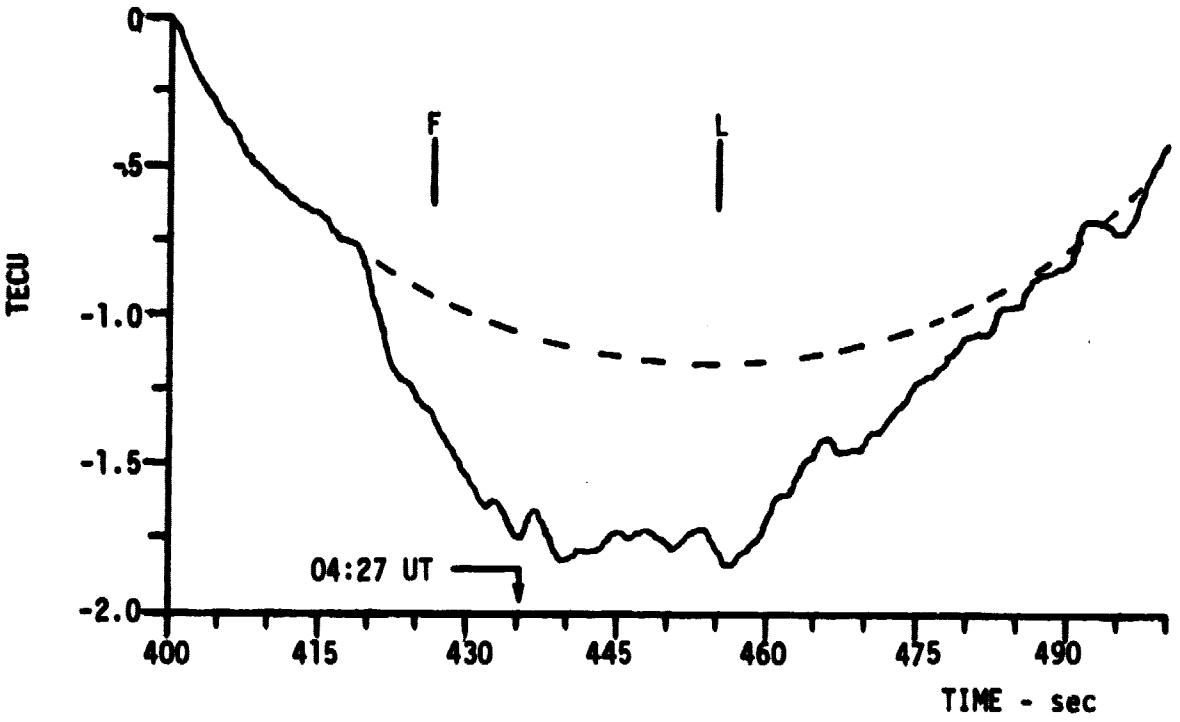

(a) N_c versus TIME AROUND BEAM CROSSING

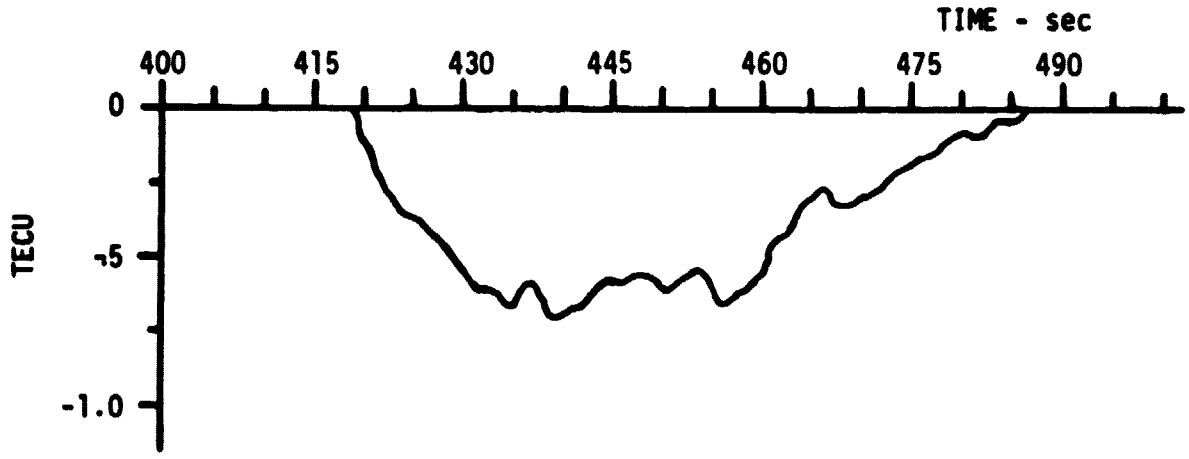

(b) DIFFERENCE BETWEEN SMOOTH CURVE AND DATA

FIGURE 40

ELECTRON COLUMNAR CONTENT AROUND HEATER BEAM

The detrended data have been analyzed in several ways. First, spectra were computed for 10 sec time blocks. This length was used to avoid the discontinuities between each 10 sec detrended block. Groups of ten of these spectra were ensemble averaged to reduce the noise level. Three spectra produced in this manner are shown in Fig. 41. Data from a fairly quiet region of this pass form the lowest curve, while the upper curve includes the beam crossing data. It shows a slightly higher level overall and several conspicuous bumps in the 15-40 Hz region. Since the LOS had a horizontal velocity of 2.4 km/sec through the ionosphere at this time, this frequency band corresponds to spatial dimensions of 40-100 m.

Due to the quantization system used with the raw data, spectral levels at frequencies over the counting rate are underestimates of the true levels. However, it is obvious from Fig. 41 that there is considerable energy beyond 20 Hz, which is above the background level of the quiet area.

The last spectrum is of the small scintillations prior to beam crossing and matches the beam crossing spectrum below 10 Hz. All these spectra represent about the same spatial scales since the LOS velocity was about the same. A spectrum of the heavy scintillation during the end of this pass was computed; its level is about 10 dB higher than the pre-crossing scintillation. However, if the horizontal axis is adjusted for the difference in velocities to compare spatial frequencies, the curves are identical beyond 2 Hz to within the variation in the line. This implies that similar physical structures were responsible for the two scintillations.

The autocorrelation functions of each 10 sec detrended block were computed from the spectra and the autocorrelation lengths (1/e points) determined. These lengths varied greatly and averages of 10 autocorrelation lengths (100 sec of data) were computed. The average values were about 1.25 sec with a standard deviation of about 0.3 sec for all cases except the 300-400 sec region, which had an average of

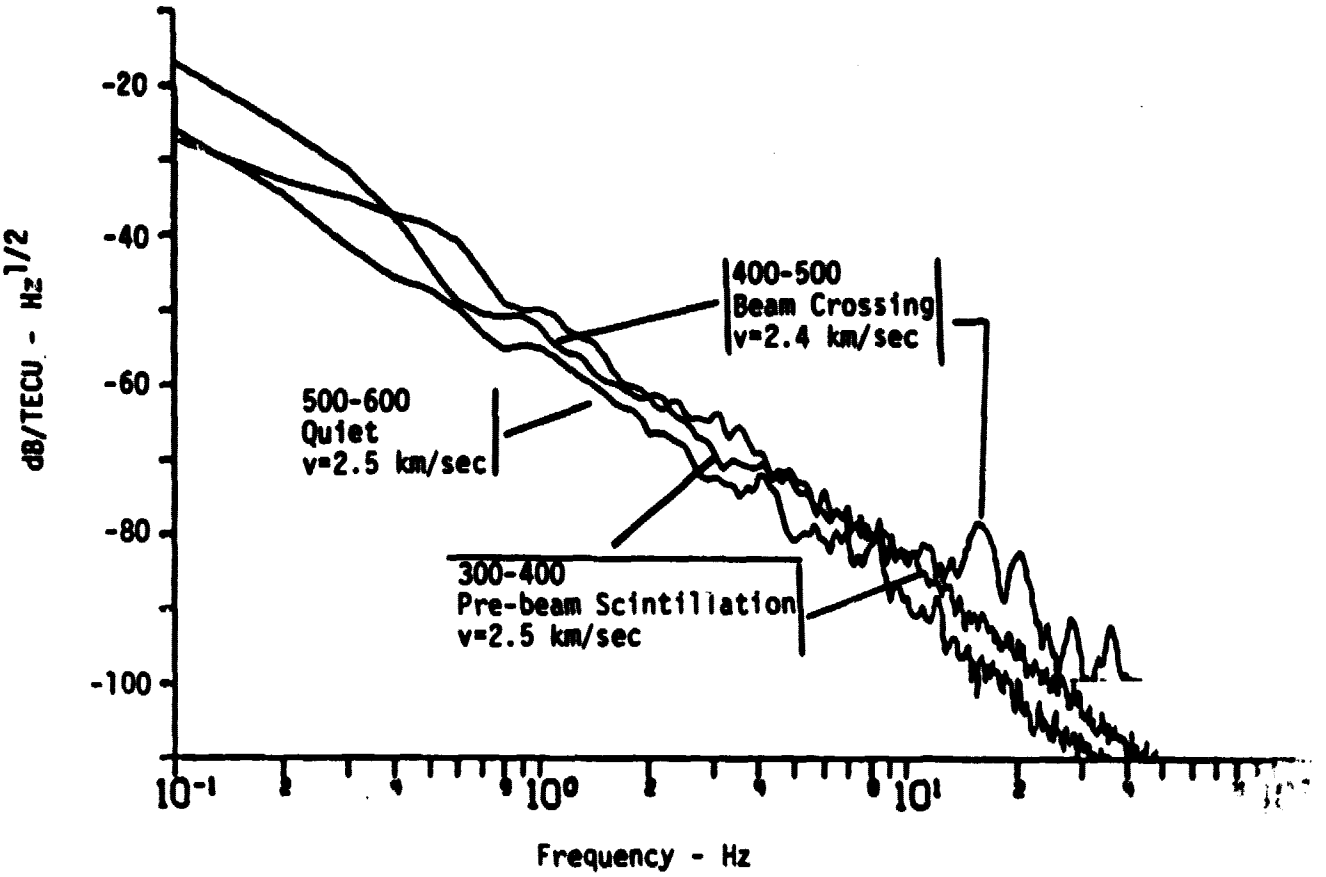

FIGURE 41

TEMPORAL SPECTRUM OF DETRENDED N_c

Satellite 93 Day 106 Rise 04:18 UT

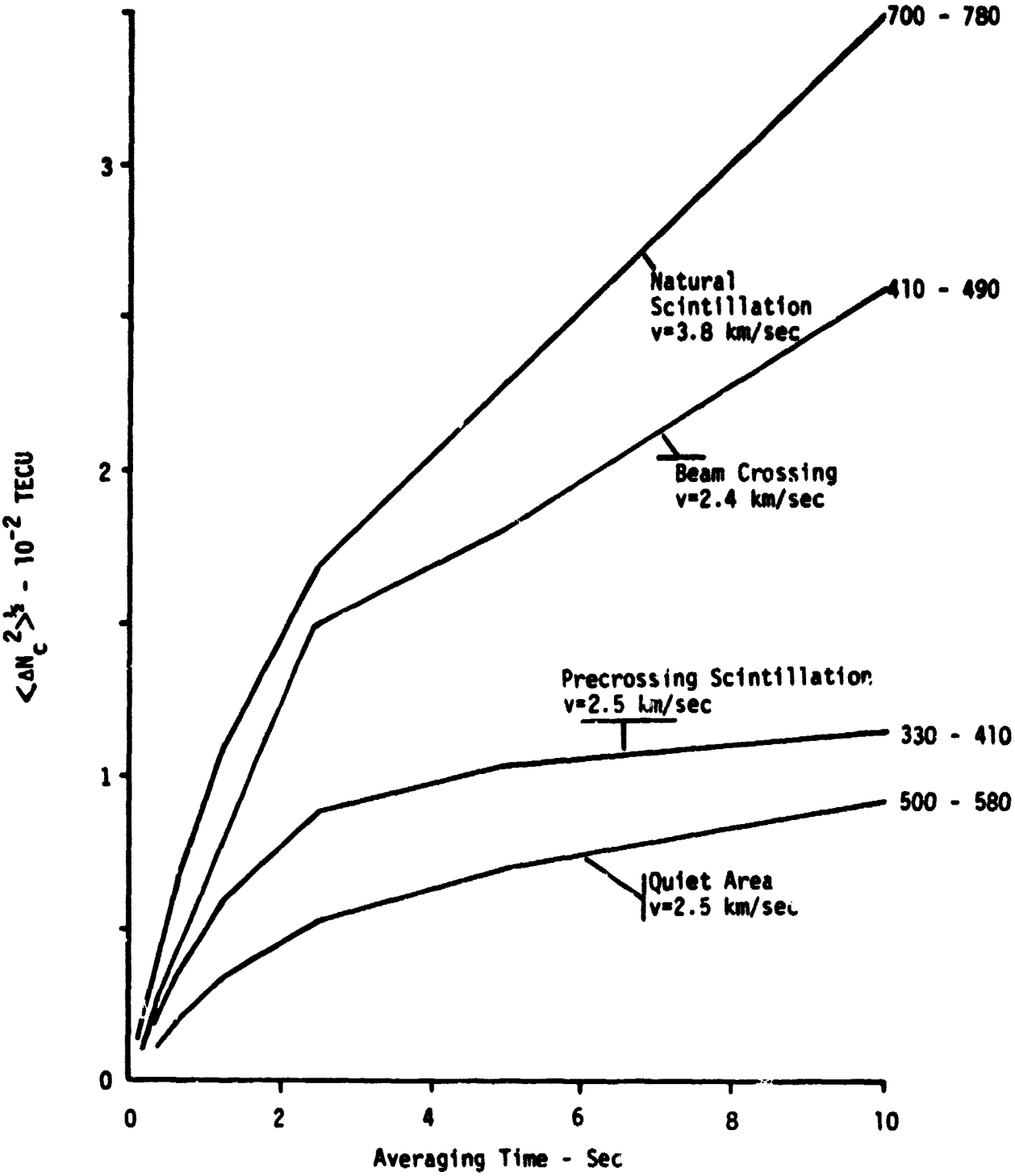

FIGURE 42

rms N_c VARIATION versus AVERAGING TIME

Satellite 93 Day 106 Rise 04:18 UT

0.75 sec. The similarity of these values in terms of time indicates that this measurement was probably dominated by processing artifacts (probably the discontinuities in slope at the times of the raw data points). If the values had been similar when an adjustment was made for differing LOS velocities, physical structures would have been the likely candidates for the dominant mechanism. However, this does give a lower limit of about 4 km to the autocorrelation distance along the LOS motion.

To compute rms phase variation, the rms value of the detrended TECU variation over an autocorrelation distance is required. The rms values were computed in time windows of various sizes from 40 msec to 10 sec. These values were then averaged over 80 sec. The results for four 80 sec cases are shown in Fig. 42. Three of these correspond to the spectral data in Fig. 41. The quiet case and the early scintillation both appear to have an asymptote at about 10^{-2} TECU, which corresponds to 2° of phase at 2.45 GHz.

The data from the beam crossing time have a much higher rms N_c and do not asymptote within the area of this graph. If a value of 1 ? sec is assumed for the autocorrelation length of these data, the appropriate rms value to use would be $1\text{-}1.5\times10^{-2}$ TECU. The value could be 2-3 times as large, however, if the true autocorrelation distance were on the order of 10 km.

The last curve is for the area of intense natural scintillation. Plotted as a function of averaging time, it lies considerably above the other curves. However, if the curves are plotted in terms of the spatial extent of the averaging region, this curve and the beam crossing curve are virtually identical. This indicates that the medium scale structures (5-50 km) are statistically identical in the beam region and in the northern auroral area.

2. Pass of Satellite 60, Day 108, 0650 UT

This pass was observed at Loveland, CO, just northwest of the antenna beam in the ionosphere. It probed the heated region over an

extensive range of altitudes as discussed earlier in Sec. III.A (Fig. 8). The receiver lost lock (LOL) at first contact and no data of any kind are available through the beam.

The high resolution $\dot{N}_c$ data for this pass are shown in Fig. 43. The intentional dropouts used to establish a time reference can be clearly seen. The LOS crossing of the beam as well as the LOL period are also marked. Prior to the LOL, the signal became slightly more erratic and this higher level of irregularities persisted after recquisition for about 50 sec. An expanded view of $\dot{N}_c$ just prior to LOL is shown in Fig. 44, where the increase in irregularity can be seen beginning at about second 415. The integral of the data in this region is shown in Fig. 45, where, on this scale, the irregularity is unnoticeable.

Spectra of detrended N_c during periods just before and after the LOL are shown in Fig. 46. The pre-LOL spectrum is essentially identical to the early scintillation spectrum of Fig. 41 (marked as seconds 300-400). The autocorrelation times computed from 10 sec spectra are similar to these of the previous pass, around 1.0-1.4 sec with standard deviations of 0.4 sec.

The rms variation in 80 sec blocks for various averaging times is shown in Fig. 47. The segments just prior to and after the LOL are plotted. In both cases, the levels are at or below the quiet level of the previous pass. This indicates that the medium scale (5-50 km) variations were smaller in these times than in the previous pass. No statement can be made about the region within the beam.

3. Pass of Satellite 68, Day 109, Rise 1102 UT

This pass was also observed from Loveland, CO. However, the LOS stayed below the F region as it cut through the heater beam. The equipment maintained lock through beam crossing, but lost lock soon thereafter.

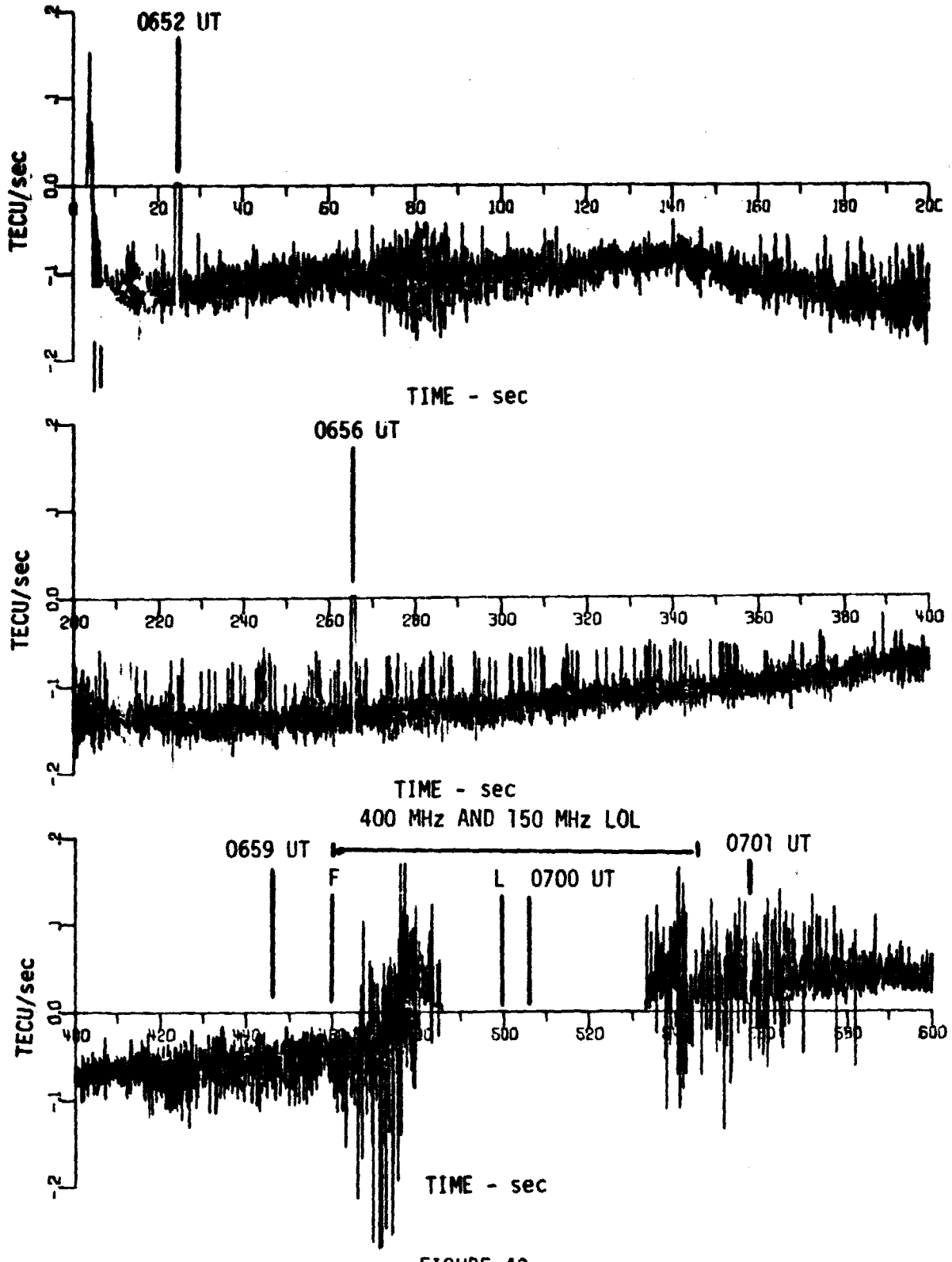

FIGURE 43

$\dot{N}_c$ versus TIME FROM AUXILIARY TAPE SYSTEM

Satellite 60 Day 108 Rise 06:50 UT AE-81-59(a)

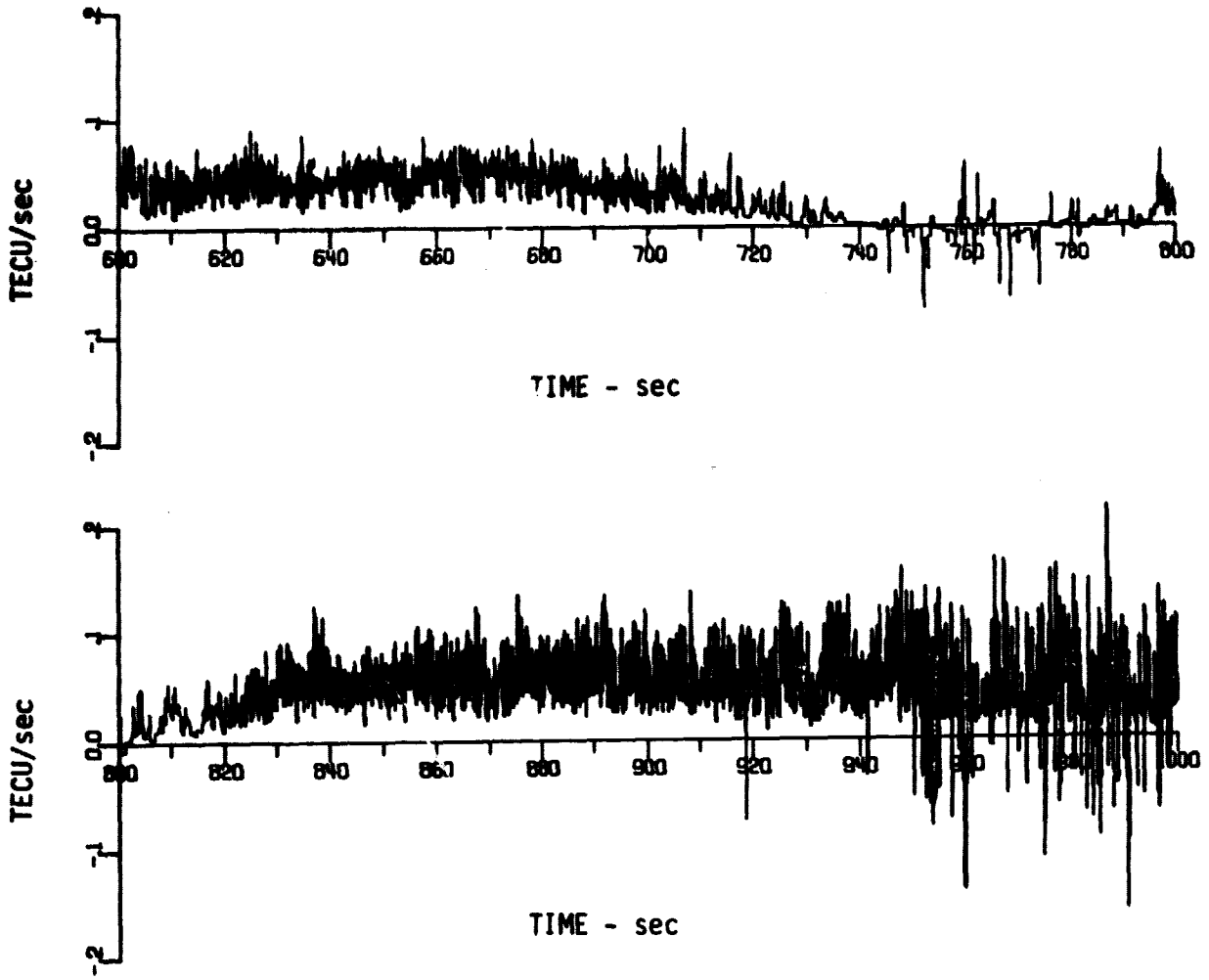

FIGURE 43 (cont'd)

$\dot{N}_c$ versus TIME FROM AUXILIARY TAPE SYSTEM

Satellite 60 Day 108 Rise 06:50 UT

AE-81-59(b)

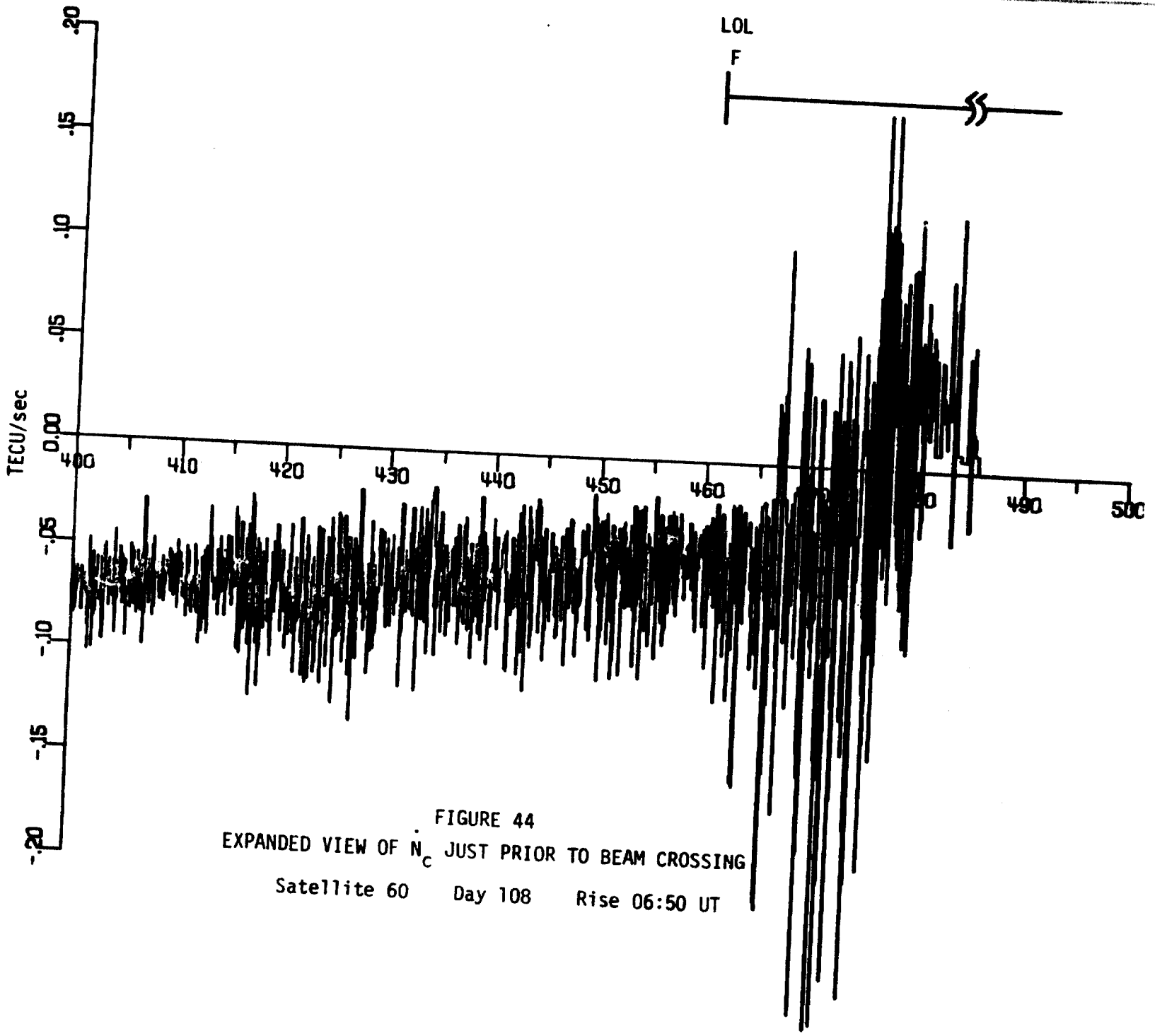

FIGURE 44

EXPANDED VIEW OF $\dot{N}_c$ JUST PRIOR TO BEAM CROSSING

Satellite 60 Day 108 Rise 06:50 UT

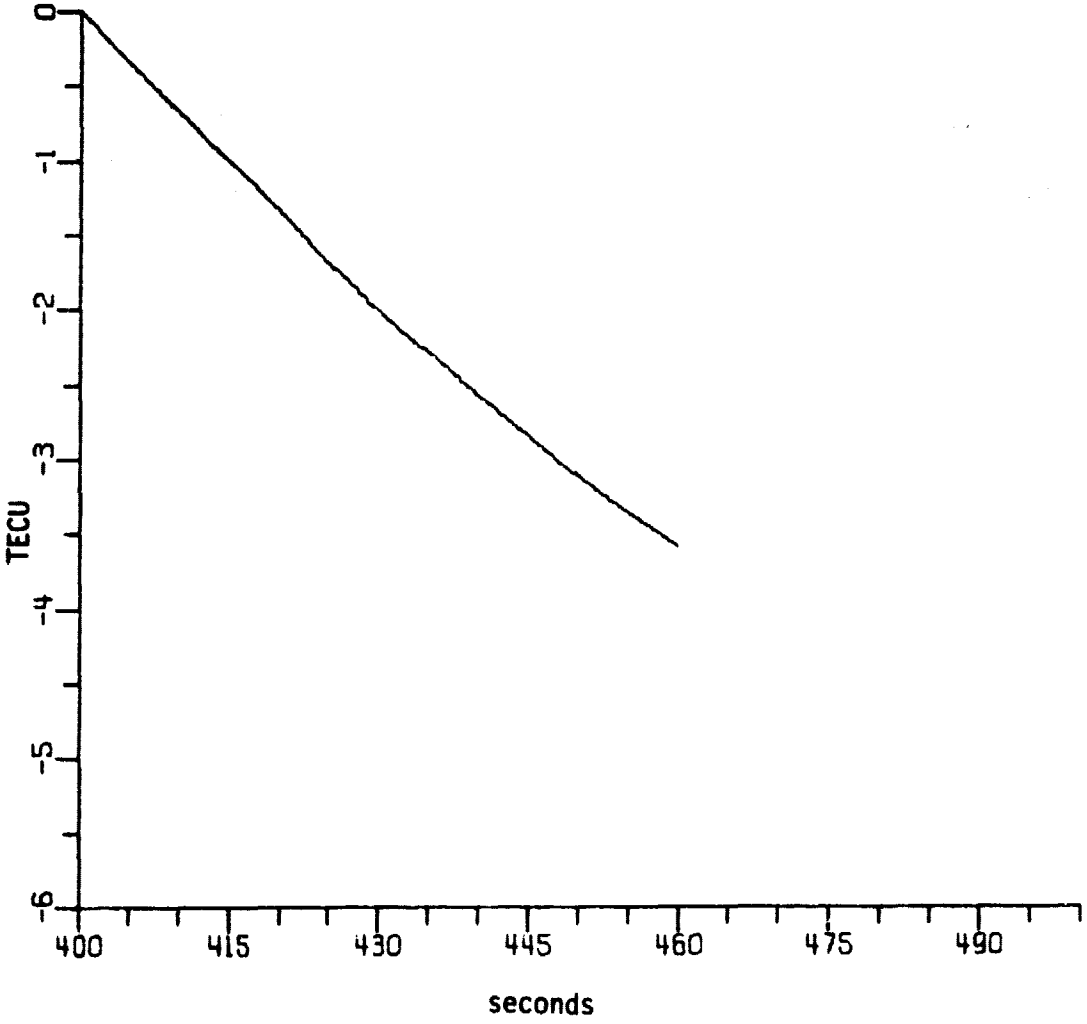

FIGURE 45

N_c versus TIME JUST PRIOR TO BEAM CROSSING

Satellite 60 Day 108 Rise 06:50 UT

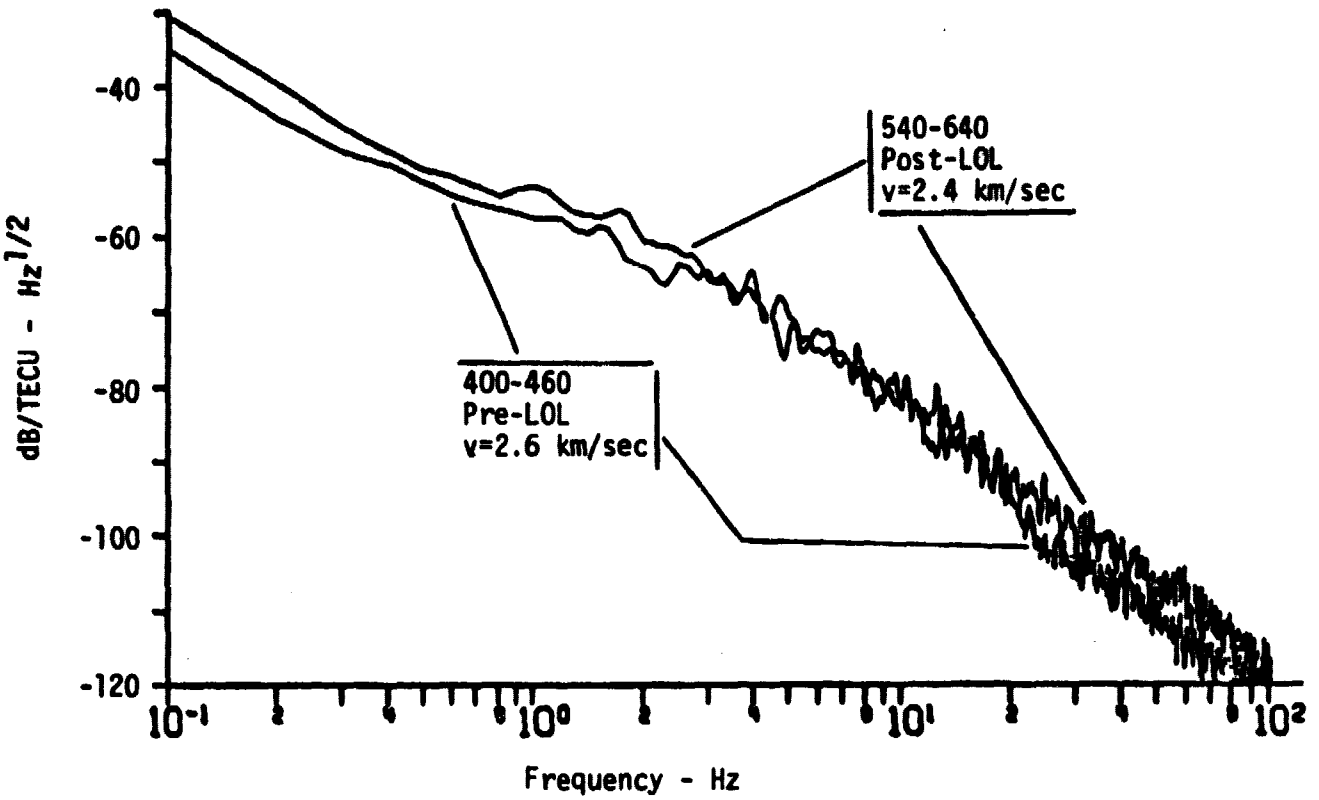

FIGURE 46

TEMPORAL SPECTRUM OF DETRENDED N_c

Satellite 60 Day 108 Rise 06:50 UT

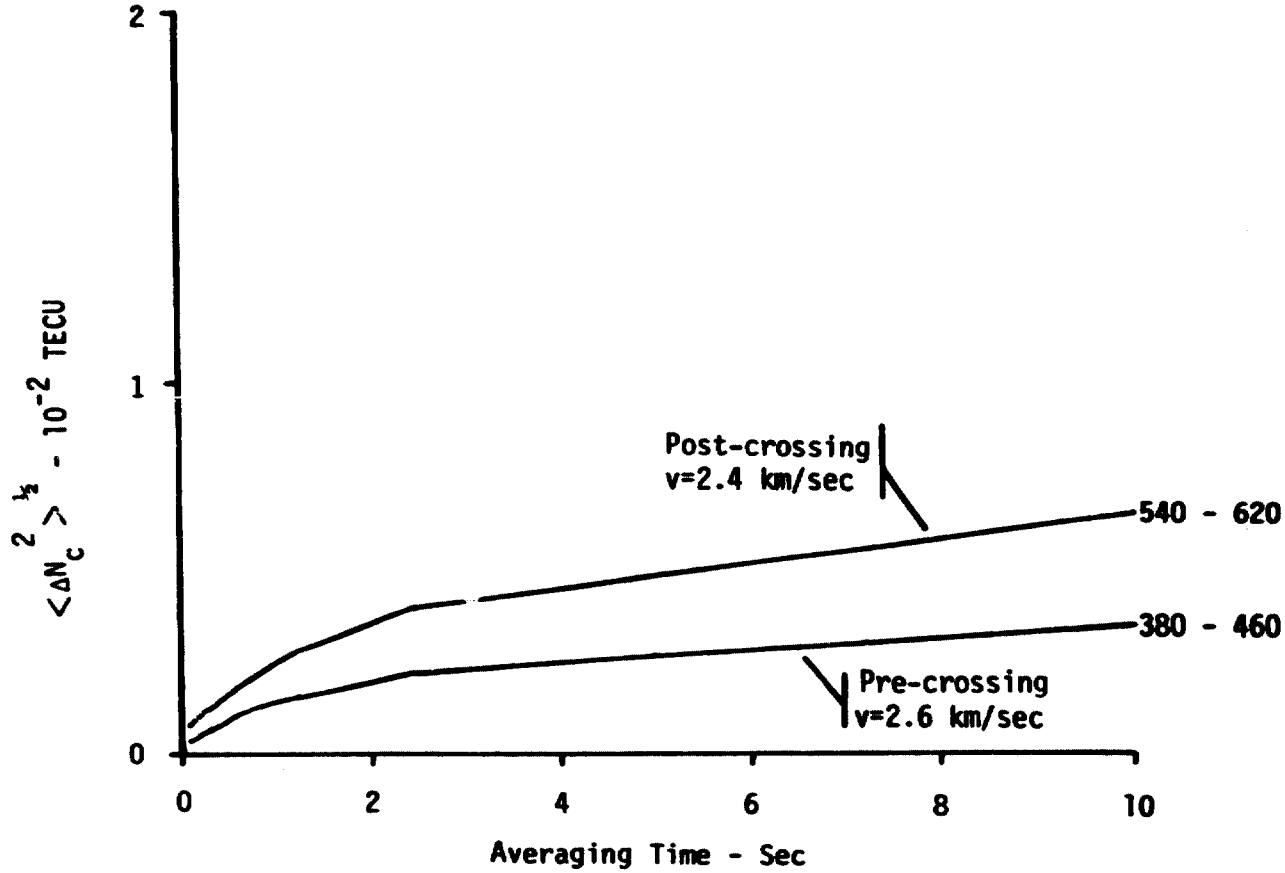

FIGURE 47

rms N_c VARIATION versus AVERAGING TIME

Satellite 60 Day 108 Rise 06:50 UT

The auxiliary tape $\dot{N}_c$ data are shown in Fig. 48, where several LOL's prior to and after beam crossing, as well as the first and last contact with the beams, are marked. Visually, the data appear to get a little noisy just prior to contact, but not nearly as erratic as during a natural scintillation at the end of the pass. An expanded view of the crossing region is shown in Fig. 49. The crossing itself was smooth compared to the region just prior to it. The integral of these data, N_c, is shown in Fig. 50. As expected, no obvious irregularities or large structures are visible. It should be remembered that, through beam crossing, the LOS is below the ionosphere and sampling the ionosphere to the east of the heater.

The spectra of the detrended N_c during and just before beam crossing are shown in Fig. 51. The beam crossing spectrum includes the noise just prior to entry while the other spectrum is of a quieter region. The beam has clearly increased the small scale turbulence in the ionosphere south and east of the beam.

Averages of the rms variation for various averaging times are shown in Fig. 52. The lowest curve is for the quiet reference region whose spectrum is given in Fig. 51. The next higher curve is for the beam crossing region and the last two are for scintillation regions. The highest is of a natural scintillation near the end of the pass and the other is of the noise just after the end of LOL. This latter curve is probably sampling beam induced turbulence.

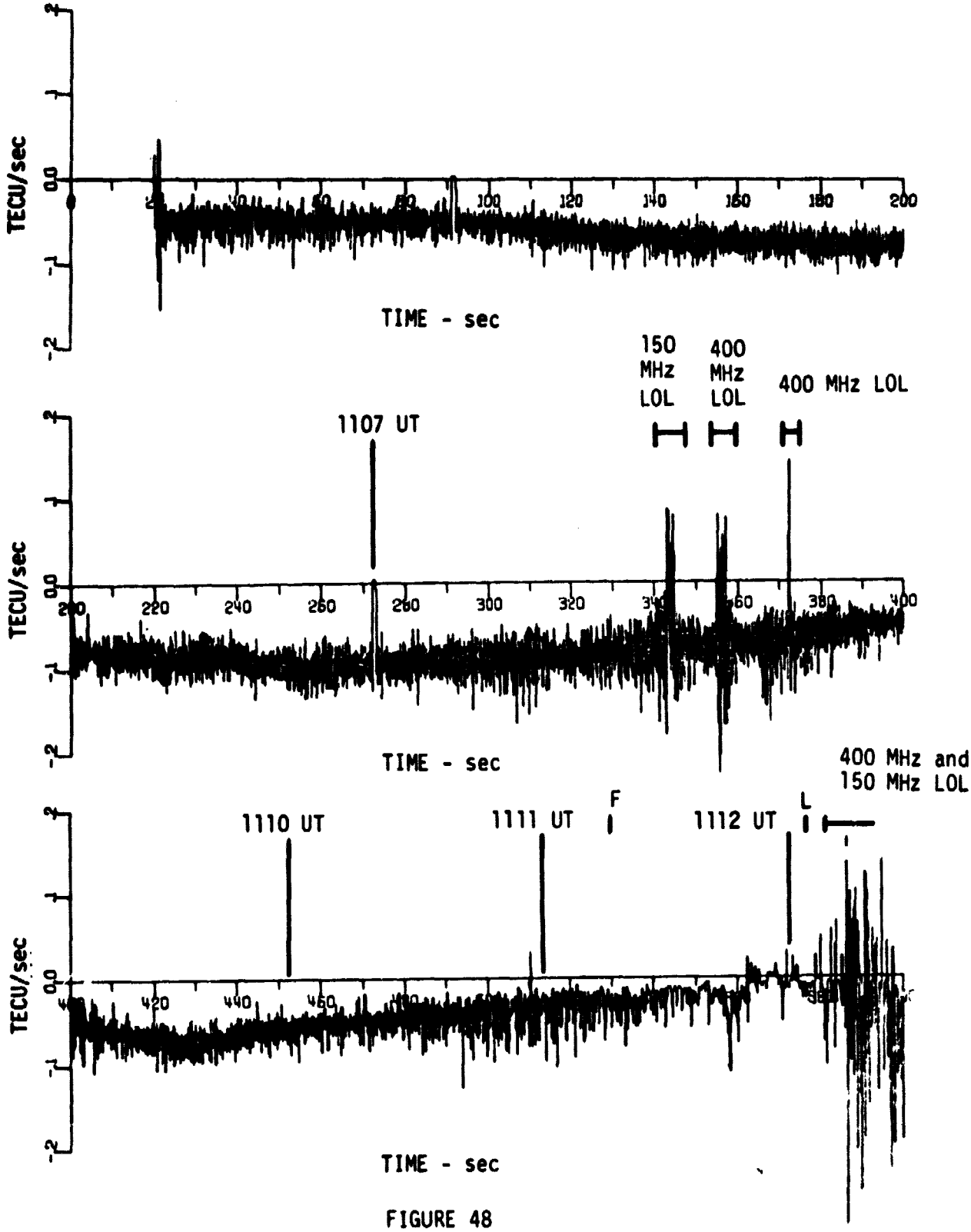

FIGURE 48

$\dot{N}_c$ versus TIME FROM AUXILIARY TAPE SYSTEM

Satellite 68 Day 109 Rise 11:02 UT

AE-81-64(a)

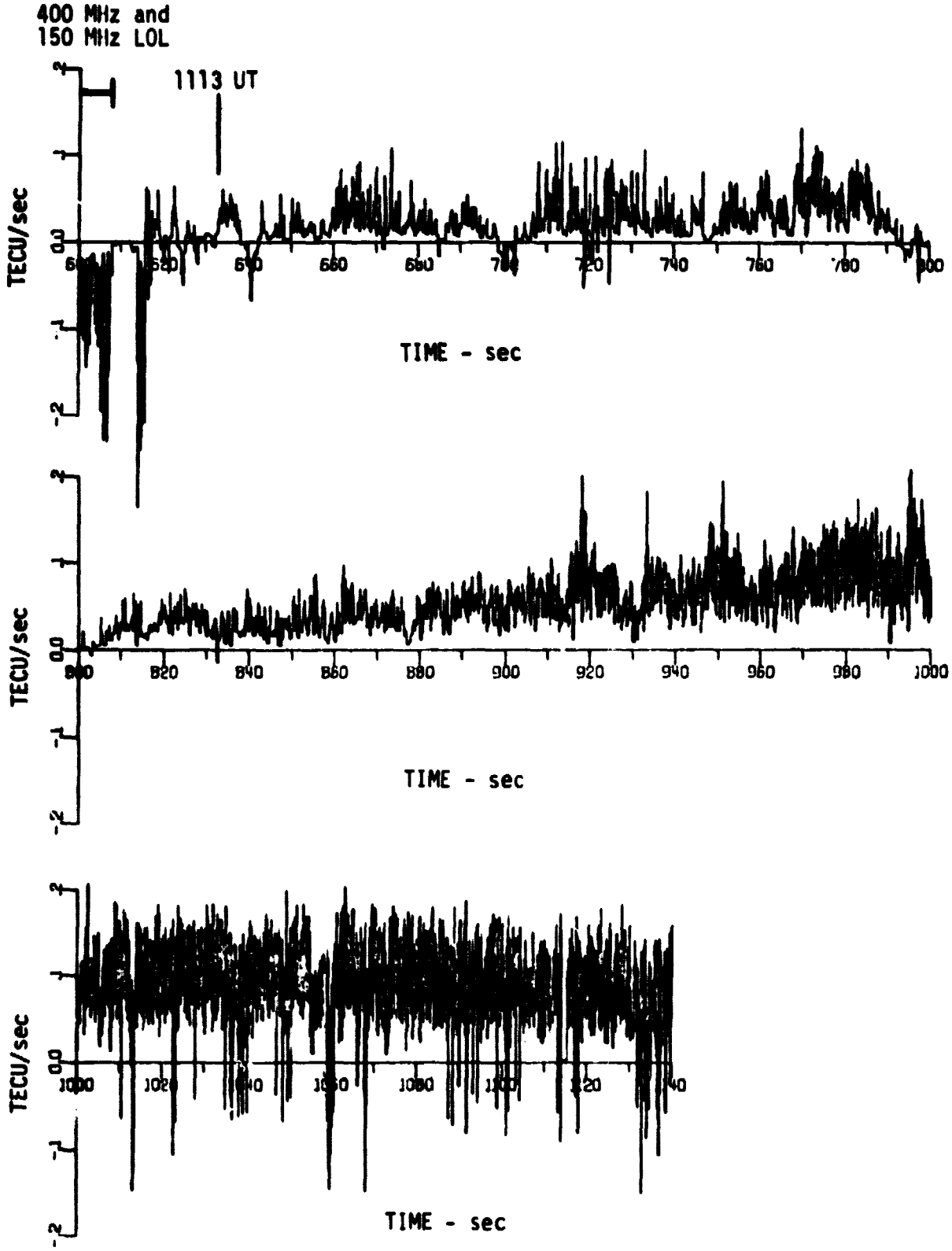

FIGURE 48 (cont'd)

$\dot{N}_c$ versus TIME FROM AUXILIARY TAPE SYSTEM

Satellite 68 Day 109 Rise 11:02 UT

AE-81-64(b)

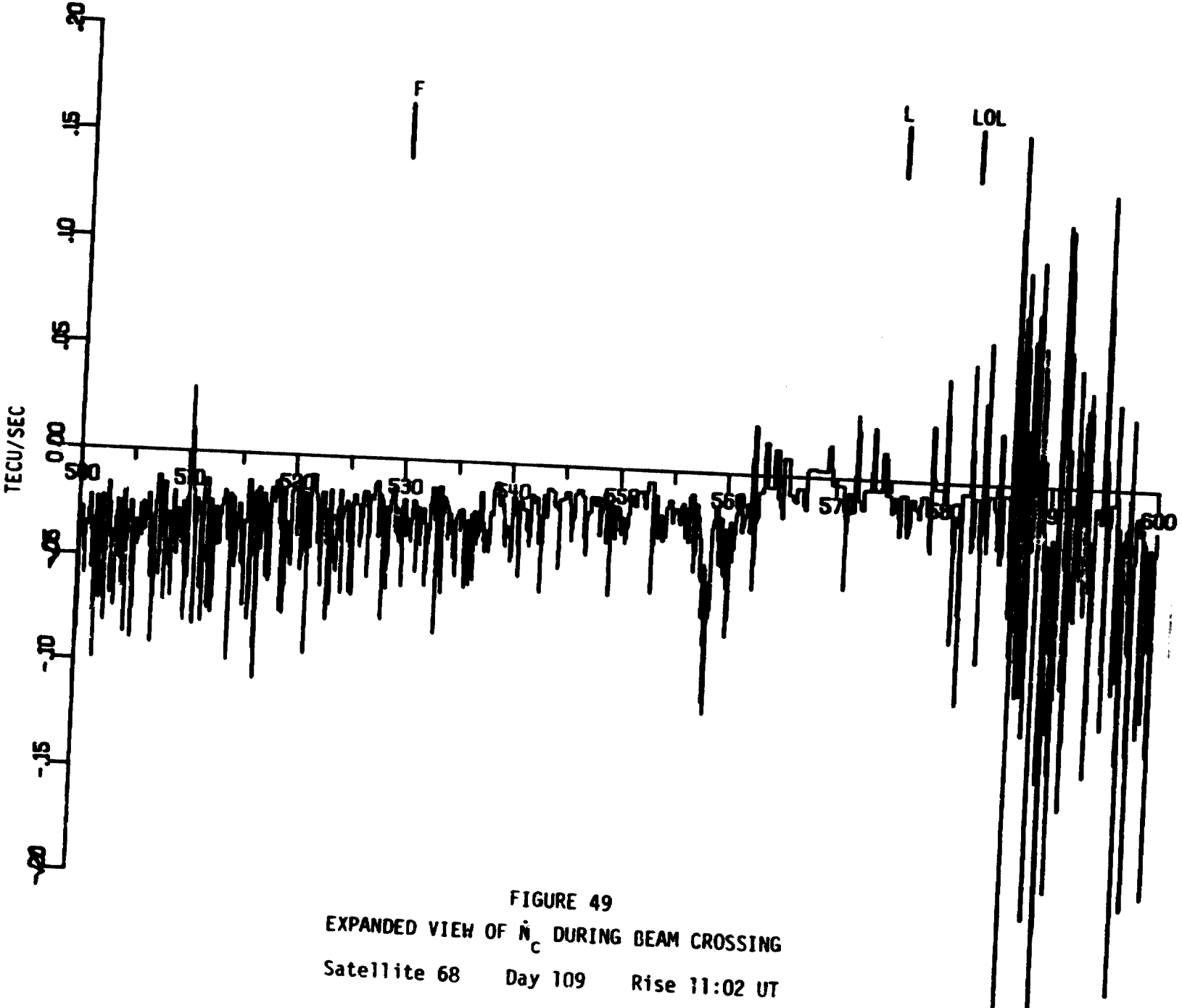

FIGURE 49

EXPANDED VIEW OF $\dot{N}_c$ DURING BEAM CROSSING

Satellite 68 Day 109 Rise 11:02 UT

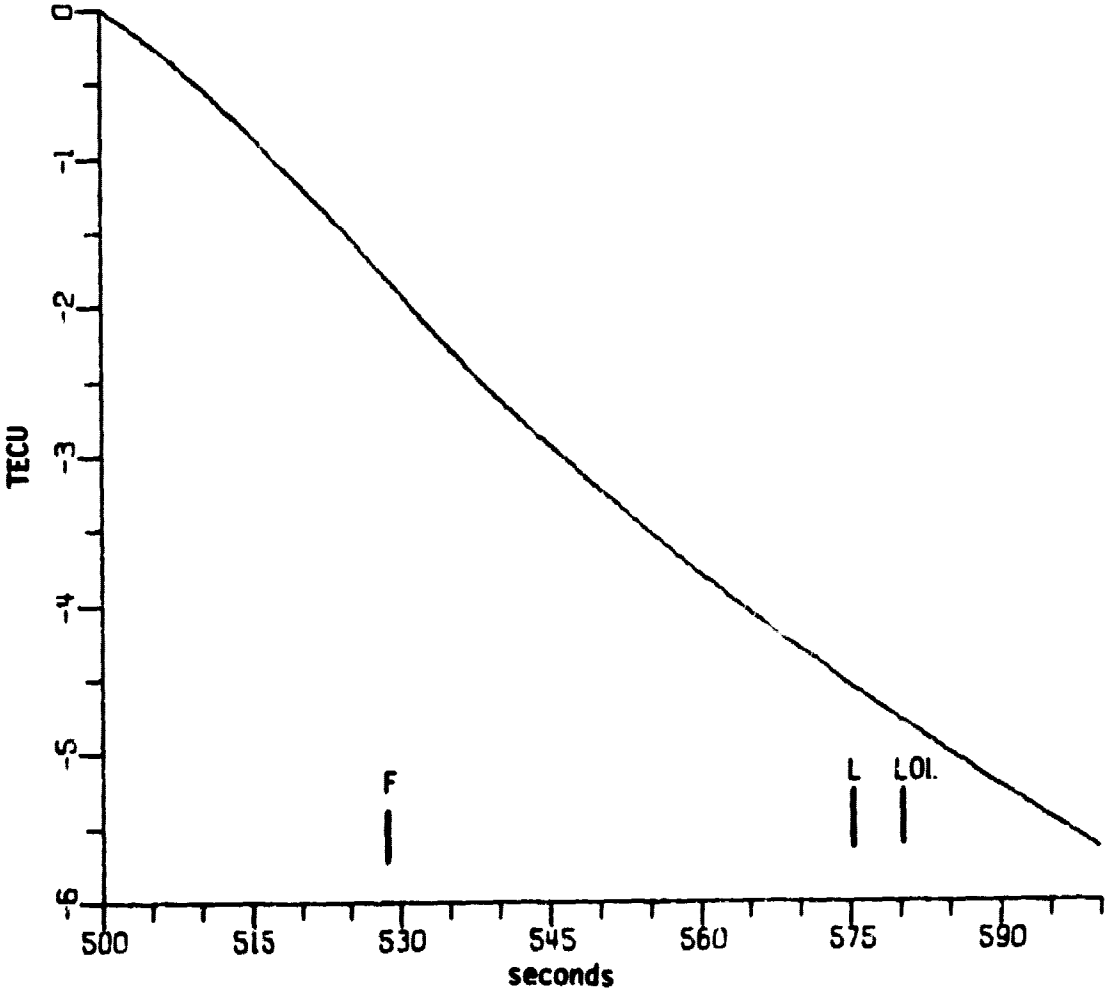

FIGURE 50

N_c versus TIME DURING BEAM CROSSING

Satellite 68 Day 109 Rise 11:02 UT

AE-81-66

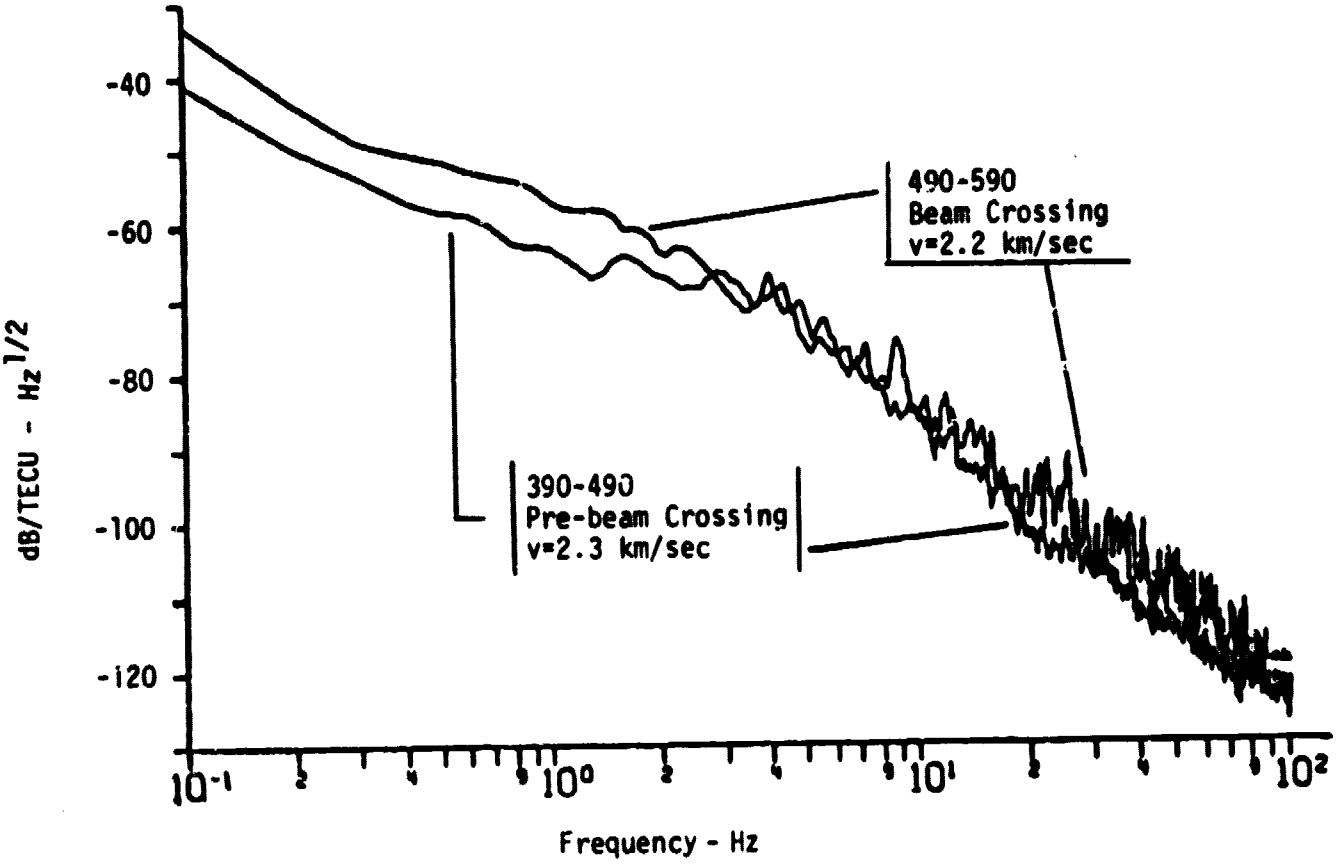

FIGURE 51

TEMPORAL SPECTRUM OF DETRENDED N_c

Satellite 68 Day 109 Rise 11:02 UT

FIGURE 52

rms N_c VARIATION versus AVERAGING TIME

Satellite 68 Day 109 Rise 11:02 UT

AE-81-68

C-2

IV. ANALYSES OF RESULTS

There are two principal observations from these data: (1) the F region within the beam has fewer electrons than the surrounding volume, and (2) there are small scale irregularities high in the F region which give rise to scattering and multipath. These lead to the following simple model. Energy is being deposited in the F region, either directly or from the E region, which causes the electrons to expand as a free gas. The electrons travel up the field lines causing turbulence, especially at higher altitudes where the perturbation will be a greater percent of the background. Because the data are sparse this model is simple and qualitative.

The observations, independent of this model, can be used to predict some effects on the pilot signal. This, of course, assumes that the proximity of the heating frequency to the peak plasma frequency is not an important feature. The depletion within the beam will cause a focusing of the beam with possibly a small net deflection. The turbulence will cause scattering of the power beam and induce phase noise on the pilot signal.

A. Effects of the Depletion

The depletion was only observed on the first pass at Sterling. The other two passes for which high resolution N_c data are available did not see a depletion for explainable reasons: the first Loveland pass, which probed the F region, lost lock immediately on entry, and the second Loveland pass went below the F region through the beam.

The measured depletion was about 0.75 TECU in depth and the LOS extended through the beam over a distance of 230 km. The reduction at

the center of the depletion represents an average reduction in density of 3.3×10^4 el/cm^3. The Boulder ionogram shows a F_0F_2 of 7.5 MHz with a peak altitude at about 450 km. This represents a peak plasma density of 7.0×10^5 el/cm^3. The ratio of the average depletion to the maximum density is therefore 5%. Allowing for the variation in density with altitude, a uniform relative depletion of as high as 10% would be required, depending on the sharpness of the F region peak.

To examine the effects on the SPS configuration, it will be assumed that there is a 10% depletion with a horizontal extent of 80 km on each side of the beam center. In the afternoon, with a vertical columnar electron content of 100 TECU and at an elevation angle of 60°, the center of the depletion would be 12 TECU in depth. This represents 6.6 cycles at 2.45 GHz or an increased phase range of about 80 cm. If this 80 cm were to decrease linearly to zero over a distance of 80 km, the angle of the wedge it formed would be 6×10^{-4} deg. If the depletion decreased quadratically over the same distance, it would form a lens. The radius of curvature of the parabolic lens is

$$R = \frac{1}{2} \frac{h^2}{\Delta l} \quad ,$$

where h is the horizontal distance over which the range of differences changes from the maximum to zero. For this case, h is 80 km, Δl, the maximum range difference, is 80 cm, and R is 4×10^6 km.

It is clear that neither the deflection nor the focusing caused by the maximal depletion inferred from these measurements will significantly affect the SPS power or pilot signal.

B. Scattering and Phase Noise

The irregularities caused by the heating will cause energy to be scattered from the power beam and phase noise to be imposed on the pilot signal. The irregularities from the auroral scintillations observed

on day 106 caused more amplitude and phase fluctuations than any of the heating passes which maintained lock through the beam. Many auroral region scintillations do cause loss of lock in geoceiver data. Therefore, it is fair to say that, whatever irregularities are produced by the heater, they are less intense than auroral irregularities.

The one good measurement of the beam turbulence indicates that there is considerable energy in the scale region below 100 m (see Fig. 41). This is on the order of the Fresnel size for the pilot beam as viewed from earth. Therefore, this turbulence will not be significantly averaged out but will contribute to phase noise on the pilot signal.

Autocorrelation lengths of 2-4 km obtained earlier may be dominated by instrumentation artifacts. If not, the rms electron content variation in the beam car be found from the area near 1.0 sec on Figs. 42 and 52, the beam crossing data. This value is greater for the case shown in Fig. 42, where the beam probed the ionosphere in the F region. For that case, the rms N_c variation is 7.5×10^{-3} TECU. This corresponds to 1.5° of phase at the SPS frequency.

If one wishes to allow for a larger autocorrelation distance, this figure may double. Allowance must also be made for the fact that these measurements were made during the early evening and the maximum daytime plasma density could be twice the value measured here. Therefore, an overall factor of four should be applied to obtain a conservative overestimate. This implies that the rms phase variations at a point on the SPS due to turbulence induced by the power beam are likely to be less than 6°.

This error will be correlated with other receivers on the SPS. Chernov[3] has shown that the spatial autocorrelation of phase function will be very similar to the autocorrelation function of the irregularities. An estimate of phase error over 1 km can be found from the rms N_c variation corresponding to 1 km on Fig. 42. This will be at 0.4 sec since the velocity of the LOS was 2.4 km/sec. The value at this point is

2.5×10^{-3} TECU which corresponds to 0.5° of phase at the SPS frequency. This measurement needs to be scaled up by a factor of two in order to account for the daytime increases in electron density. Thus, the rms variation in phase difference to be expected between points 1 km apart on the SPS is about 1.0°.

The scattering of the energy out of the beam is a potential problem. The evidence from this experiment is highly qualitative, but suggestive. On four passes (numbers 2, 3, 4, and 8), there is evidence of multipath interference from field aligned turbulence high in the F region over the heater. This indicates that sharp edges have formed and these are significant irregularities at a few meters scale length. The high resolution N_c data do not contain clear evidence of this, although it may be below the noise floor of the equipment.

APPENDIX

RELATIONSHIP OF REFRACTION CORRECTION COUNT TO COLUMNAR ELECTRON CONTENT

The Navy navigation satellites contain coherent radio beams at 150 MHz and 400 MHz. Some geodetic satellites contain similar beacons at 162 MHz and 324 MHz. The upper or UHF beacon is used to determine the Doppler curve during a satellite pass. These data are then used (1) to determine the receiver's location given the satellite position as a function of time, or (2) to determine the satellite position as a function of time given the receiver position, or (3) for some other purpose, such as measurements of propagation effects. Because these radio waves must pass through the ionosphere where the refractive index is significantly different from unity, the lower frequency or VHF signal is included as a probe to measure the ionospheric quantities necessary to correct for propagation effects.

The refractive index in the ionosphere can be approximated at these frequencies by

$$n = 1 - A \frac{N}{f^2} \quad , \tag{1}$$

where

n is the refractive index,
N is the electron density,
f is the frequency, and
A is 4.03×10^7 $Hz^2/(el/cm^3)$.

The phase ϕ, observed on the ground, will be

$$\begin{aligned} \phi &= -\frac{2\pi}{\lambda} \int n ds + 2\pi f t \\ &= -\frac{2\pi f}{c} \left\{ \int 1 \, ds - \frac{A}{f^2} \int N ds \right\} + 2\pi f t \\ &= -\frac{2\pi f}{c} R + \frac{2\pi A}{cf} N_c + 2\pi f t \quad , \end{aligned} \tag{2}$$

where R is the slant range and

$$N_c = \int N ds \tag{3}$$

is the columnar electron content. The frequency observed will be

$$f_{obs} = \frac{1}{2\pi}\frac{d\phi}{dt} = f - \frac{f}{c}\dot{R} + \frac{A}{cf}\dot{N}_c \quad . \tag{4}$$

This expression contains two terms proportional to f and one proportional to 1/f. The former two contain the geometric information needed to determine relative positions, and the latter contains the effects of the medium.

In the geoceiver, two signals are received and a quantity proportional to the last term in Eq. (4) generated. Let ϕ_U be the UHF phase and ϕ_V be the VHF phase. Then the combination

$$\phi_{RCC} = \alpha\left(\phi_U - \frac{f_U}{f_V}\phi_V\right)$$

$$= \alpha\frac{2\pi A}{cf_U}N_c\left(1 - \frac{f_U^2}{f_V^2}\right) \tag{5}$$

is formed and counted. The result is the RCC. The constant α varies between the two frequency pairs and is 3/2 for the 150 MHz/400 MHz frequency pair and three for the 162 MHz/324 MHz pair.

A change in ϕ_{RCC} of 2π generates one refraction correction count and represents a change in N_c of -3.25×10^{-2} TECU for the NAVSATs and -2.68×10^{-2} TECU for the geodetic satellites. A total electron content unit, TECU, is 10^{12} el/cm^2, or 10^{16} el/m^2.

REFERENCES

1. W. Utlaut, and R. Cohen, "Modifying the Ionosphere with Intense Radio Waves," Science 174, 245 (1971).

2. J. A. Thompson, "Energy Deposition in Artificial Ionospheric Heating Experiments," J. Geophy. Res. 75, 6446 (1970). (See also other papers in this special issue of J. Geophy. Res.)

3. L. Chernov, Wave Propagation in a Random Medium (Dover Publications, New York, 1960), p. 110.

ACKNOWLEDGMENTS

This experiment could not have been performed without the full cooperation of Charles Rush and his colleagues at the Institute of Telecommunications Science. We are grateful to them for operating the heater in the dead of night and for technical assistance in times of difficulties. In addition, we would like to express our gratitude to the Defense Mapping Agency Hydrographic/Topographic Center for the loan of the Geoceiver used in this experiment.